THE EFFECT OF CHARGE STRATIFICATION ON THE COMBUSTION OF LEAN METHANE-OXYGEN MIXTURES UNDER CONSTANT VOLUME CONDITIONS

A thesis

submitted in fulfilment

of the requirements for the degree

of

MASTER OF ENGINEERING (MECHANICAL)

in the

University of Canterbury

by

LEONARD FRANCIS DAMIANO

Department of Mechanical Engineering

University of Canterbury

Christchurch

NEW ZEALAND

February 1993

ABSTRACT

A constant volume cylindrical combustion bomb of 100 mm diameter, and of variable length (from 250 mm to 1000 mm) has been built. The effect of charge stratification on the ignitability and subsequent flame propagation of lean ($\lambda > 6$) methane-oxygen mixtures has been investigated. The test mixtures were quiescent with initial conditions of 25°C and 1.5 bar absolute.

The stratified charge was created by injecting small quantities of a relatively rich ($\lambda = 4.57$) premixed methane-oxygen mixture through a modified commercially available spark plug so that an easily ignitable mixture formed in the vicinity of the spark electrodes. The injector used was a commercially available Bosch gasoline injector, suitably modified for gas operation. The injection pressure was 5 bar gauge. The size of the injected puff could be altered by adjusting the duration (from 0-100 ms) for which the injector was opened, and the timing of the spark could be adjusted so that it occurred either before, after or at the end of injection.

Results show that the injected premixed puff is an efficient high energy ignition source for very lean methane-oxygen mixtures. For the most reliable ignition performance a delay of 10 ms between the end of injection and the occurrence of the spark has been found to be desirable. This is attributed to the decay of the turbulence produced by the puff. Long injection durations (greater than 20 ms) also improved ignition reliability, due to the larger puff size.

The use of charge stratification did not enable combustion to continue below the ideal flammability limit. It did extend the equipment lean limit of flammability from $\lambda = 7.3$ (spark alone) to $\lambda = 8.35$, and thus demonstrated that it could be useful as a limit extender in non-ideal combustion situations. Results from the longest bomb used (1000 mm) show that the flame dies out after successful ignition has been achieved, and that a distinct lean flammability limit does not exist. Experimental evidence suggests that the flame is generating turbulence as it propagates, and this turbulence causes the flame to become self accelerating. Further, it is thought that the flame generated turbulence is the primary cause of flame extinction (in the form of turbulence induced gas phase quenching) after successful ignition in the 1000 mm bomb.

ACKNOWLEDGMENTS

I am most grateful for all the support, help and encouragement given to me by my supervisor, Dr R Green, during the course of this research. The assistance given to me by the Thermodynamics Laboratory technicians, Messrs R Tinker and E Cox, has also been invaluable.

Thanks must also go to Mr O Bolt for allowing me use of the Departmental workshop facilities, and to Messrs S Amies and K Brown for the manufacture of the bomb and other equipment. Mr G Leathwick was an invaluable help in obtaining materials and other miscellaneous items. Mr D Sallis of the Electrical Engineering Department built the timing control box and gave help in other electrical and electronic areas, as did Messrs H Anik and J Murphy. Mr B Sparks was a great help during the schlieren and other photography work.

Final thanks must go to my post-graduate colleagues, especially Vikas Ahuja and Neil Glasson, for some enlightening discussions on various aspects of the research.

TABLE OF CONTENTS

LIST OF TABLES

LIST OF FIGURES

LIST OF PLATES

NOMENCLATURE

Abbreviations

A/D	Analogue to Digital
AEI	After End of Injection
ATS	After Test Start
EGR	Exhaust Gas Recirculation
ELLOF	Equipment Lean Limit of Flammability
FACP	Fraction of Adiabatic Carbon dioxide Production
FAPPR	Fraction of Adiabatic Peak Pressure Production
FGT	Flame Generated Turbulence
ILLOF	Ideal Lean Limit of Flammability
NO_x	Oxides of Nitrogen (NO and NO_2)
O/F	Oxidiser to Fuel ratio
OPEC	Organisation of Petroleum Exporting Countries
SCE	Stratified Charge Engine
TMPI	Time to Maximum Pressure from Ignition
UHC	Unburnt HydroCarbons

Symbols

A	Area
c	Mean specific heat
c_p	Specific heat at constant pressure
c_v	Specific heat at constant volume
d	Diameter
e	Ratio of moles present after and before combustion
E	Activation energy (also energy in coil, Section 5.4.1)
f	Fraction of fuel in reactants
H	Enthalpy
i	Instantaneous current
I_{ss}	Steady state current
k	Thermal conductivity
K	Karlovitz Number
K_i	Equilibrium constant of Equation (i)
L	Inductance
m	Mass
M	Some unspecified molecule(s)
n	moles
N	Number of sparks (also number of injections, Appendix E)
P	Pressure
P_c	Critical downstream pressure for sonic flow
P_o	Injection pressure

q	Heat energy available in spark
Q	Heat
r	Radius
R	Universal gas constant (also resistance, Section 5.4.1)
S	Velocity at point in flow field
S_u	Burning velocity
S_w	Wave velocity
t	Time (also thickness, Section 4.2.1)
t_{inj}	Duration of injection voltage pulse
T	Temperature
U	Internal energy
v	Specific volume
V	Volume
w	Moles of gas in bomb
W	Work
x	Coordinate transformation in Appendix C (= t_{inj} - 20)
XA	Molar fraction of component A
y	Spline approximated molar flowrate
z_i	Spline Constants

Greek Symbols

ρ	Density
η_o	Preheat zone thickness
λ	Equivalence ratio (defined as the actual O/F ratio divided by the stoichiometric O/F ratio)
σ	Stress
ΔA	Change in quantity A
γ	Ratio of specific heats

Subscripts

b	Burnt gas
u	Unburnt gas
r	Reactants
p	Products
i	Initial state
f	Final state
e	After combustion
w	Water
m	Methane

Superscripts

A'	Rate of change in A with respect to time (eg. n' = molar flowrate)
A''	Double gradient of A

CHAPTER 1

INTRODUCTION

1.1 INTRODUCTION

Since the emergence of the internal combustion engine as a viable prime mover over one hundred years ago the reciprocating spark ignition engine has remained a most popular engine, especially for motor vehicles. This is due primarily to its light weight, simplicity of operation, versatility and low cost of manufacture. These factors have enabled it to compete successfully in all but the most specialist areas (eg. turbojets for aviation use, compression ignition engines for large stationary applications).

A measure of the success of the design pioneered by Otto, Daimler and others in the late 19th century is that the reciprocating spark ignition engine remains fundamentally the same today. Developments have concentrated on improving particular facets of the engine's performance rather than resorting to a completely new design as problems arose. This process will probably continue for some time yet, while fundamentally different designs like the rotary engine (Wankel design) will struggle to establish even a niche in the market.

The biggest problems confronting engine designers of today (and tomorrow) are the somewhat interrelated areas of fuel economy and exhaust emissions. It is generally agreed that reserves of liquid hydrocarbon fuels such as gasoline are finite and that consumption of these will increase in the future.[1] Pressure will therefore increase on engine manufacturers to improve fuel economy of the engines in use, to insure that the reserves last as long as possible. The effect on the environment of the emissions these engines produce is well known in some cases (eg. as vehicle engines they are the primary cause of photochemical smog[2]) but still debated in others (eg. carbon dioxide emissions causing a planetary-wide "greenhouse effect"). As legislators around the world respond to these real or imagined problems, engine designers will be forced to look for more effective solutions.

1.2 LEAN BURN AND STRATIFIED CHARGE

1.2.1 Lean Burning Engines

Burning a lean mixture decreases the maximum power output of an engine, but this is generally of little concern as most vehicle engines do not operate at maximum power for more than very short periods. Lean mixtures are however especially conducive to improved part load fuel economy due to the reduced flame temperature (leading to lower heat losses). A good deal of research was initiated in the early 1970's (in response to the OPEC inspired "oil shock") in an attempt to achieve the improved fuel economy promised by lean burn engines. Specially

designed engines were built to use leaner than stoichiometric fuel-air mixtures, but achieved little success for three primary reasons:

(a) Ignition of a lean mixture is considerably more difficult than a stoichiometric one, which can lead to misfire.[3,4]

(b) Even if ignition is successful a lean mixture increases the cycle to cycle variation, leading to a decrease in optimised engine performance.[5]

(c) Burning velocity can be so slow that combustion is not complete when the exhaust valve opens.[6] This is especially a problem in high speed engines.

Interest in lean burning as the basis of a new range of practical engine designs faded away at the beginning of the 1980s. The problems described above could probably have been solved, but a more practical reason why the lean burn engine has not been adopted has to do with the level of exhaust emissions.

1.2.2 Exhaust Emissions and Treatment

A spark ignition engine burning a hydrocarbon in air produces three main kinds of pollutant, namely unburnt hydrocarbons (UHC), oxides of nitrogen (NO_x) and

carbon monoxide (CO). UHCs are mostly created due to wall quenching, which occurs because the flame is unable to propagate within a certain distance (known as the quench distance) of the combustion chamber wall due to heat losses to the wall. The level is dependent on such things as compression ratio, spark timing, induction system and load.[7,8,9] The fuel remaining in this quench layer remains essentially unburnt. Small quantities of UHCs are also created by post flame reactions. NO_x is formed by equilibrium chain reactions occurring at the flame temperature and its production is further influenced by the pressure and temperature prevailing in the burnt gases, a higher temperature leading to a greater level.[10,11] Long residence time (ie. slow engine speed) is an important factor in NO_x production as are combustion chamber shape, spark timing, compression ratio and inlet mixture temperature.[12,13] CO is primarily formed due to the incomplete combustion of fuel. Small quantities are also created by various dissociation reactions at the flame temperature.[14,15] Some believe that CO_2 is also a pollutant, but until very recently it has not been considered so, due to its naturally occurring presence in the atmosphere.

In most modern spark ignition engines the three major pollutants (UHC, NO_x and CO) are treated by means of a three-way catalytic converter. This has evolved into a highly efficient and reliable device after a somewhat inauspicious beginning. However the use of such a converter requires that the engine run at exactly stoichiometric mixture conditions, and these engines demand a complex engine management system to continually adjust the mixture in response to changing conditions. A lean burn engine cannot use a three-way catalyst because the excess

oxygen in the exhaust would make catalytic reduction of NO_x impossible. NO_x levels are generally of less concern with lean burning, as the reduction in flame temperature can significantly reduce the production of NO_x. However, the lower flame temperatures and slower burning velocity of a lean burn engine can actually increase production of UHC and CO, due to the reduction in post flame front oxidation reactions. Research has been carried out to produce systems which can reduce these emissions to acceptable levels, but the catalytic converter is generally simpler, needs no maintenance and is now proven technology. In addition the inherent limitations of the lean burn engine (that is difficulty of ignition, increased cyclic variation and slow burning) remain.

1.2.3 The Stratified Charge Engine

Interest in the lean burn concept has increased again due to the promise of significantly improved fuel consumption figures, which catalytic converter engines cannot match. Rising to prominence is the stratified charge engine (SCE), which was developed in the 1970s to retain the best features of the lean burn concept, but eliminate the problems of poor ignition performance, increased cyclic variation and slow burning.

The SCE functions by burning a stratified mixture, ranging from stoichiometric around the spark plug electrodes to lean near the combustion chamber wall. The majority of the mixture in the combustion chamber is lean, the richer volume near

the electrodes being small. Once ignited the flame from the richer volume can burn the lean volume, which may be non-ignitable if a spark alone were used. Being lean near the walls reduces UHC production from wall quenching and improves part load fuel economy as for the lean burn engine, but the richer mixture near the plug improves ignitability (less misfire) and speeds up the time to burn the whole charge by decreasing the ignition delay time (time between the spark occurring and the start of the pressure rise). This helps negate the tendency of a lean burn engine to produce high levels of UHC and CO due to insufficient time for the occurrence of post flame front oxidation reactions. UHC and CO levels may still be high compared to a conventional engine with a three-way catalyst, but these can be treated by using a thermal reactor or oxidation catalyst. NO_x levels are usually lower than a conventional engine due to the reduced flame temperature, and may be further treated using EGR.*

Thus the SCE promises to produce emission levels as low as or lower than the best of the conventional catalytic engines, while significantly improving fuel consumption. Many SCEs have been developed, and the major ones are shown in Table 1.1.[16]

The way in which the stratified charge is created can be divided into two main methods. The divided chamber forms a rich mixture in an auxiliary prechamber connected to the main combustion chamber by a torch passage.[17] In this case the stratification division is fairly sharp, and can give good results but is complex, requiring an additional fuel mixing and induction system. The open chamber

---

* Exhaust Gas Recirculation

Table 1.1 Various Stratified Charge Combustion Processes

RESEARCH ORGANISATION AND PROCESS	FUELLING AND COMBUSTION SYSTEM	OPERATIONAL CHARACTERISTICS
FORD Programmed Combustion Process (PROCO)	Low pressure direct injection. Open chamber enhanced swirl. Twin plugs.	EGR and oxidation catalyst required.
HONDA Compound Vortex Controlled Combustion (CVCC)	Carburation into divided combustion chamber.	Low fuel consumption. Good emission control. Developed into production engine.
M.A.N. FM System	Open chamber high swirl direct injection. Employs surface evaporation.	Modified plug. Exhaust catalyst. Multi fuel capability including methanol and ethanol.
MITSUBISHI Mitsubishi Combustion Process (MCP)	Open chamber. Fuel injection with variable retraction delivery valve.	Multi fuel capability including kerosene. Production engine for agricultural machines.
TEXACO Texaco Controlled Combustion System (TCCS)	High pressure direct injection. High swirl, late ignition. Included turbocharged version.	EGR and oxidation catalyst. Multi fuel capability. Peak power limited by smoke emission.
VOLKSWAGEN Pre-chamber Injection System (PCI)	Variable fuel supply injected to spherical pre-combustion chamber.	Thermal reactor to reduce CO and UHC emissions.

process[18,19] is simpler, injecting a fuel spray at high pressure (up to 135 bar) into swirling air so that a rich mixture will form around the plug at the required time. The stratification is generally much smoother than in the first case but there is always the possibility that the mixture could move away from the plug by the time the spark occurred, and it has been shown that this can result in very high UHC emissions.[20]

Only the Honda CVCC* has been put into large scale production, and this was only for a short time in the early 1980s. It had been developed to meet stringent new Californian emission regulations, but legislative changes eased the impact of these, and the CVCC was unable to compete with conventional engines due to its higher manufacturing costs. The fact that the cost of designing and constructing a SCE are high compared to a conventional engine remains a problem, but the stratified charge concept remains one of the most promising alternatives available for meeting the anticipated environmental and legislative challenges of the future.

The concentration gradient formed in SCEs substantially affects flame propagation and energy release. This propagation through non-homogenous mixtures represents a much more complex situation than with a conventional spark ignition engine and the combustion process is not well understood. For example the understanding of the effects of a concentration gradient on the flammability limits, rates of flame propagation relative to those in homogenous mixtures and ignitability could benefit from further study.

1.3 INTENDED AREAS OF INVESTIGATION

This thesis will examine under controlled conditions the combustion processes arising from stratified charge combustion. The conclusions reached are intended to increase the fundamental understanding of the combustion process, although they

---

* Compound Vortex Controlled Combustion

may not be immediately applicable to a working SCE. Engine testing work by Zavier[21] has suggested that a fundamental study needs to be made of the following areas.

(a) How does the stratified charge affect the ignition of the mixture? What amount of stratification is necessary?

(b) Does a flame propagating from a richer mixture to a lean one continue propagating? How does the propagation change? Can such a flame continue in a mixture below the normally accepted lean limit of flammability?

(c) If the flame continues burning in such a mixture, for how long does it sustain combustion? Is the combustion steady state or slowly diminishing?

The fuel and oxidiser chosen for the testing are methane and oxygen respectively. Methane is chosen for its ready availability, because it is the lowest order hydrocarbon fuel and because it is commonly used by other researchers. Oxygen is chosen rather than the air more commonly adopted because it simplifies the combustion process. For example if sampling of the explosion products is required, fewer different species would be present than for methane-air. Oxygen also simplifies modelling of the combustion process. It should be pointed out that very lean mixtures of methane-oxygen and methane-air behave in an almost identical

manner, the only exception being a higher flame speed for methane-oxygen mixtures.

A constant volume cylindrical bomb of variable length is envisaged as the testing rig. The mixture in the bomb is to be quiescent and the stratified charge is to be created using a modified spark plug and injector as used by Zavier. A premixed mixture rather than the pure methane of Zavier will be injected. It was felt that pure methane would cause ignition problems because the turbulence level available in the bomb for mixing the puff with the internal mixture is low compared to that in an engine.

CHAPTER 2

METHANE AS A FUEL

2.1 INTRODUCTION

Methane (CH_4) is the lowest order hydrocarbon fuel. At room temperature and pressure it is a colourless odourless gas. Some of the properties of methane are give in Table 2.1.*

Table 2.1 Properties of Methane

Formula	Density at 0°C & 1013 mbar	Main Compo. % by weight	Boiling Point at 1013 mbar	Heat of Combustion	Ignition Temp.	Ideal Air Req.
CH_4	0.72 kg/m^3	75C, 25H	-162°C	50.0 MJ/kg	650°C	17.2 kg/kg

Gaseous fuels have a number of advantages over liquid fuels when applied to spark ignited internal combustion engines. The fact that they are a gas means they do not have to vaporise in the inlet tract, and hence they achieve a more homogenous fuel-air mixture. This insures better combustion and generally lower emissions. However gaseous fuels are difficult to store and handle, especially those of low molecular weight, like methane, as they will not liquify under reasonable pressures

* From Bosch Automotive Handbook[92]

at room temperature. For stationary engine applications this problem is not serious, but for vehicle use it limits operational range. Storage of a high pressure gas poses additional safety problems.

2.2 PRODUCTION

The largest source of methane in the world today is natural gas,[22,23] which is typically 80% - 95% methane, the remainder comprising small quantities of ethane, propane, butane, hydrogen, hydrogen sulphide and carbon dioxide. The exact ratio is dependent on the field from which the gas is taken. Natural gas is usually found in deposits associated with oil fields, although it is now being found alone in places where oil would not normally be expected. Reserves of natural gas are more evenly divided across the planet than are oil deposits. The former Soviet Union leads the way with 40% of known reserves, while Iran is the next largest with 14%. Western Europe and the USA have 5% and 6% respectively.[22] Natural gas use in all areas is likely to increase in the future as reserves of liquid hydrocarbons are depleted.[24,25] Before use any sulphur compounds are always removed, and the quantities of propane, butane and carbon dioxide are often also removed.

Methane is also associated with coal seams and is known as "fire damp".[26] The gas is released slowly during mining. This sometimes reaches concentration levels high enough to cause an explosion, and so it is removed from the mines by large ventilators. Collection of the gas in this way is not usually economically feasible,

but if the gas yield is large enough it can be recovered through a series of bore-holes behind the coal face. The gas recovered is typically 93% - 95% methane, the remainder being ethane, nitrogen and carbon dioxide.

Coal, wood and peat can be used as a source of a gas known usually as "town gas" or "coal gas".[23,26] The production method consists of high temperature (1000 - 1300°C) carbonization, that is heating in the absence of air. The gas produced is typically a mixture of methane (approximately 30%) and hydrogen (50%), the remainder being carbon monoxide, carbon dioxide and nitrogen. The byproduct of the process is low grade coke. Before the Second World War, coal gas formed the majority of gas supplied to domestic and industrial users, but since 1945 natural gas has, in most countries, gained such a share of the market[27] that the traditional method of gas production is virtually obsolete. Significant quantities of coal gas are still formed in the low temperature carbonization of coal, but the primary purpose of this process is the manufacture of high grade coke for steel making, and the gas is a byproduct, which may or may not be collected. However, with coal reserves estimated to last over one thousand years at the present rate of usage, the manufacture of gas from this source may become important once again, especially if in-ground gasification of coal seams can be achieved. This would allow the exploitation of seams that are currently too deep for mining. For example it is estimated that 60% of the coal in Great Britain is unrecoverable using present techniques.[22]

The final source of methane is ecologically promising for the future. Bio-gas is produced as a byproduct of the anaerobic decomposition of organic material and waste in a vessel known as a digester.[28] Naturally occurring bacteria are responsible for this and the products of digestion are typically 70% methane, 30% carbon dioxide. The technology for small plants is available and has been used in such facilities as sewerage treatment works. The most obvious attraction of large scale production by this method is that it turns useless and potentially damaging waste into a useful fuel that is a renewable resource. Whether sufficient quantities of suitable waste would be available for large scale exploitation has been questioned but it may become important as an independent energy source.

2.3 USES

Coal gas and natural gas can be used in their virgin state, and for uses such as heating this may be acceptable, but for maximum efficiency in heat engines it is desirable that the gas consist of as much fuel as possible with little dilution. Adaptation of heat engines to run on gaseous fuels will probably take on some importance in the future due to the probable decline in oil availability.

The virgin gas can be purified by the use of "scrubbers", which remove the undesirable components. For example, bio-gas produced at sewerage works is typically scrubbed to better than 95% pure methane.

The major problem with using methane as a fuel for reciprocating spark ignition engines is the fact that due to its low density it displaces a considerable quantity of air from the engine cylinder during induction. This lowers the volumetric efficiency and hence power output of the engine by around 10% compared to the same engine running on gasoline. However a specially designed engine could eliminate this problem by using direct injection after the closure of the inlet valve, rather than a conventional gas carburettor (or indirect injection) as used in most modified engines. Otherwise methane is a good fuel, the heating value of a stoichiometric methane-air mixture being almost identical to a gasoline-air mixture (2.74 MJ/kg compared to 2.70 MJ/kg). Better combustion characteristics are attainable with methane because it mixes more readily with the air, and its higher octane rating (approximately 120) allows the use of higher compression ratios (hence improved power and efficiency). The main obstacle to the use of methane as a spark ignition engine fuel is that no vehicle engines have been designed specifically to operate on it (a few stationary engines have appeared). Almost all engines operating on it at present are compromised by the fact that they were designed to use gasoline as a fuel.

2.4 REACTION MECHANISM FOR METHANE-OXYGEN

It is a relatively simple matter to calculate the final products for virtually any fuel-oxidiser flame using equilibrium considerations and allowing for dissociation of the products (see Section 5.2). However it tells us nothing about the mechanism by

which the final products are formed, that is what reactions lead from the reactants to the products.

This is an extremely complicated subject, because even the simplest flames have complex reaction mechanisms and sequences. Much experimental work has been performed in an attempt to determine the mechanism of methane-oxygen flames, but the process is still by no means well understood.

The major problem in proposing a mechanism is deciding which of several possible reactions are important. This relies on experimental evidence, and the measurement of the rate of production or disappearance of a particular species in the flame front. The concentration of a molecular species in the flame front can be measured using micro gas sampling or other techniques. The rates of reaction for this species can then be calculated. These rates are then be used to deduce which equation might be responsible for the destruction or appearance of that species. It is then possible to deduce an expression for the overall reaction rate and the burning velocity of the flame (burning velocity is the velocity of the flame front relative to the unburnt gas). As an insight into this subject the mechanism for methane-oxygen combustion proposed by Fristrom and Westenberg[29] will be described.

Experimental evidence shows that methane disappears throughout the reaction zone of the flame. The most likely steps for this disappearance are

$$CH_4 + OH \rightleftharpoons CH_3 + H_2O \quad (2.1)$$

$$CH_4 + H \rightleftharpoons CH_3 + H_2 \quad (2.2)$$

$$CH_4 + O \rightleftharpoons CH_3 + OH \quad (2.3)$$

Reaction (2.1) is probably dominant in fuel deficient (ie. lean) systems, and Reaction (2.2) is dominant in fuel rich systems.[30] Reaction (2.3) is slower than the first two and probably plays only a minor part in CH_4 disappearance in both fuel rich and lean cases.[31]

H_2O is formed throughout the reaction zone. One major source is Reaction (2.1). Another possible source is the reaction sequence (2.4) to (2.6).

$$CH_3 + O_2 \rightleftharpoons H_2CO + OH \quad (2.4)$$

$$H_2CO + OH \rightleftharpoons HCO + H_2O \quad (2.5)$$

$$HCO + OH \rightleftharpoons CO + H_2O \quad (2.6)$$

Thus we would expect the appearance of one mole of CO for the disappearance of one mole of CH_4. Experimental evidence confirms this in the early stages of reaction. Eventually CO production departs from this because of the onset of a CO loss reaction. There is doubt about the exact mechanism for CH_3 to CO transformation. Fenimore and Jones,[32] backed by some experimental evidence have suggested Reaction (2.7) in place of Reaction (2.4).

$$CH_3 + O \rightarrow \bullet\bullet\bullet CO \quad (2.7)$$

However they were unable to specify a viable route that would lead to CO production, so uncertainty remains.

The most probable reaction by which CO disappears is

$$CO + OH \rightleftharpoons CO_2 + H \qquad (2.8)$$

The other main possibility is

$$CO + O_2 \rightleftharpoons CO_2 + O \qquad (2.9)$$

but this is discounted because of its very low reaction rate.[33]

In addition to the above reactions, there are the chain-branching reactions which are responsible for the proliferation of the radicals necessary for the other reactions.

$$H + O_2 \rightleftharpoons OH + O \qquad (2.10)$$

$$O + H_2 \rightleftharpoons OH + H \qquad (2.11)$$

$$O + H_2O \rightleftharpoons 2OH \qquad (2.12)$$

Reaction (2.13) is also important although it is not of the chain branching type.

$$H + H_2O \rightleftharpoons H_2 + OH \qquad (2.13)$$

The radicals produced by these reactions can also recombine in various three body reactions as given below, where M is some unspecified third body, which stabilizes the new molecule on the right hand side of the reaction by removing energy from it (by collision).

$$H + H + M \rightleftharpoons H_2 + M \quad (2.14)$$

$$O + O + M \rightleftharpoons O_2 + M \quad (2.15)$$

$$H + O + M \rightleftharpoons OH + M \quad (2.16)$$

$$H + OH + M \rightleftharpoons H_2O + M \quad (2.17)$$

Thus it can be seen how complex a reaction scheme becomes, and this is for the lowest order hydrocarbon flame. Even more complex mechanisms have been put forward recently for methane-oxygen flames, for example that of Tsatsaronis,[34] which includes thirteen chemical species and twenty nine different reactions.

In principle it is possible to write the rate expression for each of the above listed equations and hence combine these to get an overall reaction rate and hence the burning velocity (for example see Warnatz[35] or Westbrook[36]). This is usually accomplished using iterative computer techniques, but it is generally unrewarding given the uncertainty of much of the experimental data that must be included (for example, reaction rate "constants" vary with pressure and temperature), and the assumptions that must be made (such as the restriction to one dimensional adiabatic flame propagation - see Section 3.2.3).

CHAPTER 3

COMBUSTION WAVE PROPAGATION

3.1 INTRODUCTION

This Chapter will deal with the propagation of a burning zone or combustion wave through a mixture of flammable gases. The discussion will be restricted to initially quiescent explosive gases, which are usually mixtures of two reactants (eg. carbon monoxide-oxygen, hydrogen-air), although some gaseous compounds such as ozone are self-explosive under certain conditions. Only premixed flames will be looked at, hence diffusion flames in which the combustible mixture is created by the interdiffusion of the oxidiser and fuel[37] (eg. candle) will be excluded.

3.2 THE COMBUSTION WAVE

3.2.1 General Description of a Combustion Wave

An explosion in a combustible mixture may be initiated by a source of heat. This heat causes a chemical reaction to take place which liberates heat and chain carriers which initiate the reaction in the adjacent layer of gas. The reaction in this layer produces yet more heat and chain carriers which in their turn initiate the

reaction in the next layer and so on. By this process a burning zone moves throughout the combustible mixture. This is the definition of a combustion wave.

In the layer being consumed by the wave, the rate of chemical reaction rises rapidly due to the high temperature created by the heat transfer from the preceding layer. This increased rate of reaction is due to the increased probability of reaction in molecular collisions as dictated by an Arrhenius type function, that is $e^{(-E/RT)}$. The increase in temperature leads to self acceleration of the reaction, and this is known as a thermal explosion. Intermediate species formed by the chemical reaction such as atoms and free radicals also play some part as chain carriers depending upon the reaction mechanism, but only cause self acceleration when the chains are branched. This self acceleration is only dominant over the thermal self acceleration at temperatures less than approximately 300°C.

3.2.2 Detonation Waves

A flame may propagate in a combustible mixture in two different ways. The combustion wave already described moves more slowly than the speed of sound, the speed being determined by the rate of chemical reaction. The maximum rate is approximately 10 m/s (70% hydrogen in oxygen). Under certain conditions a detonation wave may result and travel at speeds up to 3500 m/s, well over sonic velocity. A detonation wave is a shock wave, sustained by the energy of the chemical reaction caused by the temperature and pressure of the wave, whereas a

combustion wave propagates through heat transfer and diffusion of active species. Detonations result from the coalescence of flame generated pressure pulses into shock waves, and are limited in their speed only by the physical properties of the mixture, rather than the physical and chemical properties as for a combustion wave. An explosive mixture has rich and lean limits of detonability, and when the concentration of the mixture falls outside these limits detonation cannot occur, although combustion waves may still propagate.

3.2.3 Adiabatic Plane Wave

The true plane wave does not exist in most practical situations but may be closely approximated in the laboratory by flat flames[38] or spherical flames.[39] It enables the creation of a simple model from which some valuable insights can be gained. The profile of such a wave is shown in Figure 3.1.

Heat flows from boundary b of the hot burned gas to boundary u of the cool unburnt gas. The burned gas temperature is T_b and the unburnt gas temperature is T_u. The propagation of the wave creates a flow through the wave. Since the wave is planar, the flow through the wave is constant across its area. A mass element passing through the wave passes from boundary u to boundary b. As it does so it increases in volume, due to the thermal expansion caused by increasing temperature. The mass element, upon entering the wave, initially gains more heat through conduction from the hot downstream elements than it loses to the cooler

upstream elements. When the temperature of the mass element reaches T_i, the element is transformed from a heat sink into a heat source. This is because it is now losing more heat to the cooler upstream elements than it is gaining from the hotter downstream elements. The temperature of the element continues to rise however due to the energy liberated by chemical reaction. This process continues until the temperature of the element reaches T_b, at which point the rate of heat production approaches zero due to the consumption of all the reactants. The temperature curve is convex from T_u to T_i and concave from T_i to T_b, corresponding to positive and negative values of the rate of heat flow $d(kdT/dx)$. These zones are labelled as in Figure 3.1, that is the preheat zone and the reaction zone respectively.

The change in molecular concentration as the mass element passes through the wave can be considered using similar reasoning. The concentration of reactants curve is symmetrically opposite to that of the temperature gradient. As the mass element enters the preheat zone, reactants are initially only lost through diffusion. The mass element also receives product and intermediate species, also through diffusion. Thus reactant molecules diffuse in the direction u to b, product molecules from b to u and intermediate species (atoms, free radicals) diffuse in both directions. When the mass element passes into the reaction zone, the reactant loss is increased by consumption of these by the chemical reaction, until at T_b the reaction ceases due to their exhaustion.

These gradients (temperature and reactant concentration) have been measured for a number of flames by many investigators. Methods used include miniature

thermocouples, micro gas sampling and schlieren photography. An extensive review of the subject has been given by Fristrom[40,41].

A wave propagating in a mixture will eventually reach a steady velocity because the temperature and reactant concentration gradients of the adiabatic plane wave cannot continue increasing (ie steepening) indefinitely, the limiting factor being the reaction rates of the processes occurring in the wave, these being limited by the laws of kinetics. Conversely they cannot decrease to an ever flattening profile because the burned gas temperature, and the concentration of the reactants is fixed. The chemical reaction in the wave cannot vanish, but will adjust its rate to the prevailing temperature and concentration fields.

Equations governing the gradient profiles and the rate of propagation of the adiabatic plane wave have been developed by Hirschfelder and Curtiss[42]. Solving these is very difficult, even for simple explosive systems, due mainly to the lack of information on reaction mechanisms and kinetics (as demonstrated in Section 2.4), and transport properties at high temperatures.

Generally the most readily available experimental quantity that is available to investigators is the burning velocity S_u. This is defined as the velocity of the flame surface with respect to the unburnt gas, and easily obtained using gas burners (eg. Bunsen). The adiabatic plane wave equations have been simplified in various ways in an attempt to calculate the burning velocity of a given mixture. A review of this subject has been given by von Karman[43]. These methods achieve generally no

better than order of magnitude accuracy, and as the calculated value of S_u is relatively insensitive to the reaction mechanism and kinetic data used, it shows that the true adiabatic plane wave has few specific applications in real combustion situations.

This is primarily due to the equations being unreasonably restricted by the requirement for one dimensional propagation in an infinite medium for an infinite time. Among other difficulties is that it does not predict the existence of the limits of flammability (for full explanation of these see Section 3.4), or allow for the quenching of the flame by some other mechanism. This is because even a large disturbance cannot extinguish the flame in the absence of heat losses. Consider a adiabatic plane wave flame propagating at a steady velocity. Let some large disturbance disrupt the flame so that the chemical reaction ceases, that is the propagation of the wave ceases. Because the burnt gas is still at the temperature T_b, heat transfers across the region of quenched mixture and restablises a temperature gradient in the unburnt mixture. As soon as a suitable gradient is established, exothermic reactions recommence and the flame front re-establishes itself. This was first proved by Spalding[44]. However the adiabatic plane wave is still useful in that it presents the fundamentals required for flame propagation, namely the establishment of a temperature gradient and a concentration gradient, and hence the heat transfer to the unburnt gas.

3.2.4 Flame Stretch

In the preceding Section it was assumed that the velocity gradients in the stream of unburnt gas flowing relative to the combustion wave had no effect on the wave propagation. Consider a stationary wave, with the flow impinging on the wave from the x direction. But consider also that the velocity of the flow changes with y, that is across the wave surface. The assumption of no effect on the propagation process is justified if the velocity changes over distances comparable to the wave width are slight. If the converse is true, then the propagation (now called divergent wave propagation) is significantly altered because the mass flow across the wave is not constant. This leads to non-uniform expansion of the burnt gas, and hence an area increase from the unburnt state. It can be shown[45] that there is a dimensionless similarity factor K, known as the Karlovitz Number, which is a measure of the area increase undergone by a wave in a flow field. This is given by

$$K = \frac{dS}{dy}\frac{\eta_o}{S} \tag{3.1}$$

where S is the velocity at a point in the flow field. η_o is a measure of the preheat zone thickness and is given by

$$\eta_o = \frac{k}{c_p \rho_u S_u} \tag{3.2}$$

The importance of divergent wave propagation lies in that per unit wave area a larger volume of unburnt gas is available for chemical reaction than for planar propagation. This changes the heat transfer and molecular transport properties of the wave, so that the temperature gradient is flatter than for a corresponding planar

wave. This is caused by the increased heat loss from the reaction zone to the unburned gas, and the reduced reaction zone temperature means the burning velocity is lower for the divergent wave. The temperature of the reaction zone is reduced as flame stretch increases, that is as K becomes larger. It follows that there should be some critical value of K at which the temperature reduction in the reaction zone is so great that the heat production can no longer keep pace with the heat loss and the flame becomes quenched. This idea was first postulated by Lewis and Von Elbe[45] but has since been confirmed by others.[46,47,48,49]

The usefulness of K is that flames in quite different situations can be analyzed for their resistance to stretch induced quenching, in much the same manner as the critical Reynolds number defines the stability limits for laminar fluid flow. Some work has been done to assess the validity of such applications, and order of magnitude agreement has been obtained. In general the critical value of K is in the order of unity. The concept of flame stretch is useful in many areas, some of which will be discussed in the following Sections.

3.3 FLAME PROPAGATION IN TUBES

3.3.1 Interactions Between Flame and Induced Flow

When a flame is confined in a tube or channel, flow of the unburnt gas induced by the thermal expansion of the burnt gas is confined by the vessel wall. The velocities

obtained by this flow increase significantly over those obtained under the conditions of free expansion encountered in an open flame.

The flow and the flame augment each other by a feedback mechanism. The flow has some turbulence associated with it (however slight) and this produces a wrinkling of the flame front.[45] The resulting increase in the surface area of the flame leads to a greater reaction per unit time. This in turn increases the flow of the gas which leads to yet greater turbulence and hence more wrinkling. Thus the progress of the wave becomes unsteady and self accelerating. This produces pressure pulses which can coalesce into shock waves and in this situation the flame continues as a detonation wave (see Section 3.2.2). However it is possible to obtain steady flames under certain conditions.

3.3.2 Open Tubes

One method for obtaining a steady flame is to use a small diameter (less than 50 mm for lean hydrocarbon-oxygen or hydrocarbon-air flames) open tube, with the flame propagating from the open end to the closed end. Propagation in the reverse direction generally leads to detonation.[45] Completely closed vessels will be discussed in Section 3.6. For the initial propagation of a flame in a open tube, with the flame propagating toward the closed end, the flow pattern created by the thermal expansion of the burned gas can be seen in Figure 3.2.

Ahead of the flame the unburnt gas forms a stationary column. Behind the flame the burnt gas expands and creates a flow toward the open end. This flow is retarded at the wall due to viscous drag, and accelerated at the centre. This acceleration produces a thrust which pushes the unburnt gas toward the closed end of the tube. This gas cannot escape there so it is forced to reverse its direction so that it flows in a curved path toward the open end. Thus the wave is driven toward the closed end at the centre and toward the open end at the walls, assuming a curved shape. Figure 3.2 is the view of the velocity field that a stationary observer would see at any instant. The burning velocity S_u of the flame remains essentially constant across its diameter, this being because S_u is the velocity of the front relative to the unburnt gas.

There is however, a local reduction in S_u near the wall of the tube. This is due to some heat loss to the walls which reduces the temperature and hence S_u. This is basically a variation of the wall quenching phenomena, whereby the wall removes sufficient heat from the flame to make combustion impossible for a certain depth adjacent to the wall. This depth is known as the quench distance.

3.3.3 Wave Velocity

If the wave propagates along the tube as a plane, the wave velocity S_w would be equal to the burning velocity S_u. Because of the wave curvature, S_w is greater than S_u. This can be proven by considering the following. If the wave is at rest, the

unburnt gas and the tube move against the wave with a velocity S_w. Thus the mass flow is given by

$$m' = \rho_u A_{tube} S_w \tag{3.3}$$

However the mass flow is also approximately equal to

$$m' = \rho_u A_{wave} S_u \tag{3.4}$$

Since A_{wave} is greater than A_{tube} due to the curvature of the wave, then continuity of mass flow gives that S_w is greater than S_u.

This method can be used to obtain burning velocities and is quite successful, although the values obtained are slightly lower than other methods, probably due to the slight reduction in S_u at the edges of the vessel.

3.3.4 Consequences of Wave Curvature

The process described in the preceding Sections steadily increases the curvature of the wave as it propagates. This argument suggests the flame should not attain a steady state, that instead the acceleration should be continuous with continually increasing turbulence. For small tubes (less than 50 mm diameter), the viscous drag exerted by the wall on the flow prevents unlimited acceleration. For larger diameter tubes, the flow does become more turbulent and the propagation of the flame becomes unsteady. This and other sources of flame generated turbulence will be discussed further in the Section 3.7.

3.4 LIMITS OF FLAMMABILITY

3.4.1 Definition

An explosive gas or mixture may be rendered non-flammable by the addition of sufficient quantities of dilutent. This dilutent may be some inert gas, or in the case of a mixture it may be either excess fuel or oxidiser. This discussion will confine itself to explosive mixtures. A limit mixture is defined as a combustible mixture such that a slight change in the concentration of fuel to oxidiser produces a non-flammable mixture in one direction and a flammable one in the other. The lean limit of flammability is the mixture that has the minimum concentration of fuel required for combustion, and the rich limit of flammability is that which has the maximum concentration of fuel allowable for combustion. Hereafter these limits will be called the lean limit and the rich limit respectively.

It was felt at one time that limits of flammability were fundamental properties of explosive systems, and should therefore be described by a well developed combustion theory. It is generally believed that the limit is caused by heat loss to the unburnt gas, but as was explained in Section 3.2.3 there exists no solution to this problem within the framework of the one dimensional adiabatic plane wave. By including heat loss in the form of radiation, Spalding[44] managed to retain the one dimensional wave, and this inclusion did produce flammability limits, with small but finite burning velocities at these limits.

However the radiation loss theory is not particularly satisfactory, as it fails to explain many aspects of the problem. Linnett and Simpson[50] show that convection plays a significant role in determining the limits. They also conclude that flammability limits observed to date are not fundamental properties of an explosive system, and that the convection determined limits are probably well inside any fundamental limits. Gerstein and Stine[51] go further and state that no fundamental limits exist.

Thus it would seem that mixtures at the convection limit are fundamentally capable of supporting combustion, but combustion waves are quenched by convection currents, the heat sink being the unburnt gas. However the mechanism by which this occurs is not yet understood. This is supported by Egerton *et al* [52,53] who stabilised flames with a burning velocity of 50 mm/s, and Dixon-Lewis and Isles,[54] who stabilised flames with burning velocities as low as 15 mm/s, compared to normal limit mixture velocities of 70-100 mm/s. This work was done using flat flame burners and a burner with an electrically heated perforated plate atop a chimney enclosing the burner for Egerton and Dixon-Lewis respectively. The contention that limit mixtures are quenched by convection currents seems likely.

3.4.2 Determination of Limits

For the reasons described above the bulk of data regarding flammability limits is experimental. Many investigators, using a variety of methods have carried out

experiments since the beginning of the century. A review is given by Andrews and Bradley.[55]

The most common method of determining the limits has probably been to observe the propagation of a flame in a suitably large tube. This is generally about 50 mm in diameter, to avoid wall quenching effects. All studies regardless of explosive mixture, have found one common result, in that the limits of flammability are wider for upward flame propagation than downward, with those for horizontal travel being approximately in between. Burning velocity is also higher for upward flame propagation than downward.

The difference in burning velocity is due to the buoyancy effects of the hot gas bubble behind the flame. For upward propagation, the bubble rises with the flame, with the heavy cool unburnt gas sitting above. This helps to keep heat in the flame front, whereas for downward propagation, the bubble can rise unconstrained by the unburnt gas. This removes heat from the flame. The difference in flame temperatures so created reduces the burning velocity.

The same phenomenon is responsible for the differences in the flammability limits, although for a different reason. When the flame is propagating upward, the downward flow velocity produced by the burnt gas expansion is to some degree offset by the rise in hot product gases due to buoyancy. For downward propagation the flow velocity (now upward) is augmented by the buoyant rise. This increases the velocity gradient across the wave, and hence increases the likelihood that the

flame will be extinguished by flame stretch (Section 3.2.4). It will be realised that limit flames are particularly susceptible to stretch quenching due to their low burning velocities (The Karlovitz Number K is inversely proportional to burning velocity).

3.5 IGNITION

3.5.1 Theoretical Aspects

An ignition source is a source of heat. This can take many forms, such as electric sparks, hot wires, matchheads and sudden compression of the explosive mixture. This discussion will be restricted to electric sparks, which are probably the most common form of ignition source at the present time.

Ignition is defined as the successful establishment of a combustion wave that propagates from the ignition source. Electric sparks, created by either capacitive or inductive circuits are very hot, fast acting energy sources. Small sparks can be passed through an explosive medium without producing ignition. As the energy of the spark is increased, a point is reached at which a successful ignition is achieved. This point is known as the minimum ignition energy of the explosive mixture.

This minimum ignition energy is a function of the explosive mixture (ie. the fuel and oxidiser, and their relative concentrations), and the configuration of the spark

gap. Several models which describe ignition in thermal terms have been developed.[56,57,58,59,60] These rely heavily on the original concepts of Lewis and Von Elbe[45] which will now be described.

The spark functions as an ignition source by instantly creating a small volume of very hot gas around the electrodes. The temperature in this volume then begins to decrease due to heat flow to the unburnt gas and the spark electrodes. In this adjacent layer the temperature will eventually rise to a level high enough to initiate the chemical reaction.[61] The combustion then begins to propagate in the normal fashion, but this propagation may die out if the ignition energy was insufficient.

The criterion for continued propagation is that the by the time the gas temperature at the point of ignition has dropped to the normal flame temperature, the temperature gradient between the outermost unburnt layer and the point of ignition should be approximately the same as that of an adiabatic plane wave propagating under the same conditions. If the size of the inflamed bubble is too small, that is the gradient is too steep, the rate of heat loss to the unburnt gas exceeds that gained from chemical reaction and the temperature in the bubble will continue to fall until the reaction ceases. Therefore a minimum ignition energy is required to establish a minimum flame diameter.

The fact that the unburnt gas serves as the quenching agent if the ignition energy is insufficient associates this phenomena with flame stretch (Section 3.2.4). Although no flow field is associated with the minimum flame (assumed to be

spherical), the area increase of such a minimum flame due to thermal expansion could lead to quenching due to flame stretch. It is postulated by Lewis and Von Elbe[45] that the Karlovitz Number K may be applied to this situation.

$$K = 4\frac{\eta_o}{d}\frac{\rho_u}{\rho_b} \tag{3.5}$$

where η_o is still given by Equation (3.2), and d is the minimum flame diameter. The formulation given here is slightly different to that given in Equation (3.1) due to the absence of a flow field. K is again in the order of unity, and it can be seen that a smaller value of d would increase the likelihood of the minimum flame being extinguished by stretch. The value of d is very closely associated with the values of ignition quench distance, which is covered in the next Section.

More recent work[62,63] using activation energy asymptotics has confirmed explicitly that a flame, aided by a heat source, must reach a minimum size before it can continue unaided, although they still cannot account for the effect of the spark configuration. Most practical information rests on the large body of experimental evidence.

3.5.2 Parameters Affecting Ignition

Extensive studies of the factors affecting the ignition energy of a combustible mixture have been carried out by Guest *et al*,[64,65] Calcote *et al*,[66] and Rose and

Priede.[67] Curves of required ignition energy versus electrode spacing are given in Figure 3.3. These curves are for stoichiometric natural gas (83% CH_4 + 17% C_2H_6) and air, but the trends described are the same for all explosive mixtures.

For very large electrode spacings (approximately 5 mm), the required ignition energy is high due to the distance that the spark must bridge. As the spacing is reduced the energy required also falls until it reaches a plateau. As the spacing is reduced further the energy remains constant until a critical spacing known as the ignition quench distance is reached. What occurs now depends on whether the electrodes are flanged or unflanged. If they are flanged, ignition at this point becomes impossible. This is because the flanges act as heat sinks and remove sufficient heat from the minimum flame kernel such that ignition cannot take place. If the electrodes are unflanged, a reduction in electrode spacing below the quench distance can be compensated for by increasing the supply of energy. It is of note that the point at which the curve begins to rise is the same as the quench distance. It might be thought that the quench distance would be independent of the spark energy used, but for very high energy sparks (greater than approximately 20 J), the quench distance actually increases. This is due to the very high levels of turbulence generated by such large sparks. This turbulence increases heat transfer to the flanges, hence larger electrode spacings are needed to compensate.

The electrode material is significant in determining the minimum ignition energy. The energy required decreases in the order of platinum, aluminium, silver and cadmium.[67] This is because some of the spark energy is spent bringing the

temperature of the electrodes up to boiling point. Theoretical estimation of these losses predicts this order.[68,69]

For a given spark configuration, the minimum ignition energy depends on the strength of the combustible mixture, its pressure and temperature. Increased pressure reduces the minimum ignition energy, this being because the increased pressure leads to a higher gas density and hence to a higher reaction rate (increased probability of molecular collisions). Required ignition energy is reduced as the mixture strength approaches stoichiometric, although it must be pointed out that the minimum is usually displaced from stoichiometric by some degree (due to diffusional stratification, which is described in Section 3.7.2). The effects of pressure and mixture strength can be seen for methane-oxygen mixtures in Figure 3.4. Other hydrocarbon fuels show similar trends. Initial mixture temperature is important in that energy needed to establish the required temperature gradient falls as the initial temperature increases.[70]

3.6 COMBUSTION IN CLOSED VESSELS

3.6.1 Differences Compared to Open Vessels

In the discussions preceding this Section it has always been assumed that the burned gas can expand freely, that is the combustion takes place at constant pressure. With a constant volume vessel (hereafter called a bomb), the propagation of the

combustion wave is accompanied by a rise in pressure, and a mass flow which is initially directed away from the ignition, and later toward it (the induced flow will be considered in the following Section).

The slowness of the combustion wave propagation insures that the pressure throughout the bomb, although increasing with time, is virtually constant at any given instant. The reaction rate and hence the burning velocity of the flame varies continuously in response to this changing pressure, due to the rise in temperature of the unburnt mixture caused by its compression. Fast burning mixtures are susceptible to the formation of pressure pulses near the end of flame travel due to the high velocity fields created by the unburnt gas motion (see next Section).

Certain slow burning mixtures (eg. lean methane-oxygen, methane-air, ethene-air) exhibit the tendency to produce relatively low frequency pressure pulses which are sometimes audible.[71,72] In this case the pressure fluctuations are due to the spontaneous diffusion of the mixture as it enters the combustion wave. The diffusion mechanism that causes the pressure fluctuations is described more fully in Section 3.7.2.

A characteristic feature of constant volume combustion is the creation of a temperature gradient in the burned mixture due to compression and expansion effects. The temperature is a maximum at the point of ignition, and decreases to the wave surface, the difference being as much as several hundred degrees Celsius. The cause of this phenomena can be visualised as follows (see also Figure 3.5).

When the gas is ignited, an initial mass element of volume V_i burns and expands to V_e at almost constant pressure, this pressure being the initial pressure P_i. When the combustion in the bomb is completed, the pressure has risen to P_e, and the initial mass burnt has been compressed back to its original volume. Because the expansion of this initial mass element took place at P_i and the compression took place over a range from P_i to P_e, it is clear that the compression work is greater than the expansion work, hence the temperature of this initial element is higher that it otherwise would have been. The reverse is true of a mass element at the end of the bomb, that is it is first compressed by pressures ranging from P_i to P_e and then expands to its original volume at P_e. Hence its temperature is lower. This temperature gradient is responsible for the reillumination of the burnt gas that is always observed in photographic studies of constant volume flames.[73] Constant pressure flames do not exhibit this effect.

Theoretical treatments have been established that enable the calculation of flame speeds and burning velocities from the pressure-time record for an explosion in a sphere with central ignition. The application of these methods to other bomb shapes (cylinders, cubes) is difficult and unrewarding, in view of the number of simplifying assumptions that must be made regarding the shape of the combustion wave.

3.6.2 Flame Propagation

For totally closed vessels, the response in the early part of the flame travel is virtually identical to an open tube such as that described in Section 3.3.2. During this stage, much of the unburnt gas is pushed ahead of the front, leading to a greater mass concentration in the unburnt portion of the bomb mixture. Upon further burning, this mass flow reverses itself (the gas having no other place to go). The drag is highest at the wall, giving the greatest flow velocity at the centre. This leads to an increasingly cone shaped flame front and the generation of high levels of turbulence, especially at the end of the flame travel, where gas movements are greatest. A diagram showing approximately how such a flame would appear is given in Figure 3.6.

3.7 COMBUSTION GENERATED TURBULENCE

3.7.1 Flame Generated Turbulence (FGT)

The idea that a flame generated turbulence as it propagated was first put forward in the 1930s, by David,[74] and David and Leah.[75,76] This idea was taken further by Karlovitz *et al*,[77] and Scurlock and Grover.[78] These investigations produced theories on turbulent burning velocity, and both included the assumption that the kinetic energy of the burnt gases behind the flame could be converted into turbulence which distorts the flame front.

The turbulence generated can be basically divided into two groups. The groups are differentiated by whether or not the generation of turbulence is independent of the mode of propagation (ie. whether the flame is in a tube, sphere, burner, etc).

3.7.2 FGT Independent of Propagation Mode

If a flame begins to propagate in a quiescent mixture it can remain laminar under certain conditions. The reason why it may begin to degenerate into a turbulent flame is explained by Lewis and Von Elbe.[45]

The effect (known as diffusional stratification) occurs in very lean or very rich mixtures where the diffusivity of the deficient component substantially exceeds that of the excess component (for lean mixtures the deficient component is the fuel, and for rich mixtures it is the oxidiser). In such a case the mixture spontaneously stratifies upon entering the combustion wave, creating local variations in the fuel/oxidiser ratio (that is, the mixture is now non-homogenous). Because of these regions of varying concentration the local burning velocity varies over the surface of the wave (burning velocity is dependent on mixture concentration). Hence the wave wrinkles and acquires a cellular structure corresponding to the local accelerations and retardations. Photographs of this phenomenon have been obtained by Manton[79] and Markstein.[80]

Once the wrinkled front is established it is augmented by a process that can be visualised as follows. Each element of the combustion wave introduces into the gas a velocity component normal to the wave front (parallel to the direction of propagation) due to thermal expansion. With a wrinkled front, the orientation of each small combustion element varies randomly, and this introduces random velocity components (ie. turbulence) into the wave.

3.7.3 FGT Dependent on Propagation Mode

When a flame is confined in a tube, flow of the unburnt gas induced by the thermal expansion of the burnt gas is confined by the tube wall. This leads to the self acceleration of the flame as described in Section 3.3.1. The turbulence produced by this process at first augments that created by the diffusional stratification process described above, but because its generation is self accelerating, it quickly becomes the dominant source. For a totally closed vessel a similar phenomenon is encountered, but the generation of turbulence, especially near the end of the flame travel, is more severe due to the reversal of the flow in the tube centre (Section 3.6.2).

For a horizontal tube or bomb the effects of buoyancy can also create an additional level of turbulence. As was described in Section 3.4.2, it is well known that the buoyancy of the hot burnt gas is primarily responsible for the difference in the lean limit of flammability between upward and downward flame propagation. In a

horizontal tube, this effect tends to lead to the flame shape shown in Figure 3.7. This is due to the hot product rise removing heat from the bottom of the flame and adding it to the top. This causes a difference in the flame temperature and hence the rate of reaction between the top and bottom of the bomb. This shape has been photographed by Coward and Hartwell[81,82] and Smith *et al.*[83]

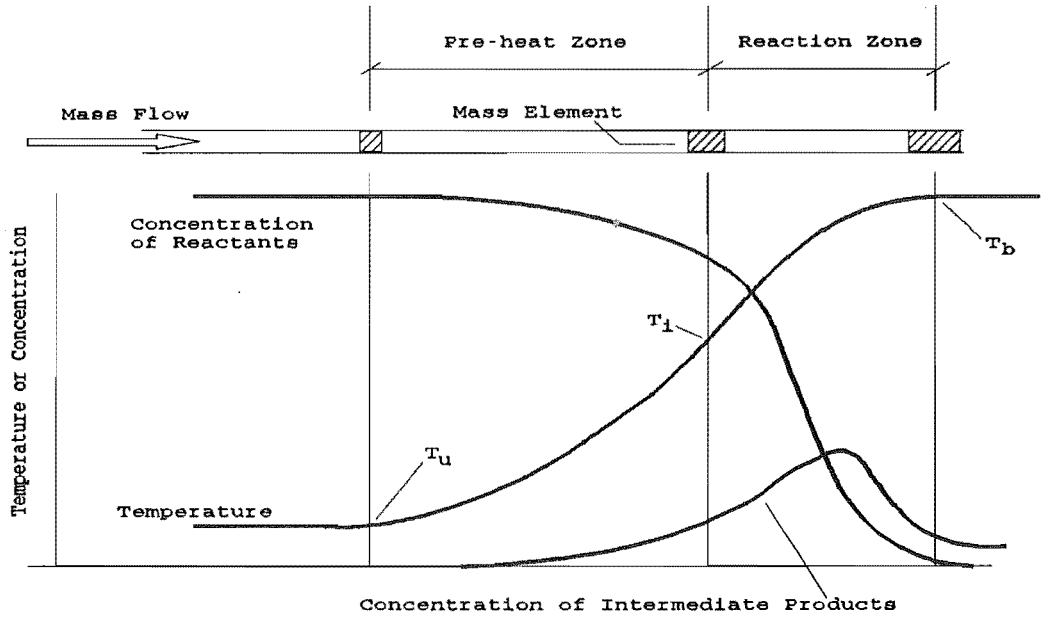

Figure 3.1 Adiabatic Plane Wave Profile

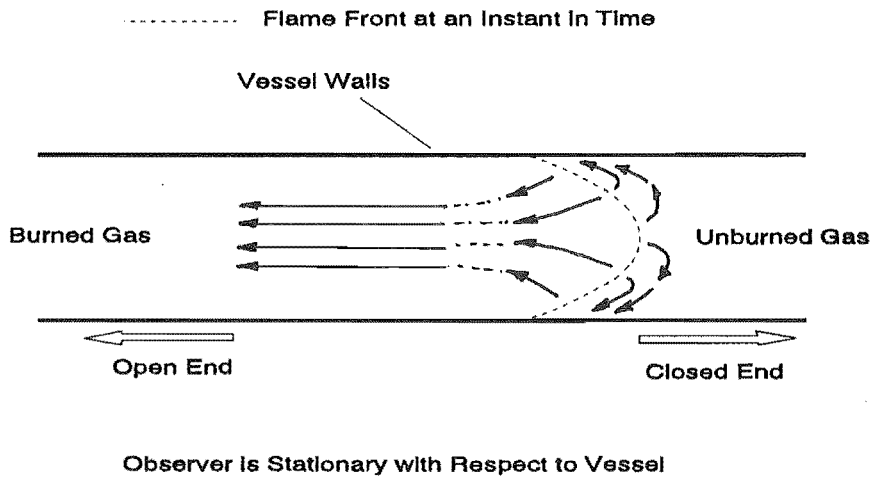

Figure 3.2 Induced Flow Due to Thermal Expansion (From Lewis and Von Elbe, p.292)

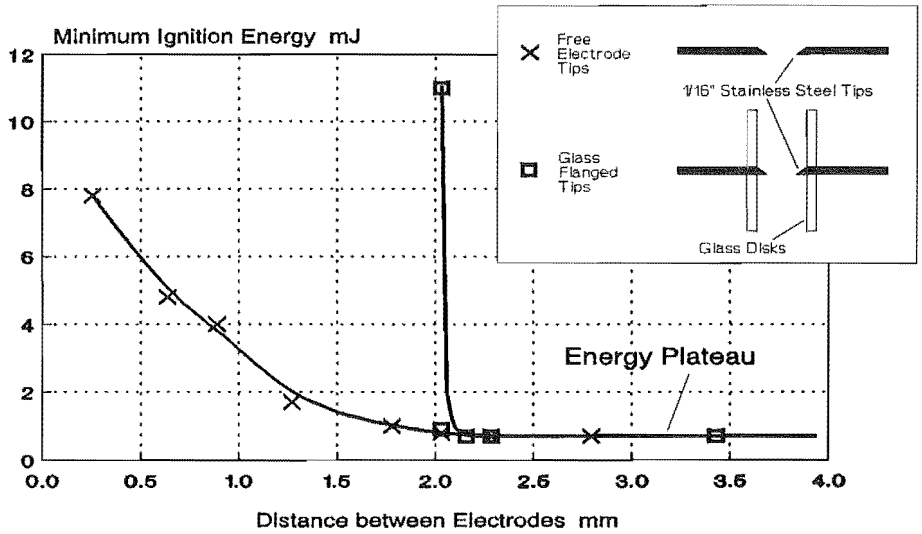

Figure 3.3 Ignition Energy v Electrode Spacing for Stoichiometric Natural Gas-Air Mixtures (From Lewis and Von Elbe p.326)

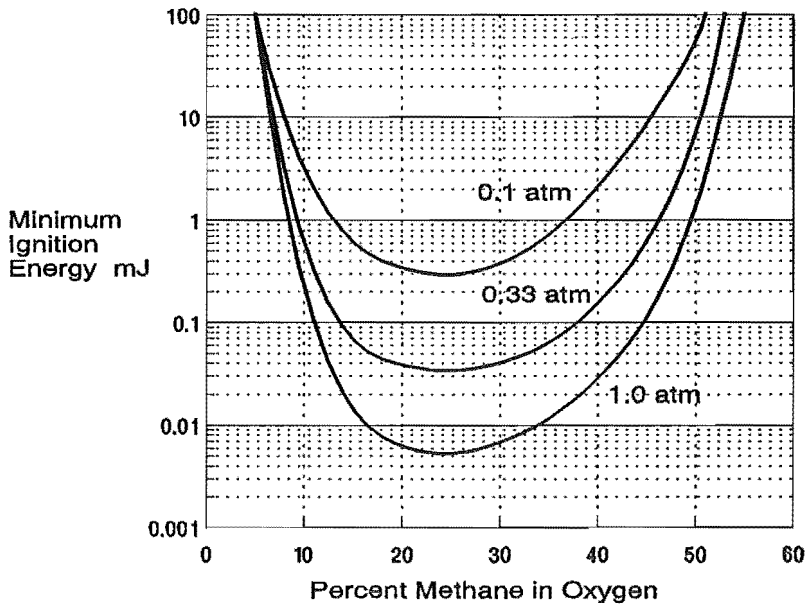

Figure 3.4 Methane-Oxygen Minimum Ignition Energy Curves (From Lewis and Von Elbe p.330)

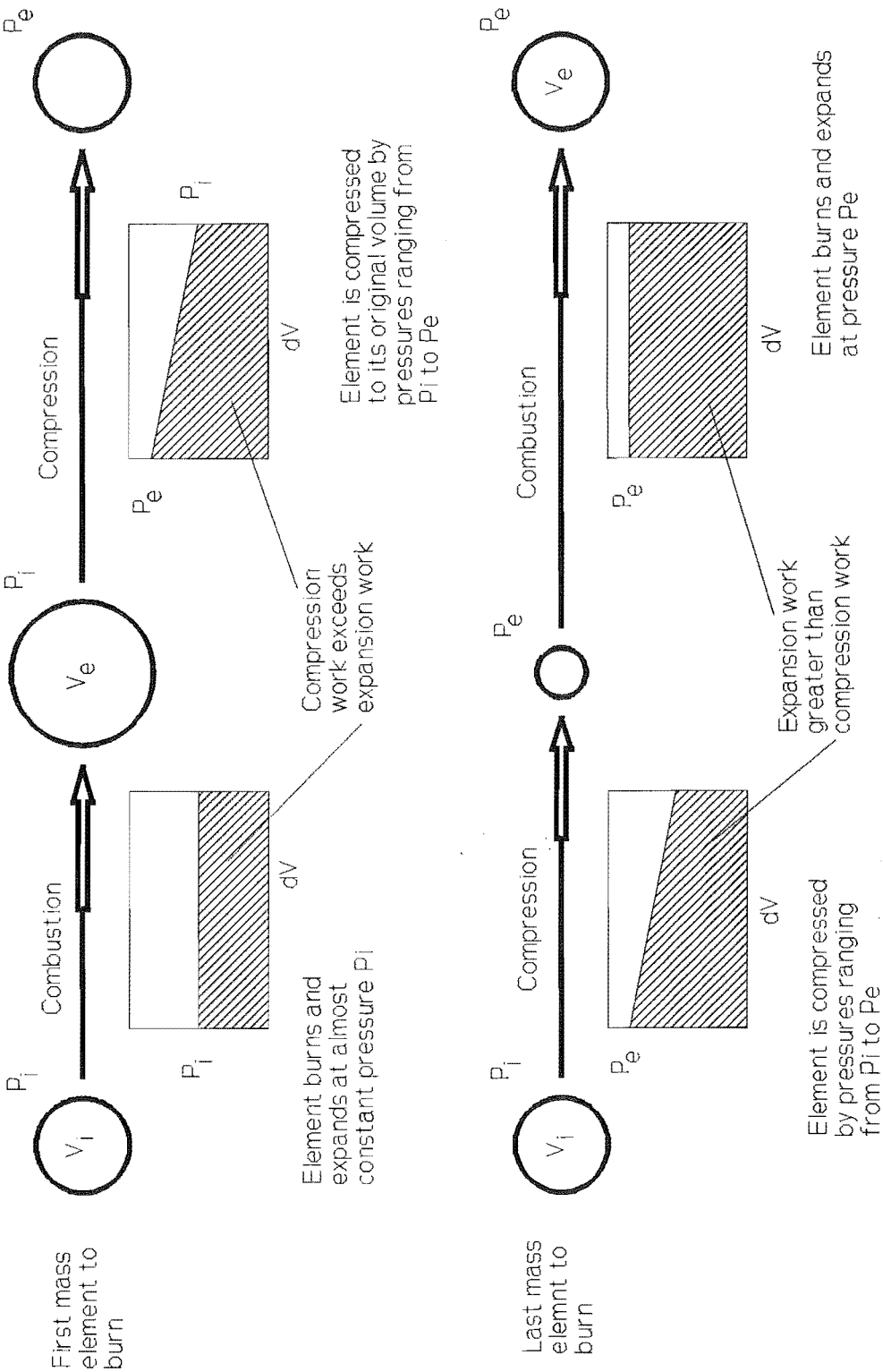

Figure 3.5 Effects Leading to the Formation of a Temperature Gradient in Closed Vessel Explosions

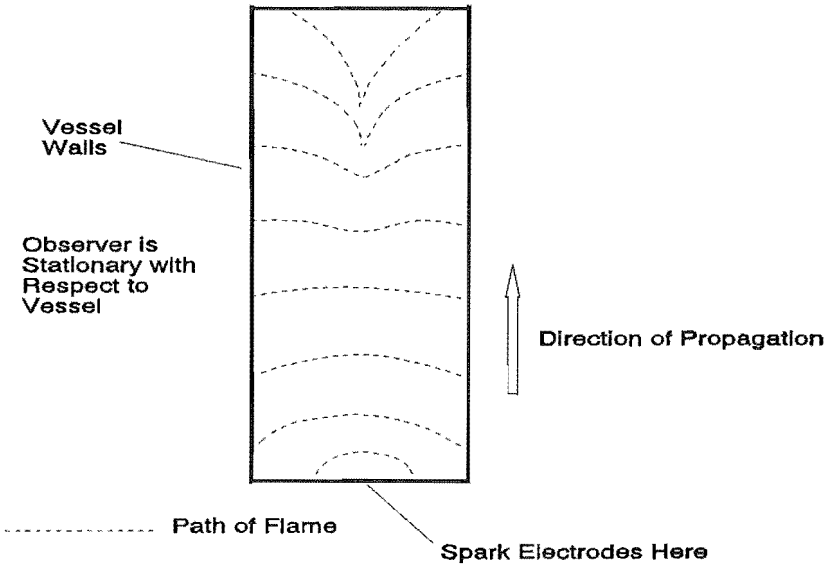

Figure 3.6 Cone Shaped Flame

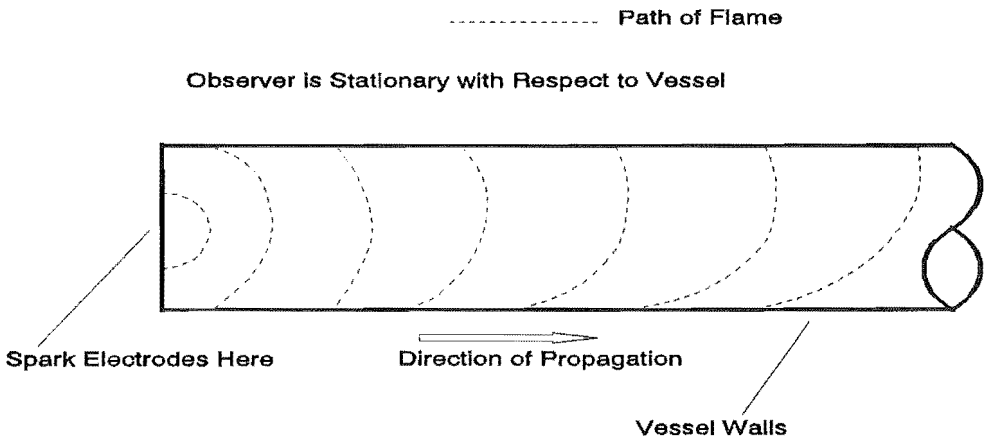

Figure 3.7 Hook Shaped Flame

CHAPTER 4

DESCRIPTION OF APPARATUS

4.1 INTRODUCTION

To conduct the investigation a constant volume combustion bomb was designed and built. A constant volume bomb was chosen primarily because it simulates, in a simplified manner, the combustion process taking place in an engine. In addition it simplified the construction of the rig (eg. constant pressure devices must make provision for the exhaust of the hot burnt gas to the atmosphere), reduced the likelihood of charge contamination through the entrainment of unwanted air and gave additional parameters that could be measured to ascertain the completeness of combustion, these being the pressure rise and the composition of the burnt gas products. It also introduced complications in that flame speed along the bomb is not constant as it varies with pressure.

A schematic diagram of the final layout of the rig is shown in Figure 4.1, along with photographs of the whole rig in place (Plate 4.1 and Plate 4.2). A brief summary of the operation of the rig can be given as follows:

(a) The bomb is of 100 mm diameter, and, by the addition or removal of 250 mm long sections can be varied in length from 250 mm to 1000

mm (Plate 4.3 to Plate 4.5). The bomb is mounted horizontally in a frame which allows for the simple adjustment of its position.

(b) Mixtures of methane-oxygen are created in the mixing cylinder by the partial pressure method. When full the cylinder contains enough mixture for at least five separate tests on that mixture.

(c) A stratified charge can be created in the bomb by injecting a methane-oxygen mixture (hereafter referred to as the injected puff) through a modified spark plug. This mixture is created in the injection cylinder, also by the partial pressures method.

(d) The duration of the injected puff and the timing of the ignition spark relative to it can be adjusted with a specially built time duration controller.

(e) An oscilloscope records the pressure rise during combustion and the flame position along the length of the bomb. This data may be downloaded to a computer for further analysis. A carbon dioxide sample is taken after combustion is completed.

It was felt that it was important that the rig be of a modular design so that it could be used to test a variety of fuels under whatever conditions the experimenter wished, without the need to resort to major modifications. Thus the final design

reflects these intentions. The length of the bomb can be changed with ease, as can its valving arrangement and ignition system. It could also be mounted vertically (for the study of upward and downward propagating flames) with little effort. One or more regulators could be added to enable the creation of mixtures with more than two constituents (eg Hythane + Air, which is Hydrogen + Methane + Air, or any fuel + oxidiser + dilutent).

Having looked at a brief description of the rig and some of the rationale behind its creation, the remainder of this Chapter deals with the detailed design and development.

4.2 THE BOMB VESSELS

4.2.1 Sizing and Design

The initial problem was in deciding what diameter the bomb cylinder should be. It was assumed that the mixtures of methane-oxygen to be used in the bomb would be very lean (λ ranging from about 5 to 10), and thus if the bomb was too small then extinguishing of the flame due to wall quenching was likely (the wall quenching limits increase asymptotically as the mixture strength approaches the lean limit of flammability). A brief review of various methods for measuring the lean limit of flammability along with the investigators who used them is given in Table 4.1. Some of these figures are for methane-air mixtures but the use of these is still valid

as lean mixtures of methane-air and methane-oxygen behave in an almost identical fashion with regards to their quenching distance at the lean limit of flammability.[45]

Table 4.1 Methods for Measuring The Lean Flammability Limit of Methane-Oxidiser Mixtures

Author(s)	Method
Burrell & Oberfell[84] (1915)	30 cm Box
Jones et al[85] (1933)	10.2 cm Tube
Coward & Hartwell[86] (1926)	5 cm Tube
Egerton & Powelling[87] (1948)	5.3 cm Tube
White[88] (1924)	2.5 cm Tube
Hsieh & Townend[89] (1932)	4.5 cm Bomb
Bone et al[90] (1928)	5 cm Bomb
Roglingson et al[91](1960)	5 cm Bomb

It can be seen that there is a wide variation in the size of the combustion device, but it is noticeable that few experimenters use a bomb or tube smaller than 25 mm in diameter. It was therefore decided to build a bomb of approximately 100 mm diameter, which would be large enough to effectively eliminate the wall-quenching problem, but be small enough that large quantities of methane and oxygen would not be required. It might be thought that from Table 4.1 a 50 mm bomb would be the obvious choice but this was rejected mainly because it seemed that the intended system for measuring the flame position (see Section 4.2.2) could obstruct the flame path to an unacceptable degree.

It was decided that the maximum bomb length should be 1 metre in the anticipation that this would be long enough to show whether the flame continued to burn after it had progressed into the ultra-lean region, yet small enough to allow a reasonable number of tests from the mixture in the mixing cylinder (the size of this had already been determined - see Section 4.3.1). Horizontal mounting was chosen because it simplified the installation problems associated with vertically mounting a bomb of the maximum length proposed (1000 mm).

From the work (yet to be described) in Section 5.2, the maximum pressure expected in the bomb after combustion should be no more than 13.5 bar absolute (from a initial reactant pressure of 1.5 bar absolute). This is for a mixture of 10% methane-oxygen (λ = 4.5) as it had already been decided that this would be richest mixture that would be tested. Assuming then a maximum gauge pressure in the bomb of 16 bar, the application of classical thin walled pressure vessel theory gives the maximum stress in the bomb wall as

$$\sigma = \frac{\Delta Pr}{t} = \frac{16.10^5 * 50.10^{-3}}{t} \qquad (4.1)$$

Some 100 mm diameter steel linepipe was available and this had a thickness t = 6 mm. Substituting this value gives the maximum stress as σ = 13.3 MPa, which is well within acceptable limits if we take the yield strength of steel as 220 MPa[92]. Mild steel was used in preference to stainless steel because of cost, availability and ease of working. It was expected however that this would lead to the formation of large amounts of rust in the bomb due to the presence of water and oxygen at high

temperature during and after the explosion. This undesirable effect was overcome by painting the inside of the bomb with antirust paint. This worked very well and the presence a flame did not appear to damage it.

The flanges of each section of the bomb were designed to meet BS 4504:1969. Each flange is 18 mm thick and 220 mm in diameter. Each flanged connection is secured by 8 M16 bolts. The endcaps of the bomb are identical in dimensions to the flanges. One endcap is designed to hold a normal automotive spark plug (thread M14 x 1.25) and the other to hold the main inlet valve of the bomb. Sealing between all flanged joints is with either Loctite Master Gasket Cement or Silicone RTV.

4.2.2 Ionisation Probes

A system of ionisation probes was designed and built to show how far the flame travelled along the bomb. The principle behind the probe is relatively simple but the probes used were of a slightly unusual design.

Gaydon and Wolfhard[93] give a review of the theory and design of the traditional ionisation probe (also known as a Langmuir probe). It consists of a bare wire inserted into the flame, with a voltage potential applied between the wire and a convenient earth, typically the vessel or burner wall. The wire must be insulated from earth and, if this is the case, then no current will flow. If the wire is in the

presence of a flame however, there exists numbers of charged particles, the generation of which is due to the equilibrium formation of ions at the flame temperature and the production of ions and electrons by various flame reactions[93]. This allows a path for current to flow from the wire to the earth, and this can be detected as the voltage across a resistor.

The probes used in this work were based on the experiments carried out by Campbell.[94] Campbell's design consisted of a 1 mm stainless steel wire as the probe and an engine cylinder head as the earth. A gap of 0.25 mm separated the probe from the earth. Campbell discovered that the probe gave an identical response whether or not there was a potential applied across it. Exactly why the probes will give a signal when there is no potential could not be explained by Campbell but it is possible that the surface of the probe, being immersed in a relatively high concentration of charged species is simply at a higher potential than the earth, which although it is in contact with more charged particles, has a much greater area over which to spread the charge. Further research would be desirable to evaluate this hypothesis.

It was therefore decided to build essentially the same probes for the present research. However when it came to the preliminary testing these probes proved to be disappointing. The main problem was that it was almost impossible to keep the probe insulated from the earth, as water from the combustion process would condense in the insulation gap. After much experimentation, a satisfactory design was achieved and a drawing of this is given in Figure 4.2.

The most suitable material was found to be brass, and the probe is simply a 4 mm brass rod inserted through a PTFE seal (which also acts as an insulator) and clamped in place by a bolt. This form of probe was used throughout the testing programme (see Section 6.2) and generally functioned satisfactorily. The three main disadvantages of the system are:

(a) Although the probes function well in a hot flame, as the mixture strength approaches the lean limit of flammability (that is $\lambda > 7.5$) the signal strength is much reduced, to the point that it can become difficult to identify.

(b) Increasing the number of probes increases the background noise of the signal. For the present rig the practical limit is five probes. With more than five the signal is so noisy that separating the probe signal peaks becomes increasingly difficult.

(c) Probes cannot be closer to each other than 50 mm because it becomes to difficult to tell which probe signal peak is which. This problem would be eased by a slower burning mixture or made worse by a faster burning one.

Two other systems were tried in an effort to overcome the disadvantages described above.

The first consisted of replacing the ionisation probes with small thermocouples. This was not successful as it proved impossible to get clear signal peaks as the flame passed over the thermocouple. The response was the same whether there was one thermocouple or several - the only reaction was a gradual rise in signal output that reached a maximum at the point of maximum pressure. In effect the thermocouples were measuring the average temperature in the bomb at that instant. Several types of thermocouple wire were tried but there was little difference between them.

The second idea came from Karim et al.[95] This consisted of a series of fibre optic cables mounted along the bomb in place of the ionisation probes. These fed into a single photo-sensor of the type recommended by Spencer.[96] Again, the problem was in getting a response that showed where the flame was at a given point during the explosion. The behaviour was almost identical to that of the thermocouples described previously. Much effort went into attempts to eliminate the reception of stray light rays by each individual probe but these proved fruitless.

It was decided after these two attempts at replacing the ionisation probes that the testing would continue with the modified ionisation probe system. However both the thermocouple system and the photo-sensor system have been described as they indirectly led to a possible explanation of an unusual combustion effect that will be discussed further in Section 7.6.1.

4.2.3 Data Sampling and Retrieval

The constant volume bomb is fitted with a number of instruments to record a variety of data from the explosions. An AVL 8QP 500c piezoelectric pressure transducer (0 - 150 bar) and Cussons amplifier (hereafter called the piezo channel) are fitted to record the pressure rise during combustion. The transducer is calibrated (approximately once every week) using a Barnet Instruments Industrial Deadweight Tester, modified for the job by Trolove.[97] This device applies a known pressure (altered by changing the weights) to the transducer, and then suddenly releasing it. The response of the transducer can be measured using an oscilloscope. This method is necessary because a pressure transducer using a piezoelectric crystal responds only to dynamic pressure, that is its output is the same no matter what the surrounding steady state pressure is. The output from the transducer and the output from the ionisation probes described in the previous Section are connected to a Hitachi VC-6041 Digital Storage Oscilloscope. This oscilloscope can download the data to a personal computer when necessary.

A K-Type thermocouple is fitted to the bomb, to give the initial temperature of the mixture. It does not measure the temperature of the bomb during an explosion but it is useful for determining when ignition has taken place as the rapid rise in temperature is easy to identify.

The final measurement taken is the amount of carbon dioxide present in the bomb after combustion. This is achieved by drawing a small sample of combustion gas

through a Kitagawa Gas Detection Tube with a specially supplied pump. By changing the type of tube any gas sample may be taken but it was considered that carbon dioxide (tube number 126 SH, 1% to 20%) alone would be sufficient for this work as its primary purpose was as a measure of combustion completeness. The pump and CO_2 tube, in the process of taking a sample, can be seen in Plate 4.6.

4.3 THE MIXING VESSELS

4.3.1 Sizing and Design

There are two separate mixing vessels mounted on the lower shelf of the rig (see Plate 4.7 and also Plate 4.1 and Plate 4.2). The larger (hereafter called the Test Mixture Vessel) measures approximately 11 litres in volume and is used for creating the test mixture. The smaller (hereafter called the Injection Mixture Vessel) has a volume of 1.837 litres and is for creating the mixture that is injected into the bomb to create the stratified charge. Both these vessels had been used by Zavier[21] as surge chambers and required some modification for their new use.

Each vessel has a maximum fill pressure of 20 bar. Both were hydraulically tested to 35 bar to ensure that they were sound. At 20 bar the test mixture vessel has enough mixture for at least five tests in the largest (ie. 1 m long) bomb although the exact number of tests depends on how much mixture is used to flush the bomb clear of previous combustion products. The injection mixture vessel contains enough

mixture for a great many tests but the exact number depends on the duration of each injected puff.

4.3.2 Gas Supply

Methane and oxygen are supplied to the rig from conventional high pressure bottles. The rig is designed so that different combinations of fuel and oxidiser can easily be used. The methane is supplied by the Christchurch City Council, and it is manufactured from biogas produced at the Council's sewerage treatment plant at Bromley. The gas supplied is 98% by volume pure methane, the remainder being mostly carbon dioxide. The oxygen is supplied by New Zealand Industrial Gases, this being 99.5% by volume pure oxygen, the balance being mostly nitrogen and carbon dioxide.

4.3.3 Pressure and Temperature Recording

Mounted above the mixing vessels is a SenSym SSX 300 G pressure transducer. This gives (for a 12 V input) a linear response in output voltage from 0 mV at 0 bar to 60 mV at 20 bar. It will also measure a vacuum, its response simply changing polarity. It is connected to a switching valve so that it can be switched to either the test mixture vessel or the injection mixture vessel. Temperature measurement on both vessels is by a K-Type thermocouple mounted in a Swagelock fitting to ensure

leak tightness. Both pressure and temperature are read by a personal computer and then displayed on screen for the operator. By entering the value of the atmospheric pressure into the computer the pressure transducer can show the output as an absolute pressure. The atmospheric pressure is measured using a Darton mercury column vernier barometer.

The gas mixtures are created by the usual partial pressure method. This procedure is described fully in Section 6.3.

4.3.4 Safety Provisions

Since the mixing vessels are of a relatively light construction (wall thickness approximately 6 mm) it proved necessary to incorporate some method of relieving the pressure build-up should the contents of the vessels accidentally ignite.

The chosen option is an aluminium burst disk. The arrangement for this is shown in Figure 4.3. An attempt was made to calculate the required thickness and diameter for the disk, but this proved to be unreliable (that is a disk of the calculated diameter and thickness would not burst at the required pressure). Experiments were conducted with various materials by applying the pressure in the vessels hydraulically until a suitable design was achieved. The disk is made of 3 sheets of 100 micron aluminium bonded together with Loctite 401 super strength adhesive. This gives a reliable burst pressure range of between 28 and 35 bar.

In preliminary testing of the rig an accidental ignition of the contents of the test mixture vessel did indeed take place. The pressure relief system worked well and damage was limited, as shown in Plate 4.8. The tubes on the end of the vents were intended to catch any debris emerging from the vessel, but proved more of a liability than an asset as the force of the accidental ignition proved to be powerful enough to tear them from the mountings. Following the accident the remaining one was removed.

The mixture that exploded was 10% methane in oxygen (λ = 4.5). This has a relatively low ignition energy of 0.03 mJ[45] and the accident occurred when the operator touched and turned the test mixture vessel outlet valve. The ignition source was thought to be either a static discharge from the operator across the valve or a build up of static on the ball of the valve as it rotated in its teflon seat.

To eliminate the creation of static on the valve ball, an earth wire has now been attached to the valve stem through the valve handle, and all valve connections are each connected to a common earth. The operator is also provided with an anti-static strap to be worn at all times. Non-return valves are fitted between the vessels and the outlet valves so that if ignition takes place in the outlet valve, the flame will not pass into the vessel itself. Following these modifications (shown in Plate 4.9) no further problems have been encountered.

4.4 INJECTION SYSTEM

4.4.1 Modification of Injector

A stratified charge can be created in the bomb by injecting mixture from the injection mixture vessel through a specially modified spark plug, using a similar system to that developed by Zavier.[21]

The injector chosen for the testing was a Bosch gasoline injector, part number 0 280 150 201, the specifications for which (as given by Bosch) are shown in Table 4.2.

Table 4.2 Specifications of Bosch Gasoline Injector

Operating Voltage	12 V DC with 6 Ω Resistor in series
Valve Lift	0.1 mm
Gasoline Flowrate at 300 kPa	236 cm^3/min with valve permanently open
Maximum Opening Time	1.8 ms
Maximum Closing Time	0.9 ms

The injector response times were studied by Glasson,[98] who discovered that the response was very similar irrespective of whether it was operating with gasoline or gas. The major difference was that the needle suffered considerably more bounce when operating with gas, probably due to the absence of the damping provided by a liquid fuel.

For the combustion rig the injector is supplied with 3 V DC, this being equivalent to the steady state voltage when it is operated at 12 V DC with a 6 Ω resistor in series. This lower voltage obviously affects the injector opening time, but this is not considered critical for the application described here. The timing of the voltage pulse is regulated by a specially built timing control box. This is fully explained in Section 4.5.2. Using this control box it was found that the minimum voltage pulse duration that could be sent to the injector to obtain a response was 6 ms.

The rear of the injector is attached to a gas line leading to the injection mixture regulator, by which means the injection pressure can be varied (up to 15 bar). The forward fitting provides a seal for the front of the injector and provides an attachment for the non-return valve described in the Section 4.4.2. A drawing of the injector is shown in Figure 4.4 and a photograph of it is shown in Plate 4.10.

4.4.2 Injector Non-Return Valve

It was discovered by Zavier[21] that it is vital to have an efficient non-return valve between the tube attached to the spark plug (Section 4.4.3) and the injector needle. Without this the combustion products are transferred to the injector face, whereupon they cause the injector to leak. Zavier used a valve with a ball bearing in metal to metal contact with a seat. For this research it was felt that a more efficient seal would be desirable, and as the temperature of the valve could be kept low (due to the explosions not occurring continuously) a valve using a PTFE seat

was designed and built. This can be seen in Figure 4.4 and Plate 4.10. The valve was used throughout the testing program and functioned satisfactorily. The only problem is that the needle tends to stick in the closed position if left for more than a week, but this proved to be of no great disadvantage.

A major reason for building a non-return valve rather than using a proprietary item (eg. Nupro) was that it is convenient to mount the injector assembly from it (see Plate 4.10). To this end the outer body of the non-return valve is threaded and by clamping a mounting plate between two nuts the position of the injector assembly may be varied to take account of the position of the tube in the spark plug.

4.4.3 Spark Plug Modifications

A commercially available NGK B6HS spark plug was modified to incorporate a tube through which the injection mixture could be introduced to the bomb. This particular spark plug was chosen for modification because it is of the "hot" type, that is, it has only a small area of insulator in contact with the plug body though which heat can escape. This allowed room for a 2 mm hole to be drilled into the plug body without damaging or coming into contact with the plug insulator. A small length of ⅛" OD hypodermic steel tube was then silver-soldered into this hole. Connection to the non-return valve of the injector assembly is provided by a standard ⅛" Swagelock male connector. For the entire testing programme the plug-bomb connection was sealed with an O-ring, as the standard deformable plug

washer proved to have insufficient sealing capability. The modified spark plug is shown in Plate 4.11. The spark plug gap is set to 0.6 mm, as recommended by the manufacturers for automotive use.

4.5 IGNITION SYSTEM

4.5.1 Description

The ignition spark is provided by two 12 V DC automotive coils (Lucas Models SP 12 and HA 12) connected in parallel. The voltage is supplied by two Promarine Supercrank 350 12 V DC marine batteries. These may be connected in parallel or in series to give a coil voltage of 12 V DC or 24 V DC respectively. Radio suppression plug leads are used to minimise interference of a voltage spike on the oscilloscope recordings. The components described here can be seen in Plate 4.10.

4.5.2 Timing Control Box

To provide for the correct timing of the injection duration and ignition, a timing control box was built in the Department of Electrical and Electronic Engineering. The wiring diagram is shown in Figure 4.5 and the unit itself can be seen in Plate 4.10.

The timing control box has two channels, each operated by a 6 V DC relay running at 12 V DC, to get the required speed of response. Each operates independently of the other. When the "fire" button is pushed a trigger pulse of 12 V is sent to the oscilloscope. The relays activate 4 ms later. Connections are provided so that the relay can either make or break a circuit for the set duration.

The duration is set by adjusting the resistance of the two potentiometers provided for each channel, one being for coarse adjustment in increments of 10 ms and the other continuously variable for fine adjustment. The maximum duration possible is 99 ms for each channel with a tolerance of ± 1 ms.

The unit generally worked well, the only problem being the occasional destruction of the timing microchips. When this occurred the duration timing of each channel had to be recalibrated with an oscilloscope, as it was found that the response varied slightly with different timing microchips.

4.6 MISCELLANEOUS

4.6.1 Vacuum System

As a rotary vacuum pump was not available when the rig was built a water venturi pump was fitted. This device, shown in Plate 4.12, works on the principle of expanding a flow of water through a nozzle. This causes the pressure of the water

to drop below atmospheric pressure and thus a vacuum can be created. A centrifugal water pump is used to increase the pressure of the water flowing though the venturi. This helps increase the rate of evacuation, and also compensates for the variation in mains water pressure, which can drop below 2 bar. The water pump provides an extra 1 bar pressure which is a big help. A pipework system connects the vacuum pump to the bomb, and the two mixing vessels. Each vessel can be evacuated independently.

The major problem with this type of vacuum pump is that it cannot create a vacuum below that of the vapour pressure of water under the prevailing conditions (approximately 0.025 bar absolute at 20°C[99]), as this would cause the water in the venturi to boil. This meant that at least some of the water formed in the bomb during combustion would not be removed. It is not clear what effect this water would have on subsequent explosions (perhaps a slight lowering of combustion temperature and pressure) but there was little noticeable effect. This is possibly because the bomb interior was cleaned regularly during testing and that the very lean mixtures used did not produce large enough quantities of water.

It has been found that the maximum possible vacuum in the mixing vessels is 0.03 bar absolute. This agrees well with the maximum vacuum possible from the venturi pump of approximately 0.025 bar absolute.

4.6.2 Pipework, Valves and Fittings

¼" piping is used throughout the rig. Stainless steel is used when the gas inside is either at a high pressure (greater than 30 bar, for example from the gas bottles to the regulators) or is a combustible mixture. Otherwise copper piping is preferred. All pipework is connected using Swagelock fittings, stainless steel for stainless pipe and brass for copper pipe. Adapters and non-return valves are from Nupro and all the ball valves used are Whitey Series 40.

Nupro stainless steel flexible hoses connect the injector, inlet valve and vacuum valve on the bomb to the rest of the rig. This allows the extension or movement of the bomb without the need to relocate the piping.

The bomb inlet valve is of a special design as shown in Figure 4.6. This design removes any small passage leading to the valve head that would be present in a conventional valve. This eliminates the possibility of trapping small quantities of methane-oxygen which then cannot be burnt. The design also features improved sealing during combustion as the pressure rise forces the valve head into the seat. This design worked very well and gave no problems at all once initial difficulties had been overcome.

4.6.3 Data Acquisition

The combustion data from the oscilloscope and the pressure data from the mixing vessels is read by a computer using a Metrabyte Dash-8 A/D Data Acquisition System. The Dash-8 has 8 12 bit A/D channels with inputs of ±5 V that can be read simultaneously. At present there is one EXP-16 Multiplexer/Amplifier connected to one of the Dash-8 channels. The EXP-16 multiplexes 16 differential input channels to a single analog output that is suitable for connection to any of the analog input channels of the Dash-8. This increases the total number of sample channels to 23. The EXP-16 is also useful in that it can accept inputs of a lower voltage than the Dash-8 and amplify these to the required ±5 V, improving resolution.

The data acquisition programs were all written in Microsoft QuickBasic 4.50 using the machine language driver DASH8.BIN (supplied with the Dash-8) to sample the data. The driver can be called from a Basic program to perform the required sampling actions, without the need to program these from scratch.

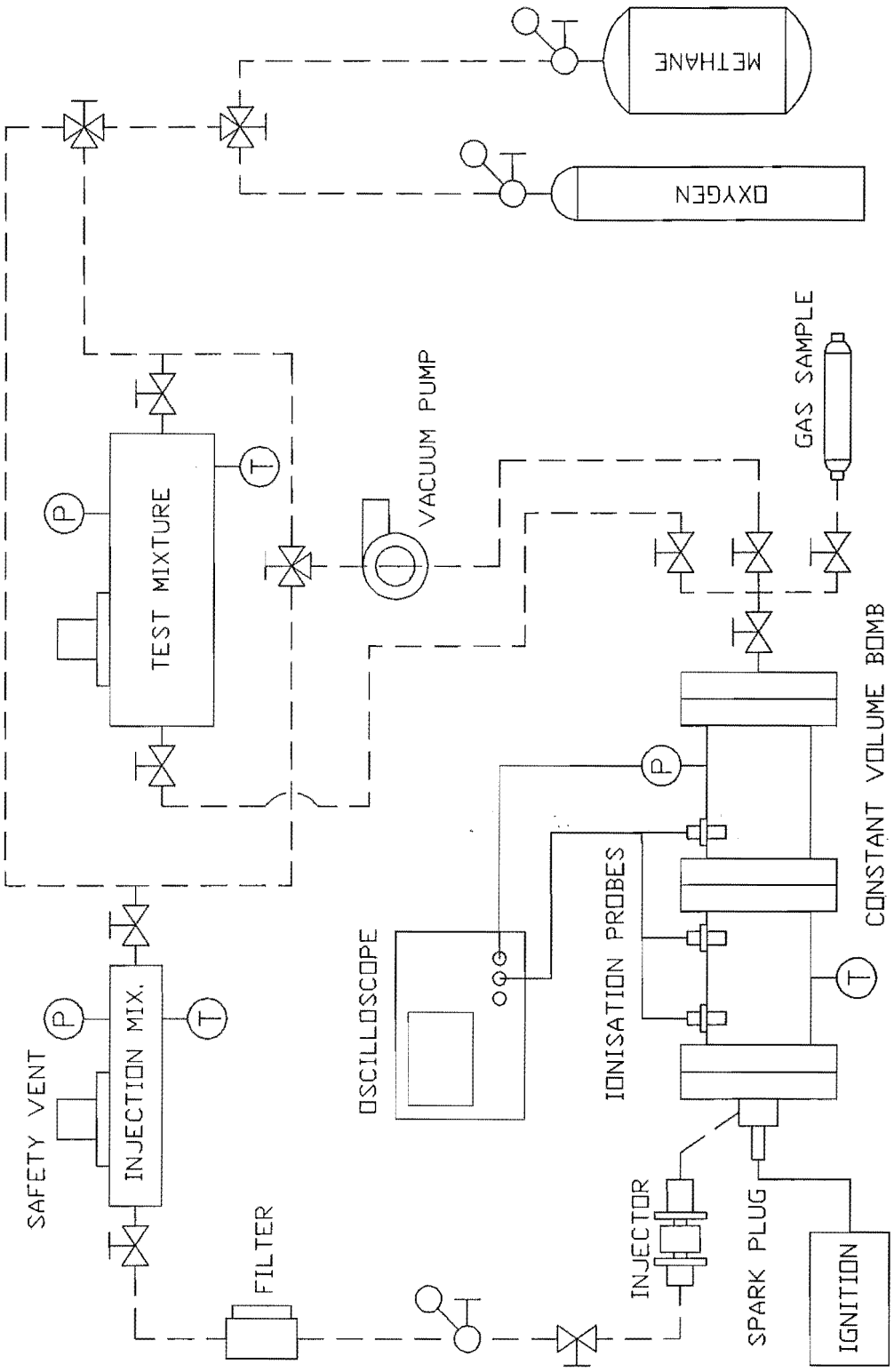

Figure 4.1 Layout of Combustion Rig

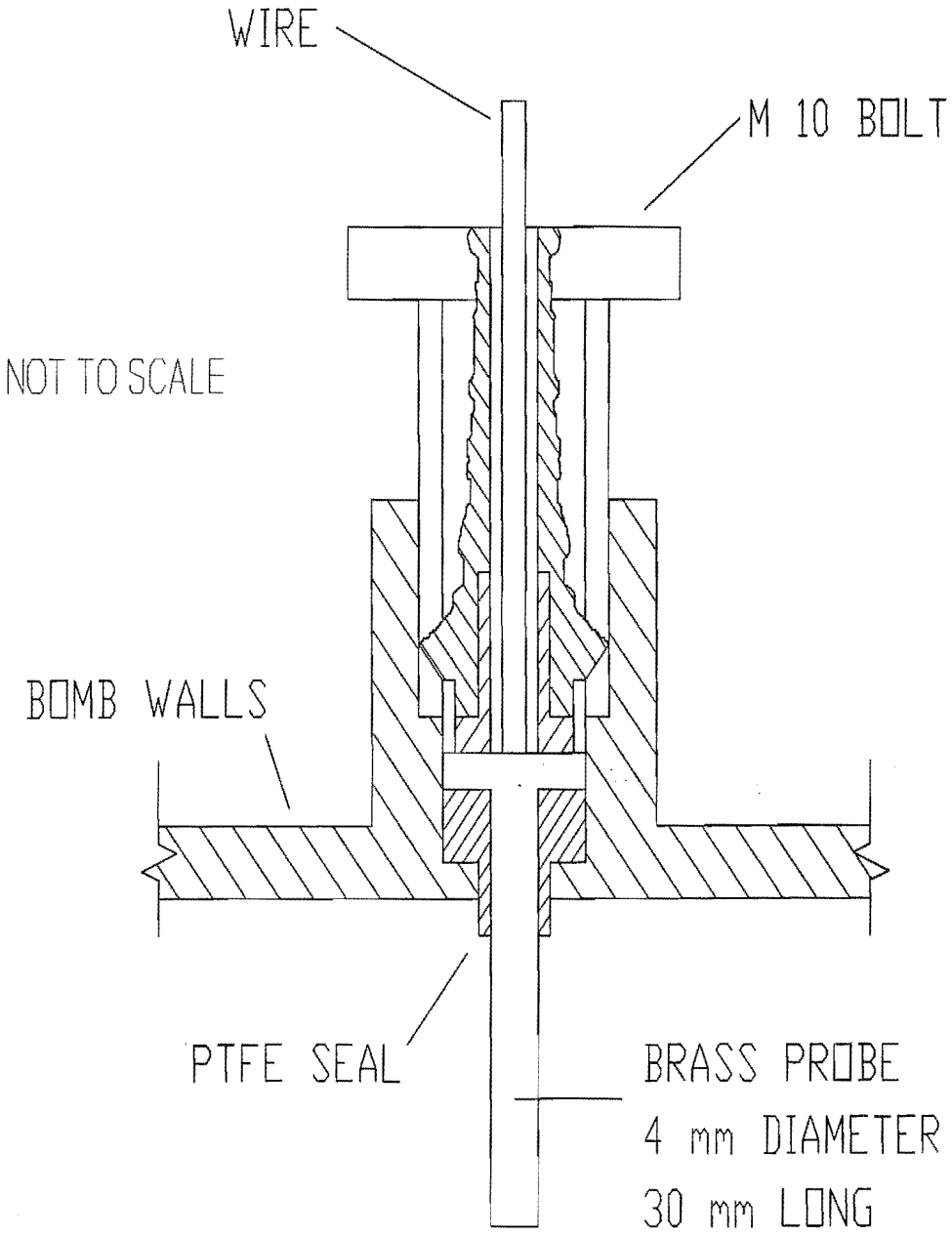

Figure 4.2 Ionisation Probe

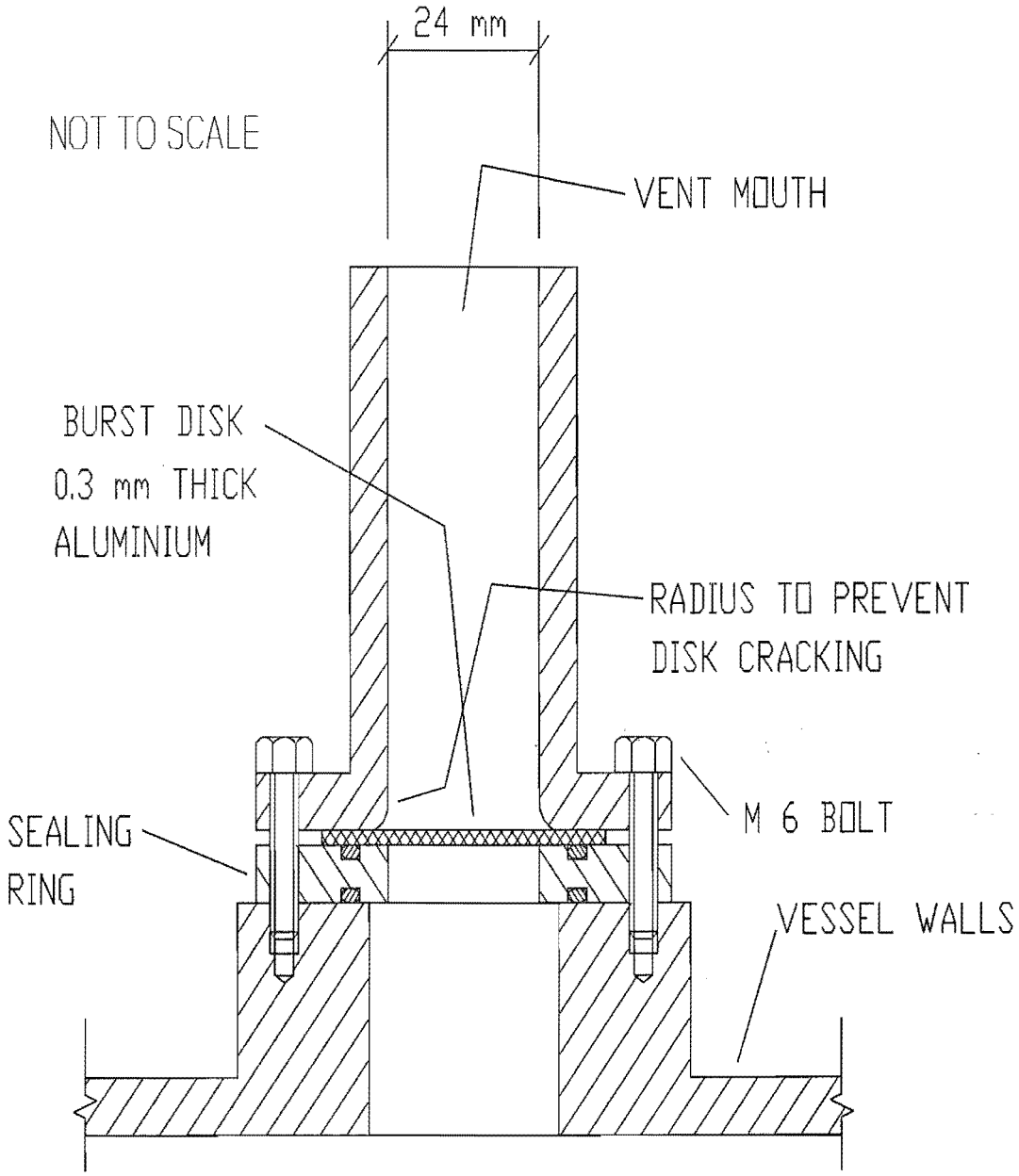

Figure 4.3 Burst Disk

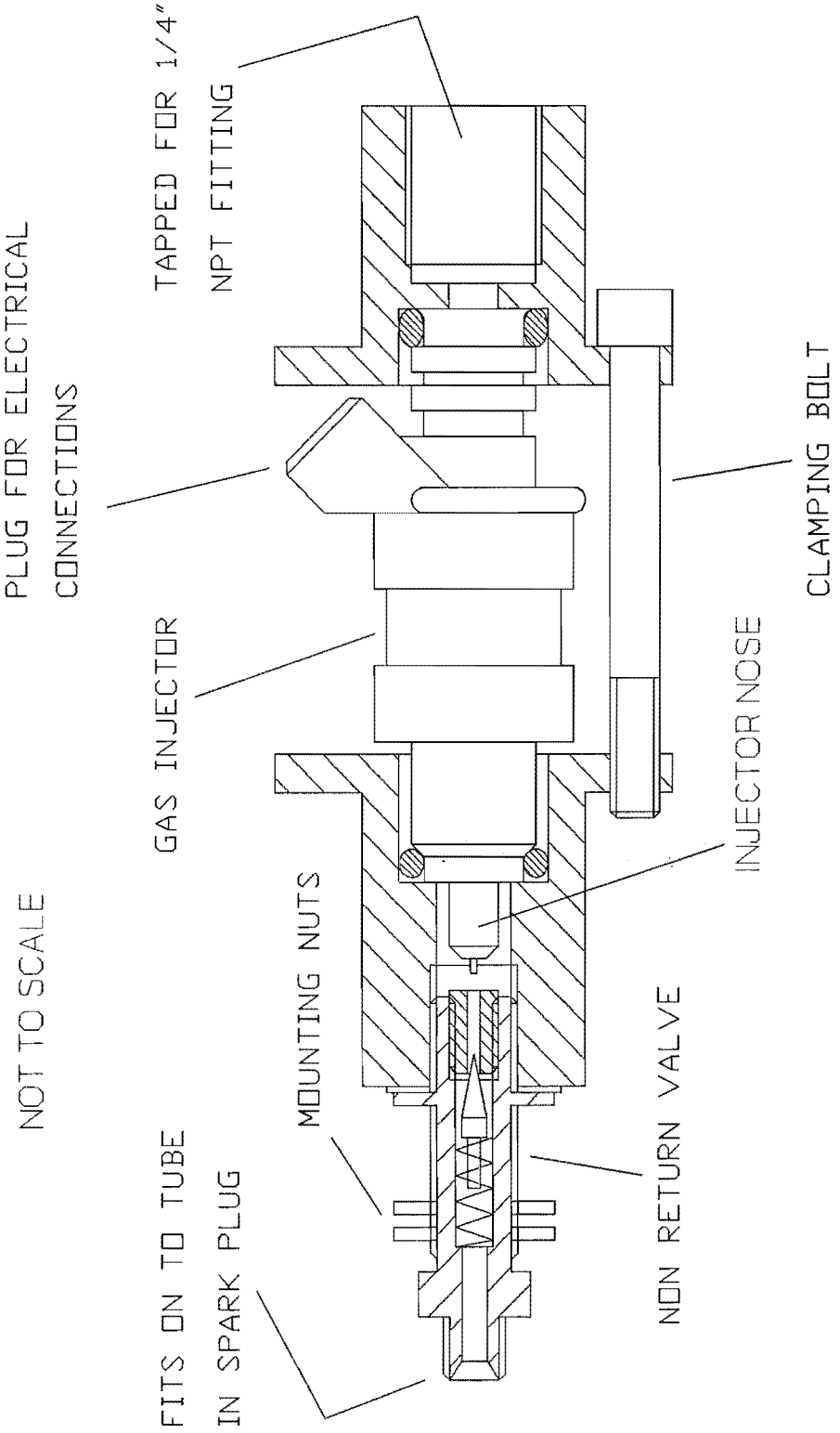

Figure 4.4 Gas Injector Assembly

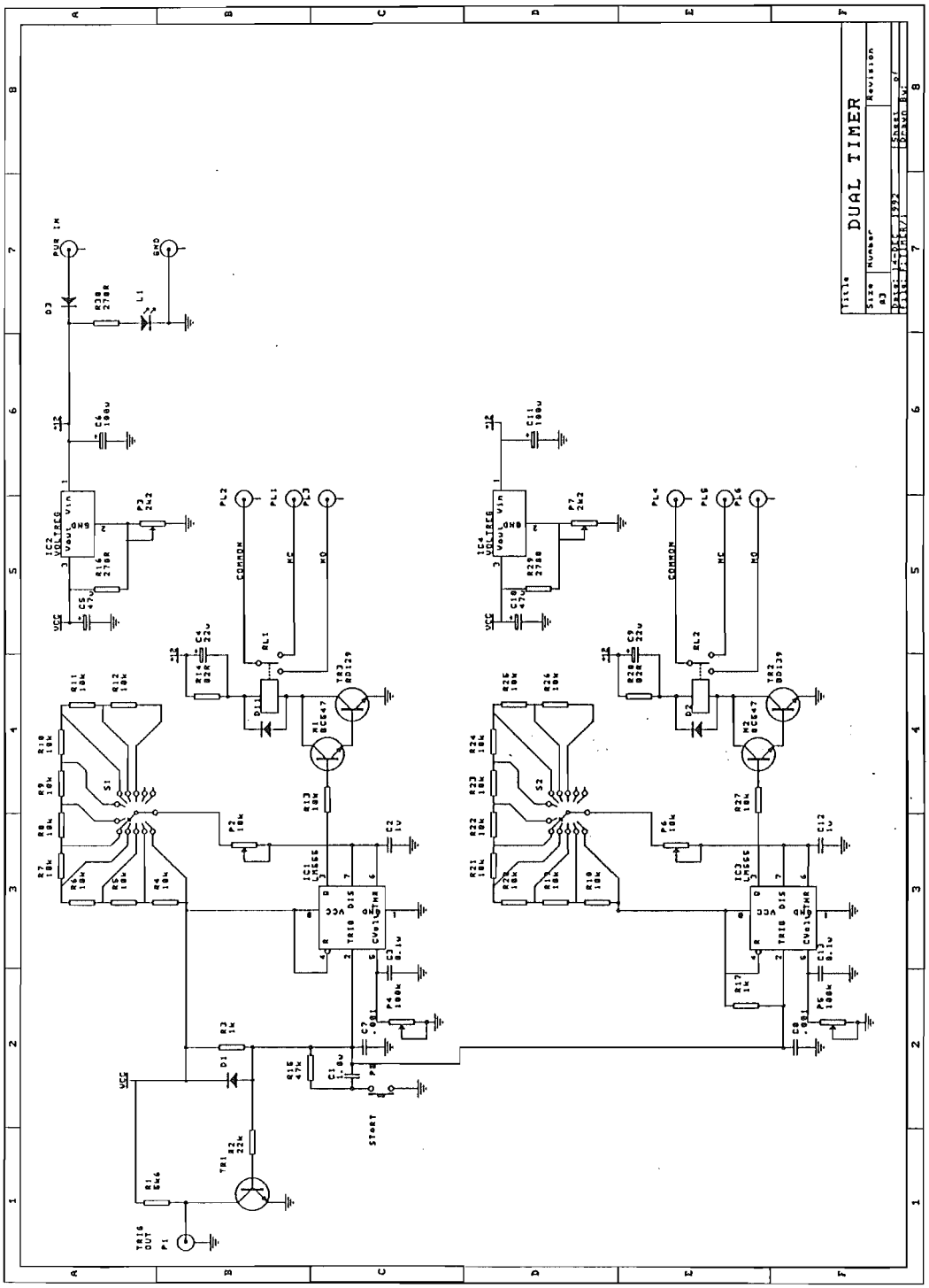

Figure 4.5 Wiring Diagram of Timing Control Box

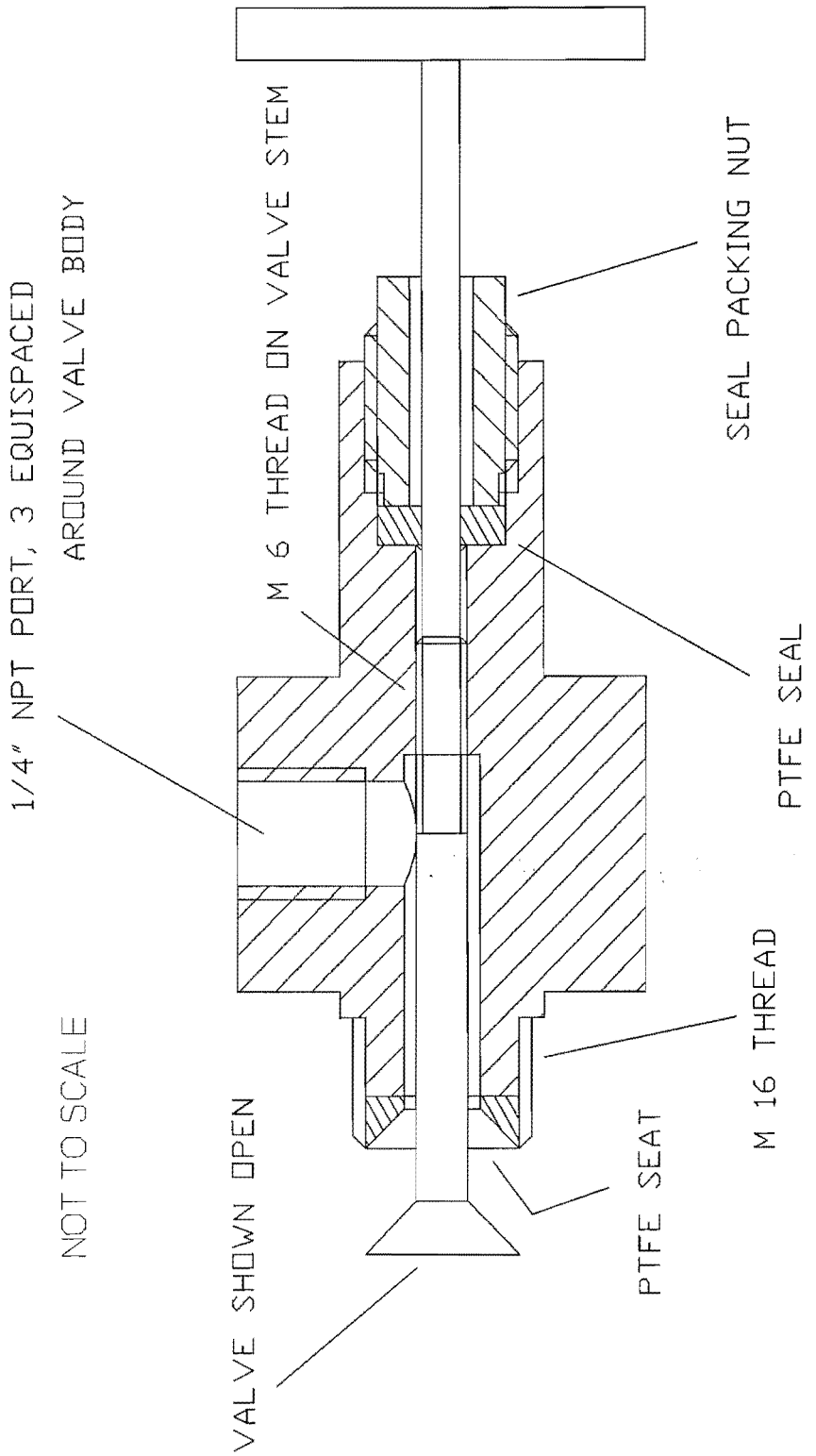

Figure 4.6 Bomb Inlet Valve

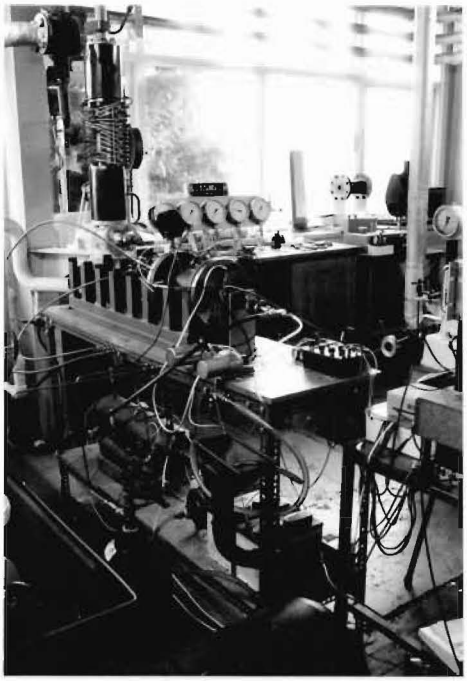

Plate 4.1 Combustion Rig from Rear

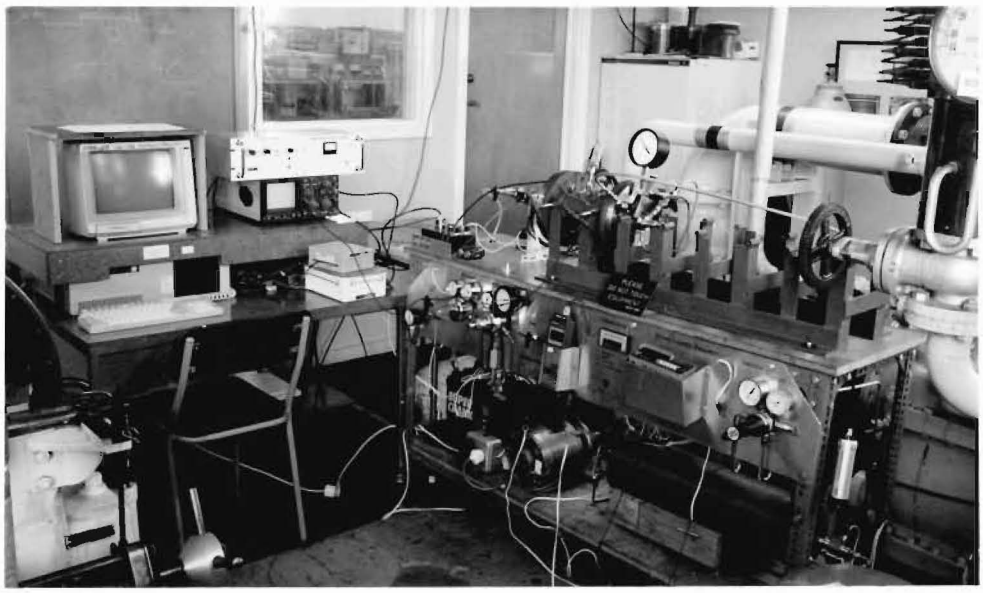

Plate 4.2 Combustion Rig from Front

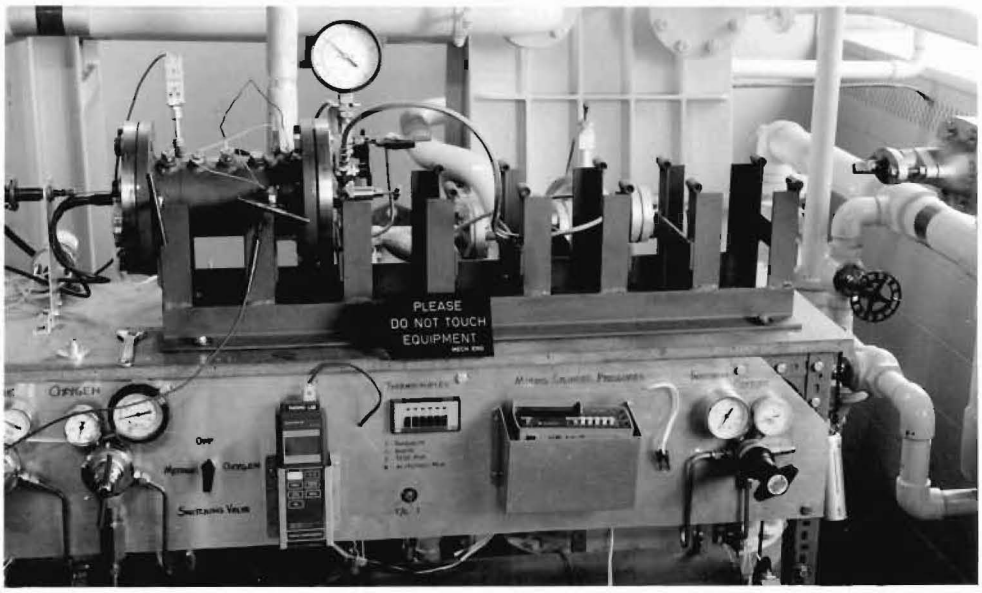

Plate 4.3 Bomb Length 250 mm

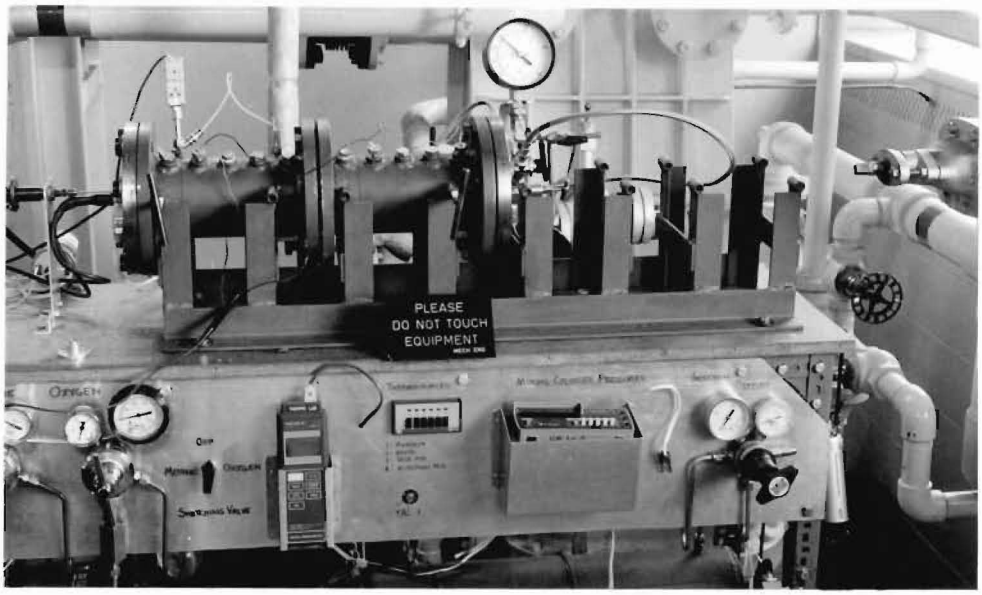

Plate 4.4 Bomb Length 500 mm

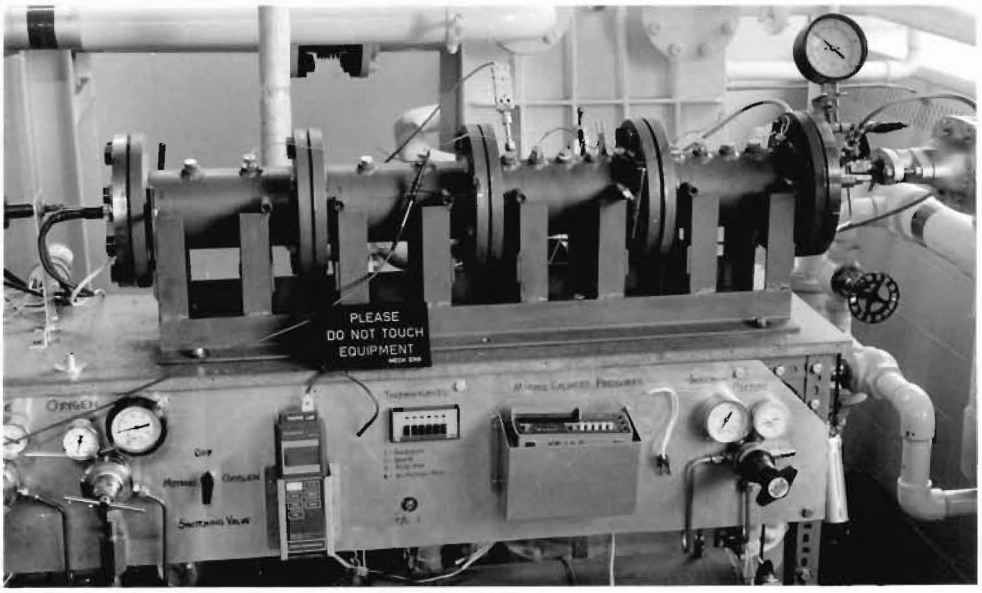

Plate 4.5 Bomb Length 1000 mm

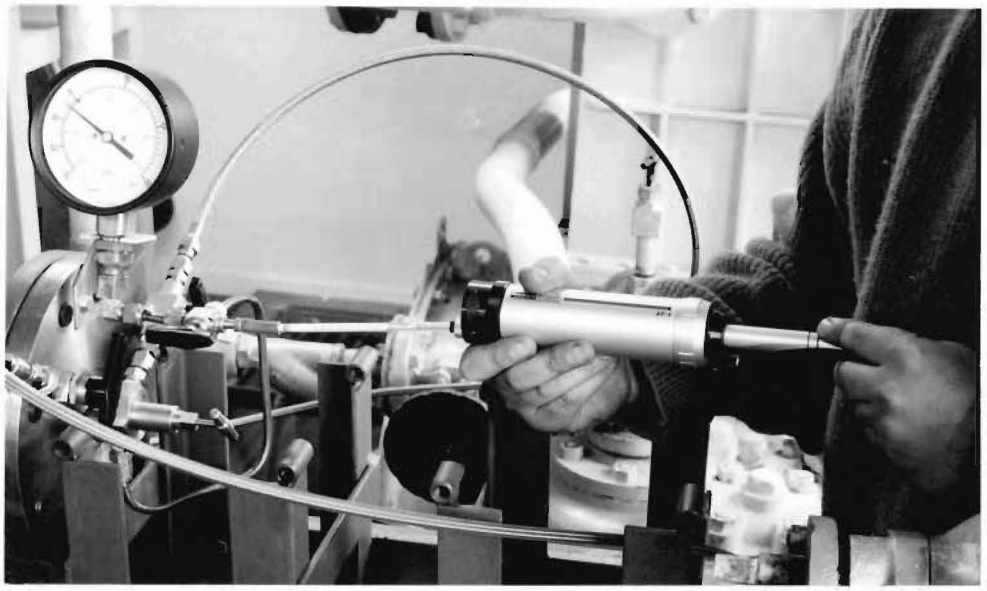

Plate 4.6 Kitagawa Gas Detector Tube and Pump

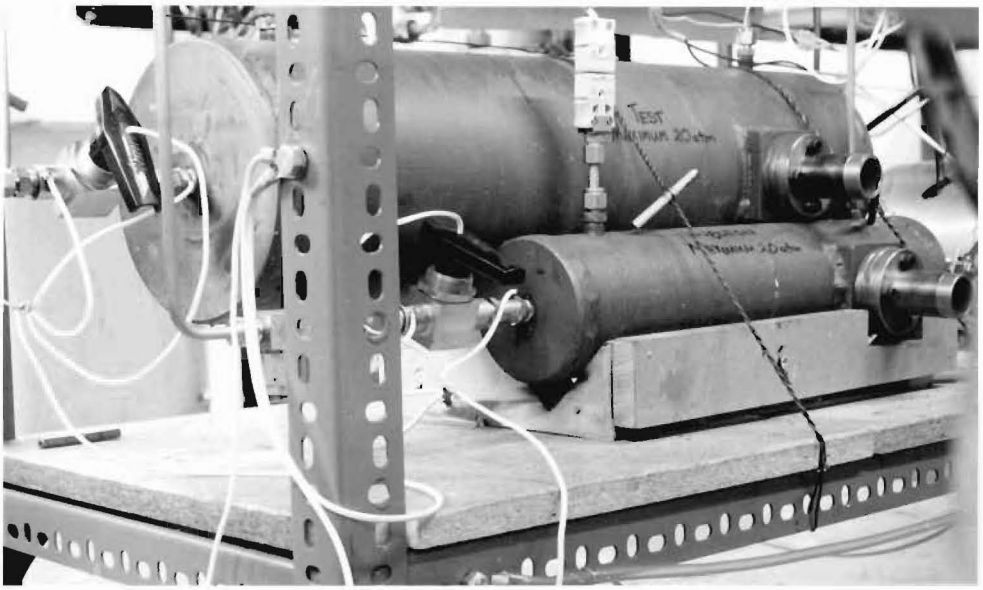

Plate 4.7 Test and Injection Mixture Vessels

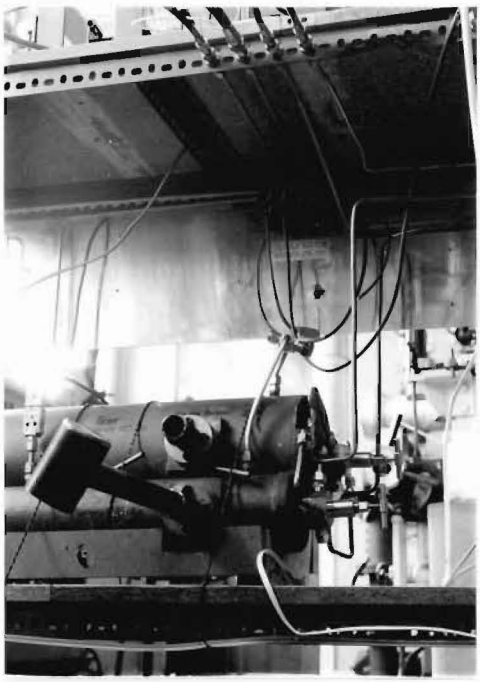

Plate 4.8 Damage to Mixing Cylinders

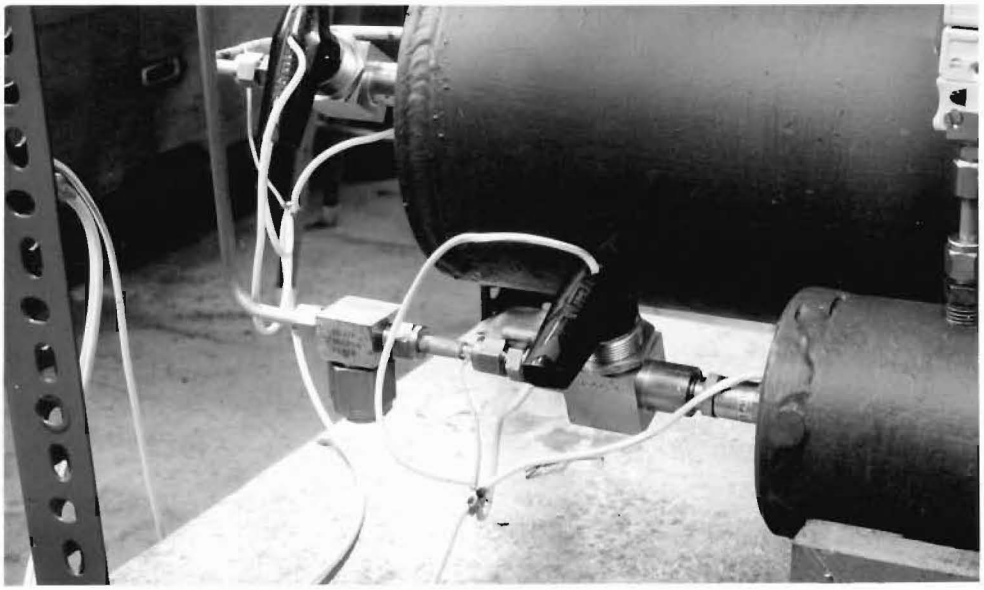

Plate 4.9 Additions to Mixing Cylinder Outlet Valves after Accidental Explosion

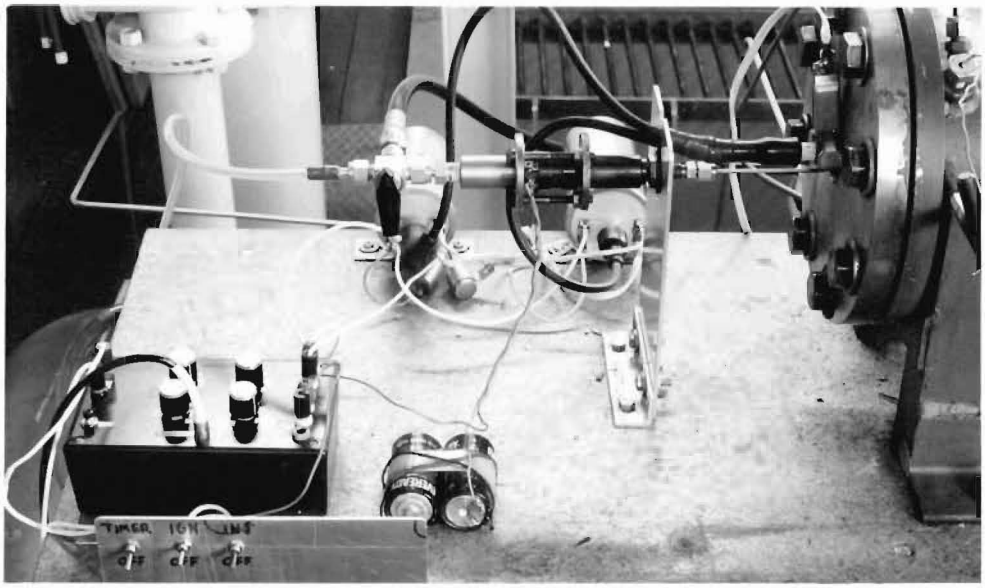

Plate 4.10 Gas Injector Assembly in Position

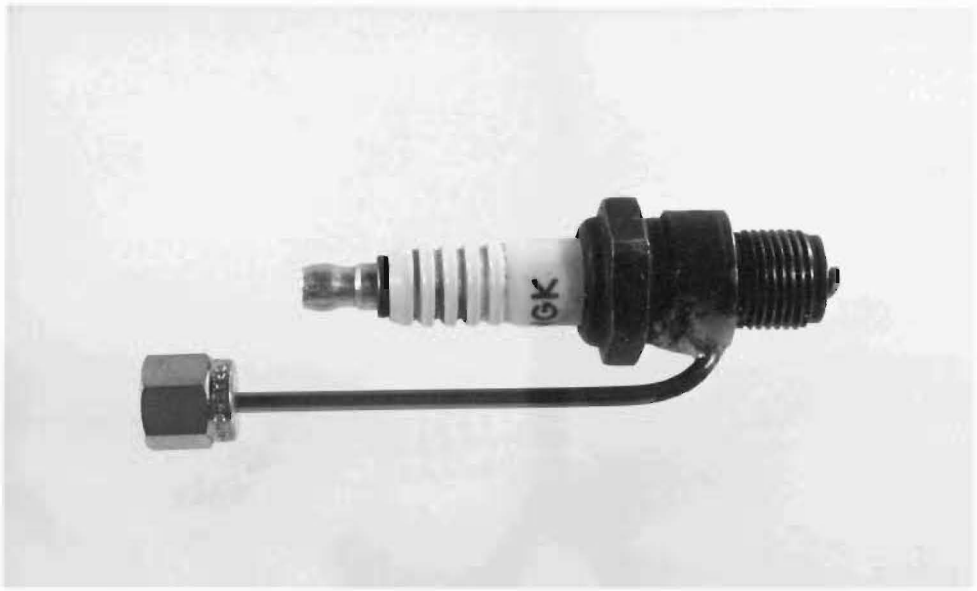

Plate 4.11 Modified Spark Plug

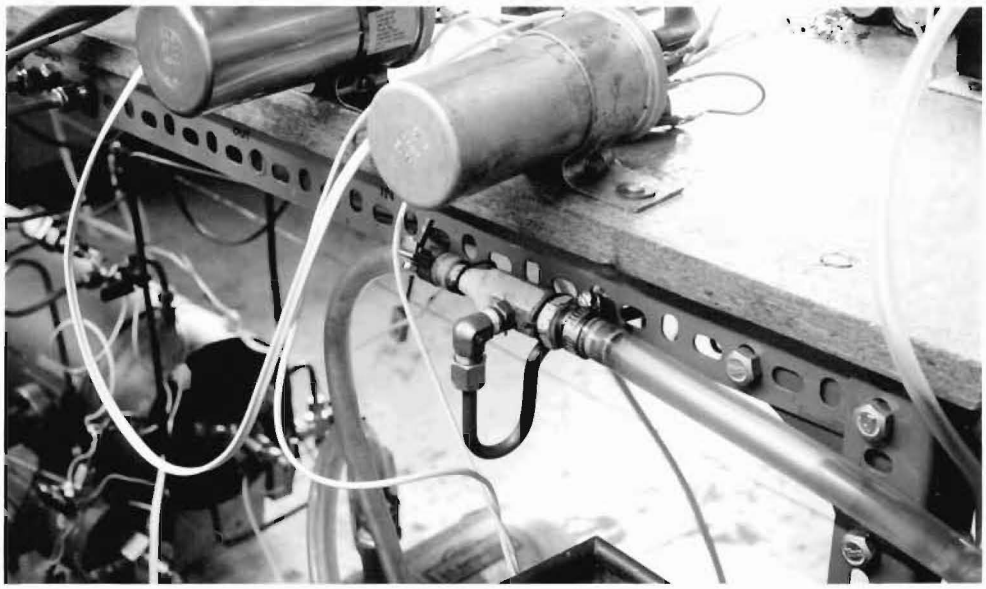

Plate 4.12 Water Venturi Vacuum Pump

CHAPTER 5

PRELIMINARY CALCULATIONS AND MEASUREMENTS

5.1 INTRODUCTION

Before any testing commenced several areas were investigated to ensure that the test programme would cover the areas of most interest, and that the experimental apparatus functioned as intended.

5.2 ADIABATIC FLAME TEMPERATURE AND PRESSURE

5.2.1 Background

The temperature to which a reactive mixture may rise after combustion can be calculated from thermochemical data. For cool burning flames such as very lean hydrogen-air or coal gas-air this procedure is fairly easy as the dissociation of the products can be neglected.[93] For very hot flames such as acetylene-oxygen large amounts of CO, H_2, O_2, OH, O and H are formed. This dissociation uses up an enormous amount of energy and limits the flame temperature. The occurrence of dissociation at high temperature considerably complicates flame temperature calculations. The temperature of the mixture must be known to calculate the

composition but the temperature itself is a function of the composition. Thus it is necessary to solve the problem with an iterative procedure.

Many systems have been proposed for the solving of the set of simultaneous equations that arise from the conditions of chemical equilibrium and molecule balances with, for example, Fehling and Leser[100] employing a graphical method. All the methods assumes that the reaction is adiabatic, ie. there is no heat loss by radiation, thermal conduction or diffusion to the walls of the vessel or burner. It is most commonly applied to constant pressure flames, but it is equally possible to apply it to constant volume explosions. Equilibrium of the burnt gases is always assumed.

The modern personal computer has made elaborate equation solving schemes obsolete for most purposes. The high speed nature of the computer means that the solution algorithm can be relatively crude but accuracy is obtained by repeating it many times. Thus, a BASIC program capable of predicting the final adiabatic flame temperature for any hydrocarbon fuel of composition C_aH_b burning lean in oxygen* under constant volume conditions was written. The program is based on the FORTRAN work of Green[101] but has been simplified a little.

---

* Further programs were developed which could predict the final adiabatic flame temperature for a fuel C_aH_b burning lean in oxygen or air under either constant volume or pressure conditions. However these programs are of little relevance to the remainder of this thesis so further details will not be given.

5.2.2 Theoretical Development

From Sharma and Mohan,[26] applying the First Law to the combustion process gives

$$Q - W = \Delta U \tag{5.1}$$

For adiabatic combustion $Q = 0$ and for a constant volume process $W = 0$ since $PdV = 0$. Thus we have

$$\Delta U = 0 \tag{5.2}$$

Now for convenience we can rewrite Equation (5.2) as

$$\Delta H - \Delta PV = 0 \tag{5.3}$$

since thermochemical data books generally tabulate H rather than U. We can also substitute in the perfect gas relationship $PV = nRT$ to give

$$\Delta H - \Delta nRT = 0 \tag{5.4}$$

We can now define n_1 as the total number of moles in the reactants and n as the total number of moles in the products, and T_1 and T as the initial and final temperatures respectively then

$$U_r = H_r - n_1RT_1 \tag{5.5}$$

$$U_p = H_p - nRT \tag{5.6}$$

Hence with $U_r = U_p$ we have the condition for constant volume adiabatic combustion.

For hydrocarbon fuel-oxygen combustion the following equations were considered to describe the chemical equilibrium of the products

$$2CO + O_2 \rightleftharpoons 2CO_2 \tag{5.7}$$

$$CO + H_2O \rightleftharpoons CO_2 + H_2 \tag{5.8}$$

$$2C + O_2 \rightleftharpoons 2CO \tag{5.9}$$

$$2OH + H_2 \rightleftharpoons 2H_2O \tag{5.10}$$

$$2H \rightleftharpoons H_2 \tag{5.11}$$

$$2O \rightleftharpoons O_2 \tag{5.12}$$

$$CO + 3H_2 \rightleftharpoons CH_4 + H_2O \tag{5.13}$$

$$2O_3 \rightleftharpoons 3O_2 \tag{5.14}$$

After combustion the following mole fractions will be present in the products

$X1$	CO_2	$X7$	CH_4
$X2$	H_2O	$X8$	O_3
$X3$	OH	$X9$	CO
$X4$	C	$X10$	O_2
$X5$	H	$X11$	H_2
$X6$	O		

From Equations (5.7) to (5.14) we can get 8 equations from the conditions of chemical equilibrium. For the general equation (i), $aA + bB \rightarrow cC + dD$

$$K_i = \frac{P_A^{\,a}\ P_B^{\,b}}{P_C^{\,c}\ P_D^{\,d}} \tag{5.15}$$

where K_i is termed the Equilibrium Constant and P_A is the partial pressure of constituent A. Now $P_A = {}^{XA}/_{e}P$ where P is the total pressure, e is the total number of moles of products and X_A the number of moles of A. Hence

$$K_i = \frac{X_A^{\,a}\ X_B^{\,b}}{X_C^{\,c}\ X_D^{\,d}}\ (P/e)^{a+b-c-d} \tag{5.16}$$

For constant volume combustion it is simpler to express ${}^{P}/_{e}$ in terms of the initial pressure P_1, the initial temperature T_1 and the final temperature T between the initial and final states. This can be done by applying the perfect gas relationship. We can express the initial state as

$$P_1V_1 = n_1RT_1 \tag{5.17}$$

and the final state as

$$PV = nRT \tag{5.18}$$

Now $V_1 = V$ and R is the Universal Gas Constant so

$$\frac{P_1}{n_1T_1} = \frac{P}{nT} \tag{5.19}$$

or

$$\frac{P_1T}{T_1} = \frac{Pn_1}{n} \tag{5.20}$$

Now let $n_1 = 1$ by definition, and with $n = e$

$$\frac{P_1 T}{T_1} = \frac{P}{e} \tag{5.21}$$

Hence

$$K_i = \frac{X_A{}^a \; X_B{}^b}{X_C{}^c \; X_D{}^d} \left(P_1 \frac{T}{T_1}\right)^{a+b-c-d} \tag{5.22}$$

The constants of equilibrium were calculated from data in the JANAF Thermochemical Tables[102] and they agreed closely with those calculated by Gaydon and Wolfhard[93], Lewis and von Elbe[45], and Green[101]. If we assume a value of final temperature we can try to solve these equations to get *X1→X16* at that temperature *T*. However we have 8 equations but 11 unknowns so we get the remaining 3 equations from balancing the atoms present before combustion with those present after.

The reactants can be represented by

$$fC_aH_b + (1-f)O_2 \tag{5.23}$$

where *f* is the fraction of fuel in the mixture. A Carbon balance gives

$$X9 = fa - X1 - X4 - X7 \tag{5.24}$$

Hydrogen balance,

$$X11 = \frac{1}{2}(fb - 2X2 - X3 - X5 - 4X7) \tag{5.25}$$

Oxygen balance,

$$X10 = 1 - f - \frac{1}{2}(fa + X1 + X2 + X3 - X4 + X6 - X7 + 3X8) \tag{5.26}$$

Thus, we have 11 equations and 11 unknowns. By assuming a trial value of final temperature we can solve these equations iteratively so that we arrive at the mole fractions $X1 \rightarrow X11$ of the various molecules that would be present at the assumed final temperature. We can then calculate the internal energy of the products and see if it is equal to the internal energy of the mixture. If this is true then we have assumed correctly for the final temperature (see Equation (5.2)). We calculate U_p by first calculating H_p.

$$H_p = \sum_{L=1}^{11} X(L).H(L) \tag{5.27}$$

where $H(L)$ is the enthalpy of $X(L)$ at the assumed temperature (obtained from the JANAF Thermochemical Tables[102]). From Equation (5.6) we can then get U_p since $n = e = \Sigma X1 \rightarrow X11$. In the BASIC program, $T = 1000$ K is assumed for the first iterative run and this is low enough so that $U_p < U_r$. The final temperature is then increased in increments of 100 K and the iterations done again until $U_p > U_r$. When this is achieved, a quadratic interpolation from Kreysig[103] is used to determine the final temperature when $U_p = U_r$ and the mole fractions $X1 \rightarrow X11$ at this temperature. The final pressure is then calculated using the perfect gas relationship.

The final form of the program, called AIDTEMP.OXY is given in Appendix A, along with tables of the enthalpies and equilibrium constants used in the

calculations. A flow diagram for the program is also given. It must be pointed out here that the order in which the equations are solved in the program is vital. As they are given in AIDTEMP.OXY, the solution will work for lean mixtures of methane-oxygen (ie below 30% methane in oxygen, $\lambda > 1.167$), but for rich mixtures the equations must be reordered to prevent the program attempting to divide by zero. Rich mixtures also present the problem that due to the lack of available oxygen the liberation of solid carbon becomes increasingly likely. This makes the calculations more difficult, although a solution is possible.[93]

5.2.3 Predicted Results

A typical output from AIDTEMP.OXY is shown in Figure 5.1. This run is for a 10% methane-oxygen mixture ($\lambda = 4.5$), and the printout lists the initial combustion conditions, the mole fractions present at the final temperature, and the final values of temperature and pressure.

As can be seen from Figure 5.2 the adiabatic flame temperature drops in a linear manner as λ increases. The maximum pressure also falls, as a function of the decreasing flame temperature. This decrease in temperature is quite severe, with it falling from approximately 3500 K at $\lambda = 1$ to approximately 2000 K at $\lambda = 9.5$.

Figure 5.3 shows the variation in the concentrations of the combustion products with λ. It must be remembered that as the initial mixture becomes leaner the

predominant combustion product becomes unreacted oxygen, but this is not shown for clarity. It is immediately obvious however that the effects of dissociation are only significant at high flame temperatures (ie. with λ close to stoichiometric). This conclusion is reached by the observation of the levels of carbon monoxide and hydroxyl radicals produced as these are only created by dissociation. When the mixture is at its leanest (λ = 9.5, which is approximately equal to the lean limit of flammability for methane-oxygen[45]) the production of CO and OH is effectively zero. Thus for very lean mixtures of methane-oxygen the flame temperatures can probably be calculated without the need for making allowances for the dissociation of the products.

5.3 FLOWRATE OF INJECTOR

5.3.1 Measurement Technique

It was obviously desirable to measure the flowrate of the Bosch injector in order to know what size of injected puff delivered a set amount of energy. The injected gas was to be a mixture of methane and oxygen (in possibly varying proportions).

The first tests concentrated on the continuous flowrate, that is with the injector constantly open. An early attempt was made using the classic gas-bubble-in-water method but this proved to be too inaccurate. The method which was used for all flowrate testing utilised the injection mixture vessel on the combustion rig, and

observing the pressure drop in it. The injector assembly was set up exactly as for the combustion tests, with it injecting into the bomb vessel, which in turn exhausted to atmosphere.

The injection pressure is the main factor in adjusting the flowrate. No study was made on the effect of increasing the pressure on the flowrate. This was considered unnecessary as there was no requirement for a high flowrate (ie. there was no limit on the injection time as in an engine). Thus all the flowrate testing and all the combustion experiments were conducted with the injection pressure at 5 bar, except where otherwise stated. This pressure was chosen because it seemed to offer an acceptable injection duration and was high enough to crack open the non-return valve (Section 4.4.2) of the injector assembly with no problems of sticking. This pressure is also high enough to attain sonic flow conditions in the injector nozzle, when the pressure in the bomb is below 2 bar. This can be shown from Equation (5.28)[104]

$$\frac{P_c}{P_o} < \left[\frac{2}{\gamma+1}\right]^{\frac{\gamma}{(\gamma-1)}} \qquad (5.28)$$

where P_o is the upstream pressure (= 6 bar absolute), P_c is the downstream pressure* (= 1 bar absolute for flow tests, 1.5 bar absolute for combustion tests) and γ is the ratio of specific heats (approximately 1.40[92] for lean methane-oxygen mixtures). Substituting γ = 1.40 into the right hand side of Equation (5.28) shows

---

* Strictly, P_c is the pressure at the throat of the nozzle, but if there is no diffuser then the assumption that the downstream pressure is equal to P_c is valid.

that P_c/P_o must be less than 0.528 for sonic flow, which it clearly is for both the flowrate testing ($^1/_6$ = 0.167) and the combustion testing ($^{1.5}/_6$ = 0.25). The relevance of this is that it can be shown that the mass flowrate is independent of the downstream pressure for sonic flow conditions,[104] thus the injection pressure should be set to the same value for both flowrate and combustion tests, even though the internal pressure of the bomb is different for these situations.

Before a flowrate test was conducted the injection mixture vessel was filled to a set pressure and the conditions were allowed to settle. The injection pressure was then set on the injection mixture regulator, which kept the flowrate constant by providing the injector with a steady pressure. The initial temperature and pressure were then recorded and the injector was opened for a set time. The conditions were then allowed to settle again and the final pressure and temperature were recorded.

This test was initially done for both pure methane and pure oxygen.* Provided that the vessel volume is known, it is possible to calculate the number of moles of gas present before the injector is opened and after it is closed from the perfect gas equation, that is from Equation (5.29)

$$n_a = \frac{P_a V}{R T_a} \tag{5.29}$$

where the subscript a refers to either the initial or final conditions. The volume of

---

* Any references to "pure" methane in this Chapter in fact mean 98% CH_4 2% CO_2. The same is true for "pure" oxygen, which is 99.5% O_2, 0.5% N_2 (Section 4.3.2). To get the actual number of moles of either methane or oxygen injected, all flowrates should be corrected for gas purity.

the injection mixture vessel, V, was carefully measured by weighing the empty cylinder, and then reweighing it after it had been filled with water. This gave V = 1.837 litres.

This system worked well, giving good repeatability. The validity of applying the perfect gas equation was checked by employing the Van der Waals equation and the Beattie-Bridgeman equation on the same initial and final conditions. The constants used for these calculations and an example of each is given in Appendix B. As shown in Table 5.1 there is no significant difference between the calculated flowrates. The molar flowrate was calculated as it was convenient but it can be easily converted to a mass flowrate by multiplying it by the molar mass of the gas. The assumption of constant flowrate with varying downstream pressure is still valid.

Table 5.1 Methods for Calculating the Molar Flowrates of Oxygen and Methane (mmols/s)

Gas	P_i Bar	T_i °C	P_f Bar	T_f °C	Time sec	Molar Flowrate mmols/s		
						Perf. Gas	Van D Waals	Beat-Brid.
O_2	18.3	13.6	5.99	12.3	155	6.097	6.267	6.209
CH_4	8.21	22.0	4.74	21.5	19.8	8.685	8.941	8.901

As can be seen the molar flowrate of methane (n'_{CH4}) is considerably greater than that for oxygen (n'_{O2}). Since it was intended to use a mixture of methane and

oxygen the question was how did the molar flowrate vary for mixtures. The next Section will address this question.

5.3.2 Variation of Molar Flowrate with Mixture Molar Mass

An experiment was conducted to show how the molar flowrate varied with the molar mass of the mixture. Three different mixtures of methane-air were compared to the flowrates for pure methane* and pure air. The results are shown in Table 5.2.

Table 5.2 The Variation of Flowrate with Mixture Molar Mass

% CH_4	% Air	Molar Mass g/mol	Flowrate mmols/s
100	0	16.56	4.584
75	25	19.66	4.295
50	50	22.76	4.029
25	75	25.86	3.782
0	100	28.96[99]	3.574

The injection pressure for the tests was 2 bar (3 bar absolute, still giving sonic flow). This was used because it allowed a longer measuring time for the methane with subsequently greater accuracy. The spring in the non-return valve was

---

* Mixture molar masses were corrected for methane impurity

removed to prevent the valve sticking closed at this lower pressure. Air was used as one of the components of the mixture (rather than oxygen) because this eliminated the need to mix combustible mixtures, that is 25% methane in air is well above the rich limit of flammability, but 25% methane in oxygen is highly explosive. The main objective of the experiment was to see if it was valid to apply a linear relationship to the variation of molar flowrate with mixture molar mass. As can be seen in Figure 5.4 this assumption is sound, certainly over the range of molar mass being considered here. Thus the molar flowrate of a methane-oxygen mixture can be calculated from the ratios of the mixture components (for a given injection pressure). This can be expressed as

$$n'_{mix} = [\%CH_4]n'_{CH4} + [\%O_2]n'_{O2} \tag{5.30}$$

where $[\%CH_4]$ and $[\%O_2]$ are the percentage concentrations of methane and oxygen in the mixture and n'_{CH4} and n'_{O2} are the molar flowrates of pure methane and pure oxygen respectively at that pressure.

5.3.3 Variation of Apparent Flowrate with Injection Duration

It was decided to conduct a series of flowrate tests based on injecting a certain number of gas puffs. This would give an apparent* flowrate for a given injection voltage pulse duration, automatically accounting for such things as the delay in the injector opening and closing and inertia of the gas stream in the injector.

---

* Apparent because the flowrate is based on the length of the injection voltage pulse, rather than on the time that the injector is actually open.

A slow speed (100 rpm) electric motor was attached to set of contact breaker points and this was used as a substitute for the manual triggering on the timing control box (see Section 4.5.2). Otherwise the injection system functioned in exactly the same way as it would have during a combustion test. The number of pulses was calculated from the speed of the motor and the duration of the entire test. The duration of the injection voltage pulse was adjusted using the potentiometers on the timing control box, and monitored by an oscilloscope. The flowrate was again monitored by observing the pressure drop in the injection mixture cylinder. The results are given in Table 5.3.

Table 5.3 Apparent Molar Flowrates for Varying Injection Pulse Duration

Pulse ms	CH_4 mmols/s	O_2 mmols/s
10	4.881	4.094
20	6.744	4.780
40	7.878	5.507
60	8.292	5.854
cont.	8.685	6.097

This data was plotted on a graph (Figure 5.5) and as expected the apparent flowrate decreases from the continuous flowrate value as the injection pulse time becomes shorter. It was then decided to fit a spline approximation between the recorded data points so that n'_{CH4} and n'_{O2} could be calculated for any injection pulse

duration. This procedure was used instead of fitting a single polynomial between given points (the best known example is that there is a unique quadratic which fits three given points), because as the order of the polynomial is increased the tendency is for the solution to oscillate. A spline overcomes this problem by calculating a piecewise solution, that is a different polynomial describes the spline between each set of two points (hereafter called nodes). The best known example of this is linear interpolation, but this suffers from having non-continuous first derivatives at the nodes.

A cubic spline was chosen for the work described here. The method used for calculating it was based on that given by Kreysig,[103] but with some slight modifications. The full procedure is given in Appendix C so only the results will be given here.

Between any two nodes the spline takes the form

$$n'(t_{inj}) = z_3x^3 + z_2x^2 + z_1x + z_0 , \quad x = (t_{inj}-20) \tag{5.31}$$

where t_{inj} is the injection voltage pulse duration (in ms). The constants z_i are given in Table 5.4 (see Appendix C regarding accuracy of constants).

Therefore all that is required to calculate the molar flowrate for any mixture of methane-oxygen at any injection duration with an injection pressure of 5 bar is;

1. Obtain the appropriate values of z_i from Table 5.4 for the required injection duration.

Table 5.4 Spline Constants

	t_{inj} ms	z_3	z_2	z_1	z_0
CH_4	10 to 20	-8e-06	-0.0074	0.1134	6.744
	20 to 40	7.6e-05	-0.0044	0.1134	6.744
	40 to 60	1.1e-05	-0.00137	0.0721	6.896
	60 to 80	-2.7e-06	2.9e-04	0.0045	7.809
O_2	10 to 20	-9.3e-05	-0.00254	0.0525	4.78
	20 to 40	1.7e-05	-0.00114	0.0525	4.78
	40 to 60	1.2e-05	-0.00144	0.07	4.586
	60 to 71	-3.1e-05	3.1e-04	0.00263	5.451

2. Substitute the values of z_i in Equation (5.31) to get n'_{CH4} and n'_{O2} for that injection duration.
3. Substitute the values of n'_{CH4} and n'_{O2} in Equation (5.30) to get the overall molar flowrate n'_{mix} for the mixture.
4. Therefore the amount of mixture injected (in mmols) is n'_{mix} multiplied by the time of the injection voltage pulse (in ms).
5. Actual moles of methane and oxygen injected can then be found by adjusting for the gas purity (Section 4.3.2).

The curves resulting from the application of the spline approximation can be seen in Figure 5.6.

5.3.4 Estimation of Molar Flowrate from Schlieren Photographs

It was thought necessary to gain some visual idea of the injected puff, so it was decided to use the Schlieren method to obtain photographs of the puff. This is described in Appendix D.

An attempt was then made to calculate the apparent molar flowrate of methane by measuring the size of the puff (only methane was used for the schlieren tests, as explained in Appendix D). The photo of the puff shown in Plate 5.1 (t_{inj} = 8 ms) was blown up to 4.35 times actual size and the outline of the puff traced. The volume was calculated by dividing the puff up as shown in Figure 5.7, and approximating each slice as a disk (effectively assuming that the puff is of circular cross section). This volume assumption is also dependent on only the injected gas being present in the puff (ie. no entrainment of the gas in the bomb).

Thus for the 8 ms puff shown in Plate 5.1, the volume is approximately 0.583 cm^3. Assuming that the puff is at the initial internal pressure of the bomb (1.5 bar absolute) and that its temperature is 15°C, application of the perfect gas equation yields

$$n_{CH4} = \frac{PV}{RT} = \frac{1.5*10^5 \; 0.583*10^{-6}}{8.314 \; (273+15)} \qquad (5.32)$$

$$= 0.0365 \; mmols$$

Thus we get

$$n'_{CH4} = \frac{n_{CH4}}{t_{inj}} = \frac{0.0365}{8*10^{-3}} \qquad (5.33)$$

$$= 4.56 \ mmols/s$$

This is approximately the same as that measured for t_{inj} = 10 ms in Section 5.3.3.

This system of measuring the apparent molar flowrate is unreliable because it depends critically on the two assumptions that the gas puff is of circular cross section and only the injected gas is present in the puff. The later in particular can lead to wild results. It has to be remembered that Schlieren photographs show only the areas of different density, due in this instance (for the most part) to the turbulence generated by the injection. After a short time this turbulence will have entrained enough internal gas to make the puff appear much larger than it actually is.

This is demonstrated by applying the same technique described above to the 10 ms puff shown in Plate 5.1. The volume was calculated to be 2.15 cm^3 which from Equation (5.32) gives n_{CH4} = 0.134 mmols. Equation (5.33), with t_{inj} = 10 ms, then gives n'_{CH4} = 13.4 mmols/s, which is much larger than the maximum possible flowrate (as measured in Section 5.3.1) of n'_{CH4} = 8.685 mmols/s. It is clear when comparing photographs of the 8 ms puff and the 10 ms puff that the puff is much more sharply defined in the first and that a significant amount of entrainment will have taken place between the two photographs.

5.4 IGNITION ENERGY

5.4.1 Energy Available in Coils

From Bartkowiak,[105] the energy E stored in a coil of inductance L, with a steady current I_{ss} flowing in it is given by

$$E = \frac{1}{2}L(I_{ss})^2 \tag{5.34}$$

Thus, to find the energy in a coil we must measure L. The voltage V in a coil is related to the instantaneous current i by

$$V = iR + L\frac{di}{dt} \tag{5.35}$$

At $t = 0$, $i = 0$ since the current cannot change instantaneously. This gives

$$\frac{di}{dt}_{t=0^+} = \frac{V}{L} \tag{5.36}$$

Hence the inductance L of a coil may be found from the initial slope of the current versus time graph.

A 3.4 Ω resistor was connected in series with each of the two coils (described in Section 4.5.1). The voltage supply to each of the coils was switched on using the timing control box (Section 4.5.2) and the voltage across the resistor was recorded on an oscilloscope. This enabled the calculation of the current and the initial slope of the current-time trace, and from this the inductance L of each coil was determined. The resulting graphs are shown in Figure 5.8 and Figure 5.9. The

steady state current for each coil was remeasured without the 3.4 Ω resistor and the energy available in each coil was calculated from Equation (5.34). The results are given in Table 5.5.

Table 5.5 Performance Parameters of the Ignition Coils

Coil	Inductance mH	Voltage	I_{ss} amps	Energy mJ
HA 12	15.54	12 V DC	3.30	84.6
		24 V DC	6.54	332.3
SP 12	15.63	12 V DC	3.34	87.2
		24 V DC	6.60	340.4

As both coils are connected together, the total energy available at 12 V DC is 171.7 mJ and at 24 V DC 672.7 mJ.

5.4.2 Measurement of Energy Available in Spark

It is well known that the energy released by the spark at the electrodes is only a small fraction of that available in the coils. To determine this energy, a simple calorimeter was built. The design was based on one described by White[106] and can be seen disassembled in Plate 5.2 and set up in Plate 5.3.

The spark energy was measured by observing the temperature rise of a small amount of water. Equation (5.37) can be used to calculate the energy, where q is the spark energy, m_w is the mass of water, c is the mean specific heat of water (4.18 kJ/kgK[92]), T_i and T_f are the initial and final temperatures and N is the number of sparks.

$$q = \frac{m_w \, c(T_f - T_i)}{N} \tag{5.37}$$

The quantity of water was measured as 4.89 g, the reason such a small volume was used being a given amount of energy will produce a greater temperature rise in a small volume than a large one. The temperature was measured with a K-Type thermocouple, the data being read by the Dash-8 data acquisition system fitted to a computer (see Section 4.6.3). This was capable of reading the temperature to ± 0.02°C. The water was separated from the spark electrodes by an ultra thin brass cap, painted black to maximise its transfer of energy from the spark to the water. The interior of the spark plug was insulated by packing it with asbestos wool, this being necessary to eliminate what would otherwise be a great source of energy loss. The screw-on cap which held the water was highly polished on the inside to minimise the absorbtion of energy by the cap itself. The entire water cap was also encased in a vacuum jacket to further minimise heat losses. Obviously, it would have been useless to attempt to measure the energy of one spark, so a set of contact breaker points were driven by an electric motor at 2800 rpm and these were used to trigger the spark. This setup can be seen in Plate 5.4.

A test was conducted by starting the electric motor and waiting for the water temperature to settle. The ignition voltage was then switched on and left for up to 5 minutes. The temperature was taken as soon as practicable after the ignition had been switched off. The plug and the vacuum jacket were then removed to allow the temperature to drop, and were then replaced while the temperature equalised for the next test.

The plug gap was the same as for the combustion tests, that is 0.6 mm, and the same spark plug was used for all the spark energy tests. Tests were done with the ignition voltage at both 12 V and 24 V. The testing procedure was very sensitive to the small changes giving wild results if the exact approach with regard to setting the calorimeter up was not carried out. If the procedure was carried out correctly the spark energy measurements were repeatable to within ± 0.3 mJ. The results are summarised in Table 5.6.

Table 5.6 Spark Energies

Coil Voltage (V)	Coil Energy (mJ)	Spark Energy (mJ)	Energy Transferred (%)
12	172	3.950	2.30
24	673	6.870	1.02

Carbon Atoms :> 1
Hydrogen Atoms :> 4
Percentage of fuel in oxygen :> 10
Equivalence Ratio Lambda :> 4.493
Initial Pressue :> 1.5 atm
Initial Temperature :> 298 K
Internal Energy of Mixture :> -9.969 KJ/mol

T(K)	CO2	H2O	OH	C	H	O	CH4	O3	CO	O2	H2	UP(KJ/mol)	E(mols)
1000	0.1000	0.2000	0.0000	0.0000	0.0000	0.0000	0.0000	0.0000	0.0000	0.7000	0.0000	-71.5982	1.0000
1100	0.1000	0.2000	0.0000	0.0000	0.0000	0.0000	0.0000	0.0000	0.0000	0.7000	0.0000	-68.5862	1.0000
1200	0.1000	0.2000	0.0000	0.0000	0.0000	0.0000	0.0000	0.0000	0.0000	0.7000	0.0000	-65.5110	1.0000
1300	0.1000	0.2000	0.0000	0.0000	0.0000	0.0000	0.0000	0.0000	0.0000	0.7000	0.0000	-62.3782	1.0000
1400	0.1000	0.2000	0.0000	0.0000	0.0000	0.0000	0.0000	0.0000	0.0000	0.7000	0.0000	-59.1916	1.0000
1500	0.1000	0.2000	0.0001	0.0000	0.0000	0.0000	0.0000	0.0000	0.0000	0.7000	0.0000	-55.9527	1.0000
1600	0.1000	0.1999	0.0002	0.0000	0.0000	0.0000	0.0000	0.0000	0.0000	0.6999	0.0000	-52.6598	1.0001
1700	0.1000	0.1998	0.0004	0.0000	0.0000	0.0000	0.0000	0.0000	0.0000	0.6999	0.0000	-49.3105	1.0001
1800	0.1000	0.1996	0.0008	0.0000	0.0000	0.0000	0.0000	0.0000	0.0000	0.6998	0.0000	-45.8943	1.0002
1900	0.1000	0.1993	0.0013	0.0000	0.0000	0.0001	0.0000	0.0000	0.0000	0.6997	0.0000	-42.4057	1.0004
2000	0.1000	0.1989	0.0022	0.0000	0.0000	0.0002	0.0000	0.0000	0.0000	0.6994	0.0000	-38.8044	1.0007
2100	0.0999	0.1982	0.0035	0.0000	0.0000	0.0004	0.0000	0.0000	0.0001	0.6990	0.0000	-35.0855	1.0011
2200	0.0998	0.1973	0.0053	0.0000	0.0000	0.0007	0.0000	0.0000	0.0002	0.6985	0.0001	-31.2031	1.0018
2300	0.0996	0.1960	0.0076	0.0000	0.0000	0.0012	0.0000	0.0000	0.0004	0.6978	0.0001	-27.1152	1.0028
2400	0.0993	0.1944	0.0107	0.0000	0.0001	0.0021	0.0000	0.0000	0.0007	0.6968	0.0002	-22.7620	1.0042
2500	0.0988	0.1923	0.0145	0.0000	0.0001	0.0034	0.0000	0.0000	0.0012	0.6955	0.0004	-18.0735	1.0062
2600	0.0980	0.1896	0.0193	0.0000	0.0003	0.0054	0.0000	0.0000	0.0020	0.6939	0.0006	-12.9684	1.0090
2700	0.0969	0.1864	0.0250	0.0000	0.0005	0.0082	0.0000	0.0000	0.0031	0.6918	0.0009	-7.3602	1.0127
2642	0.0976	0.1884	0.0216	0.0000	0.0003	0.0064	0.0000	0.0000	0.0024	0.6930	0.0007	-9.9695	1.0104

Final Temperature :> 2641.842 K
Final Pressure :> 13.43631 atm

Figure 5.1 Typical Output from AIDTEMP.OXY

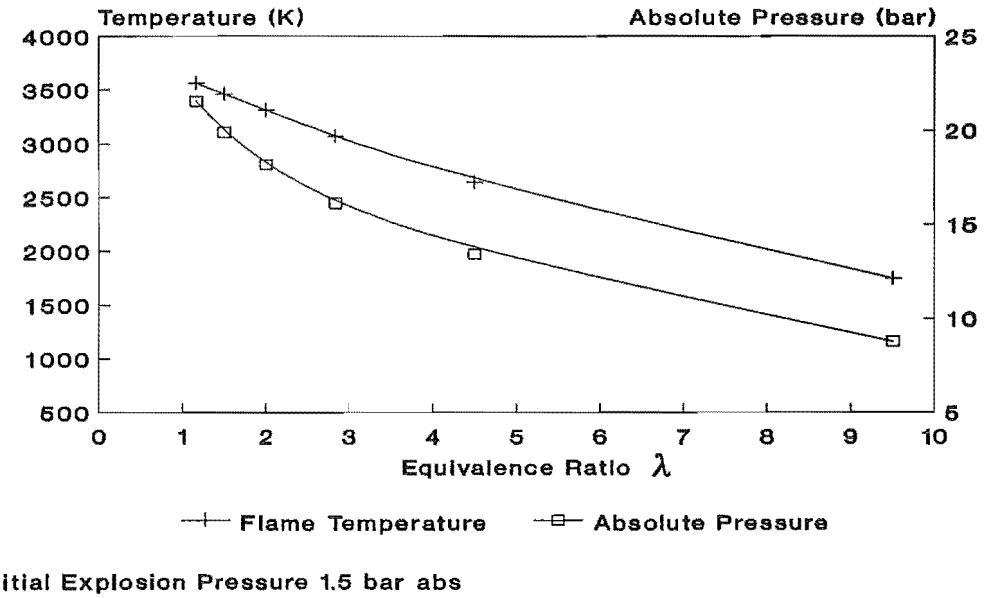

Figure 5.2 Temperature and Pressure Variation with λ

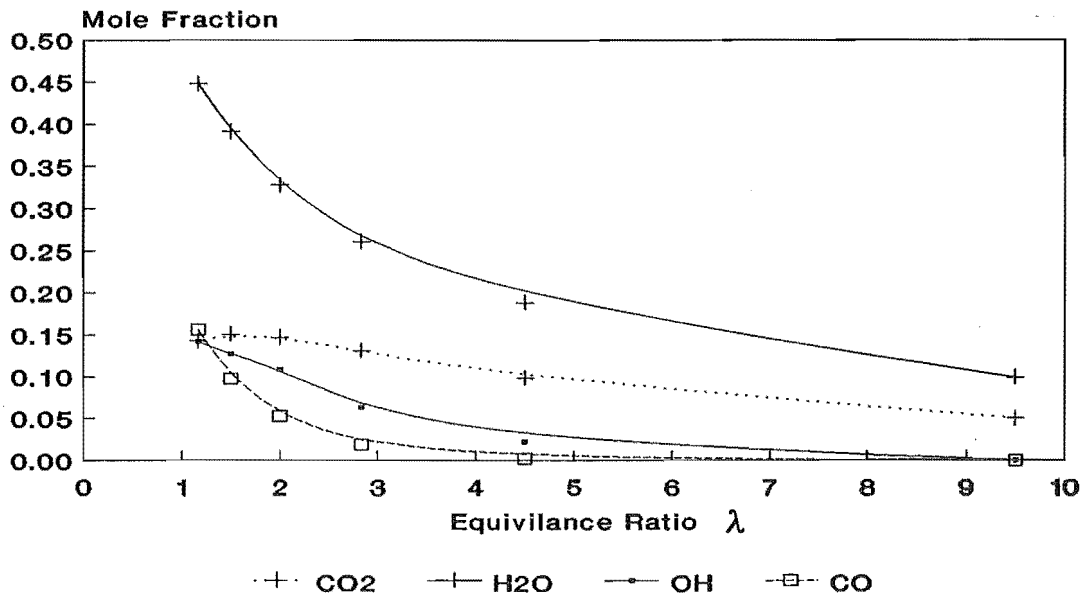

Figure 5.3 Combustion Product Variation with λ

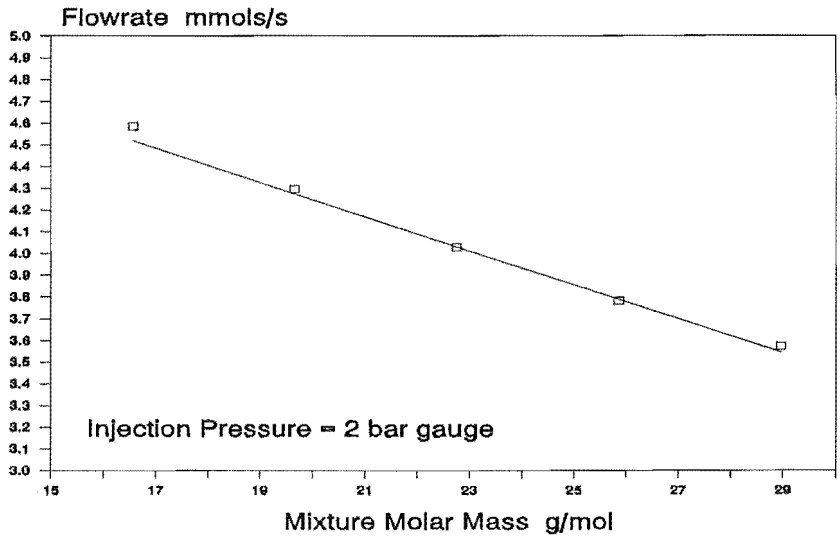

Figure 5.4 Variation of Molar Flowrate with Mixture Molar Mass

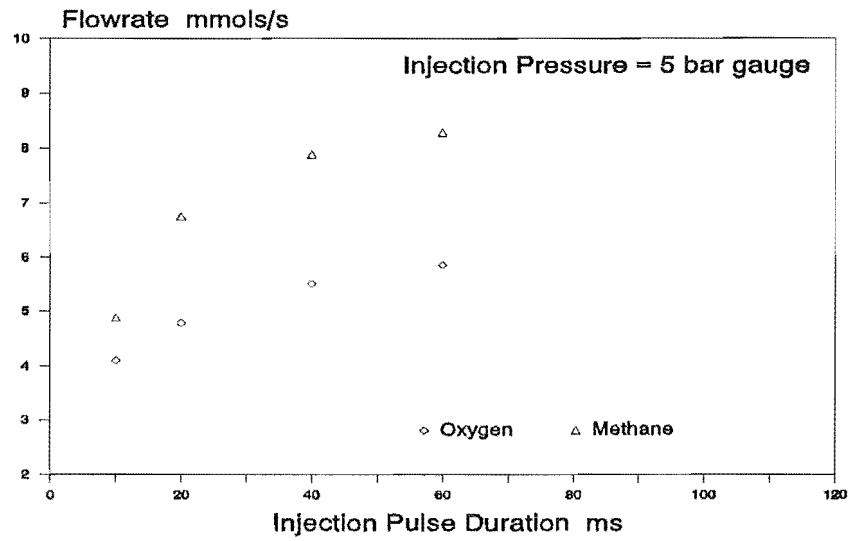

Figure 5.5 Variation of Apparent Molar Flowrate with Injection Pulse Duration

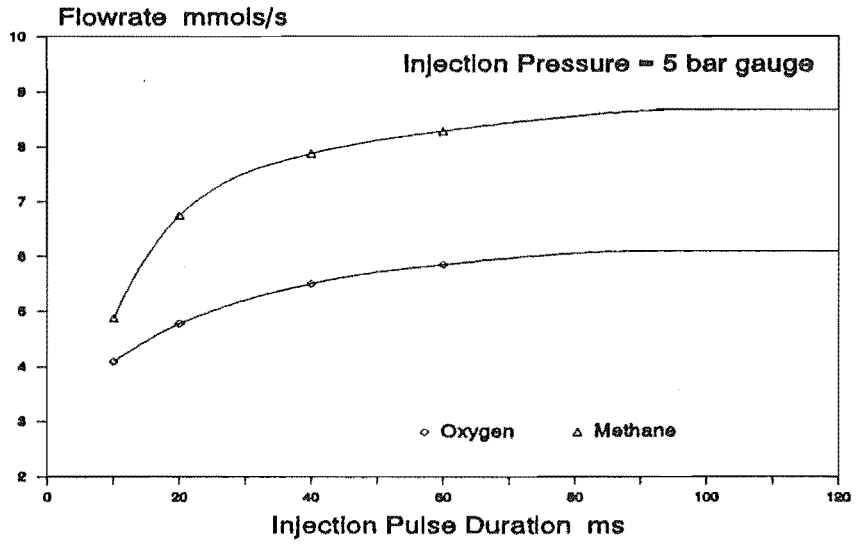

Figure 5.6 Spline Approximation of Apparent Flowrate Variation with Injection Pulse Duration

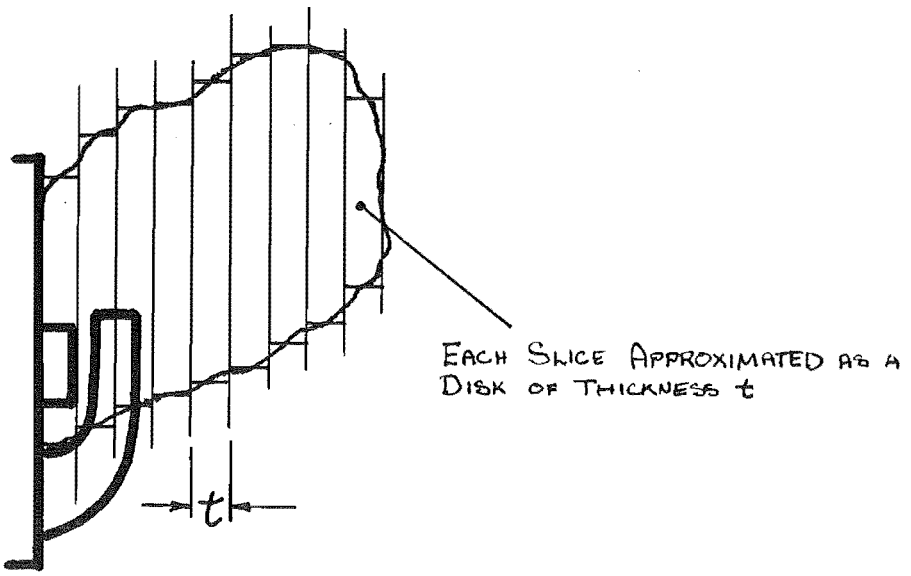

Figure 5.7 Approximation of Injected Puff Volume

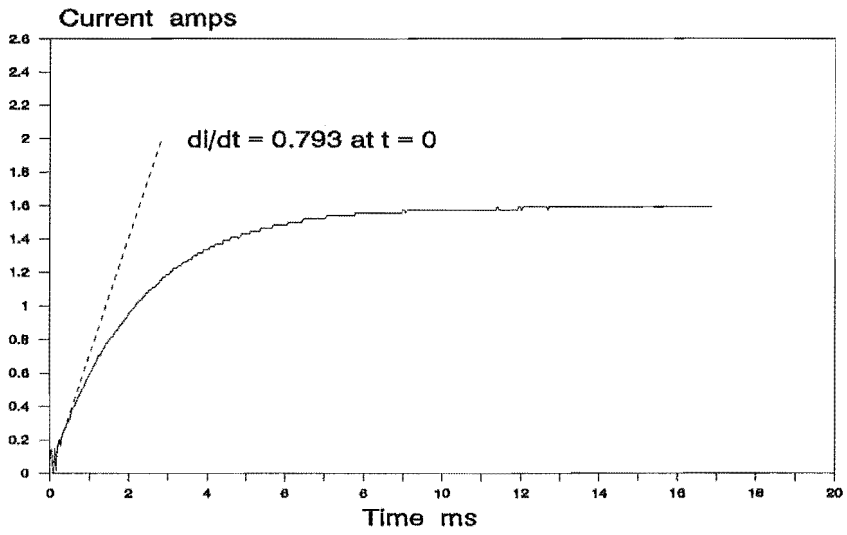

Figure 5.8 Current-Time Trace of Coil HA 12

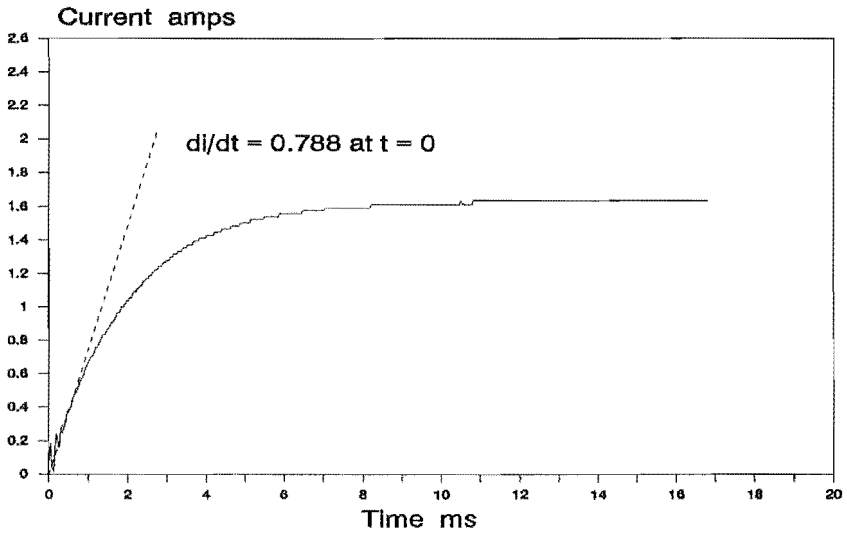

Figure 5.9 Current-Time Trace of Coil SP 12

t_{inj} = 8ms

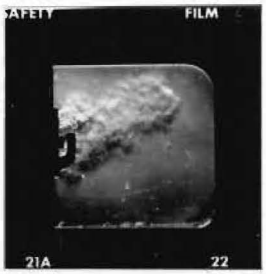

t_{inj} = 10ms

Plate 5.1 Schlieren Photographs of Injected Gas Puff

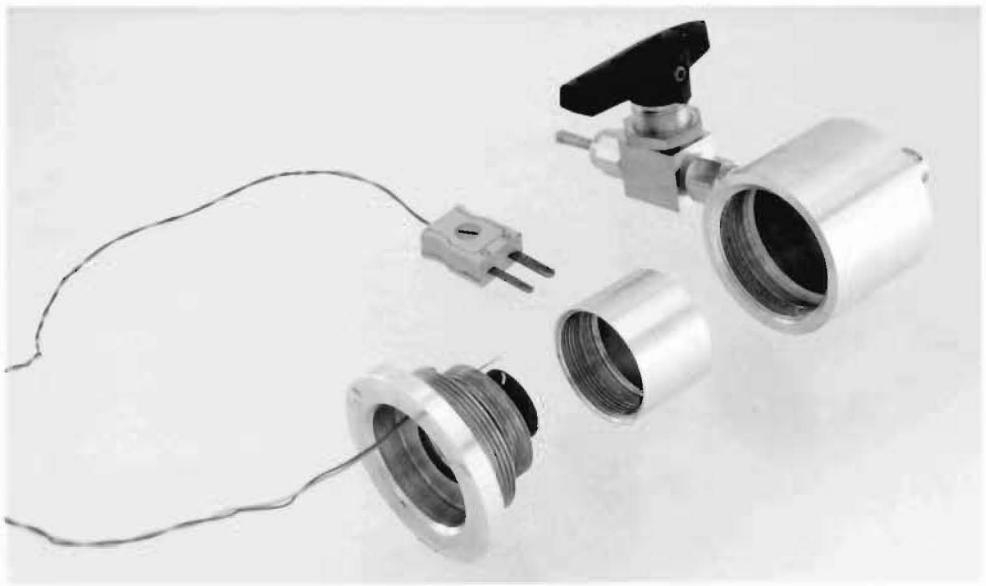

Plate 5.2 Spark Calorimeter Disassembled

Plate 5.3 Spark Calorimeter Assembled

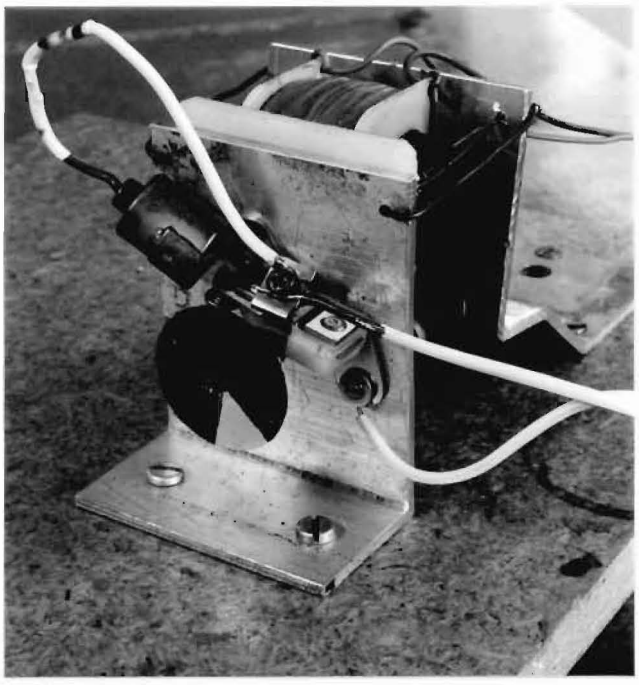

Plate 5.4 Breaker Points

CHAPTER 6

TESTING PROCEDURE

6.1 INTRODUCTION

This chapter will outline the testing programme that was undertaken. Much preliminary testing was carried out before the test programme proper began, and this helped to finalise the testing procedure. Detailed descriptions of the methods used for producing the test and injection mixtures, and the procedure used for the tests themselves will be described. Data recording methods will also be described.

6.2 TESTING PROGRAMME

The test programme needed to address the three primary objectives of the research;

(1) What effect does the stratified charge created by the puff injection have upon the ignition performance of very lean mixtures.

(2) Can a flame in a combustible mixture progress into a region where the concentration of fuel is below the normally accepted lean limit of flammability, and continue propagating.

(3) If the above does occur, is the propagation self sustaining or does the flame die after a certain period of travel in the ultra-lean region.

A programme was then devised to study the above concerns.

(a) Baseline Tests

The smallest bomb (250 mm long) would be used to find the lean limit of flammability of a methane-oxygen mixture for the rig, in its present set-up. This would involve finding the leanest mixtures that the low energy (12 V DC) ignition and high energy (24 V DC) ignition could ignite.

(b) Effect of Charge Stratification

Still using the small bomb, puffs of approximately 10% CH_4-O_2 would be used to create an easily ignitable mixture in the vicinity of the spark electrodes, ie. a stratified charge. Injection durations from 15 through to 60 ms would be used to observe the effect of the injected puff size on ignitability and combustion performance of very lean or ultra lean test mixtures. For each duration the timing of the spark relative to the end of injection would be altered from 10 ms before to 40 ms after injection ended.

(c) Length of Flame Travel

The bomb length would be increased to 500 mm and then further to 1000 mm, and the same mixture strengths as used in the tests above studied to observe how the changing length of the flame travel affected the results.

Preliminary testing showed there was no need to look at easily burnable mixtures (ie. λ less than 5) so the test program would concentrate on the very lean and ultra lean, that is with λ greater than 5. It was decided that the same injection mixture would be used for all tests due to time limitations. The strength of this mixture was set at approximately λ = 4.5, as this is easy to ignite and would ease the problems associated enrichment of the test mixture due to non-ignition (Appendix E). The initial pressure for all tests would be kept at 0.5 bar gauge as this would eliminate the chance of charge contamination from outside air.

It had originally been hoped that the gauge fill pressure would be altered to take account of the variations in atmospheric pressure, and hence the initial pressure would always be 1.5 bar absolute. However the required adjustments were so small that they were beyond the resolution of the pressure gauge used to fill the bomb, and it was therefore decided to use a constant gauge fill pressure. The injection pressure would be kept constant at 5 bar gauge (see Section 5.3.1).

6.3 PRODUCING A TEST MIXTURE

The test mixture is produced by mixing methane and oxygen in the test mixture vessel. The vessel is evacuated using the vacuum pump to approximately 0.03 bar absolute. The vessel is then filled with methane to approximately 3 bar absolute, and then re-evacuated. This procedure ensures that any remnants of the previous mixture present in the vessel are reduced to negligible proportions. This can be

carried out as many times as necessary but it was found that once was sufficient to ensure repeatable mixture creation.

After the vessel has reached the maximum vacuum once more, it is filled to the required partial pressure of methane (P_m) for the desired mixture strength (eg. for a total fill pressure of 10 bar absolute, a 5% methane in oxygen mixture requires a partial pressure of 10 * 5% = 0.5 bar absolute). It should be noted that this gives the O/F (oxidiser to fuel) ratio in volumetric terms, not on a mass basis. The pressure and temperature are allowed to settle, and then recorded. This temperature T_1 is now the reference temperature to which the remainder of the filling process must be corrected to.

After the pressure and temperature have settled the required total fill pressure (P_{fr}) is calculated, based on the actual value of P_m, which will typically not be exactly as intended. The vessel is then filled with oxygen up to P_f, which is approximately the same as the required total fill pressure. The temperature will have now risen to some value T_2 (due to the compression of the molecules already in the vessel by the incoming gas). This temperature rise depends on how fast the oxygen is added (ie. the faster the fill the less time for the extra heat to be lost to the vessel walls) and is typically about 5 to 7°C. As this drops the pressure in the vessel will also drop, so extra oxygen must be added to compensate.

There are two ways of dealing with this problem. The first is to let the mixture cool down until it reaches T_1, and then add a small amount of oxygen to bring the

pressure up to P_{fr}. This poses problems, the main one being that it takes a long time for the mixture to cool to T_1. The alternative is to compute the pressure to which the mixture will drop when it is at T_1, and then add the difference between this pressure P_f^+ and P_{fr} to the mixture. P_f^+ can be calculated by applying the perfect gas relationship to a constant volume cooling process in which no moles transfer takes place. We can say

$$\frac{P_f^+ V}{nT_1} = \frac{P_f V}{nT_2} \tag{6.1}$$

Cancelling n and V gives

$$P_f^+ = P_f \frac{T_1}{T_2} \tag{6.2}$$

where T_1 and T_2 are the absolute temperatures and P_f is the pressure in the vessel at T_2.

The best procedure was found to be as follows. After the vessel is initially filled with oxygen the pressure and temperature are left to stabilise, until the temperature T_2 drops to within 2°C of T_1, at which point any further decrease in temperature of the mixture is very slow. P_f and T_2 are then recorded and the pressure difference P_{fr} - P_f^+ calculated. It was found that calculating P_f^+ with the temperature any greater than this introduced too many errors because both the pressure and temperature were dropping to quickly (ie. it is important that the pressure and the temperature do not change while the calculation is being performed). The pressure difference is then added to P_f and the vessel filled with oxygen to this new pressure.

This pressure is again checked with Equation (6.2) to calculate the new value of P_f^+, which should be exactly the same as the required total fill pressure P_{fr}. The mixture strength is then calculated by dividing the methane partial pressure by P_{fr}, to give the percentage methane in the mixture (on a volumetric basis). Hence the O/F ratio and λ can be found.

Until now we have been assuming that the gas being used to fill the vessel is either pure methane or pure oxygen, but as stated in Section 4.3.2 this is not so. The methane is in fact 98% pure, with the remainder being mostly CO_2. The oxygen is 99.5% pure, the remainder being mostly nitrogen.

A calculation can be made relating the ideal λ_i of the mixture (assuming 100% purity for methane and oxygen) to the actual λ_a. In the reactants we have ideally

$$ACH_4 + BO_2 \tag{6.3}$$

where A and B are the concentrations of methane and oxygen respectively. In reality we have

$$A\ [0.98CH_4 + 0.02M] + B\ [0.995O_2 + 0.005M] \tag{6.4}$$

where M represents the impurities. We can now write λ_i as

$$\lambda_i = \left[\frac{B}{A}\right] \frac{1}{C} \tag{6.5}$$

where C is the stoichiometric O/F ratio (equals 2 for methane-oxygen). λ_a can be written as

$$\lambda_a = \left[\frac{0.995B}{0.98A}\right]\frac{1}{C} \tag{6.6}$$

Eliminating C, and B/A then gives

$$\lambda_a = 1.0153\lambda_i \tag{6.7}$$

A test mixture was left for at least 18 hours before use. It had been intended to leave them longer (48 hours) but preliminary experiments while setting the rig up had shown that 18 hours produced an acceptable degree of repeatability in explosions of the same mixture.

An estimation of the errors involved in these calculations is given in Appendix F, but in practice it is possible to produce mixtures to a resolution of 0.1% methane, the mixtures giving good repeatability and differentiation (ie. the differences in behaviour of mixtures differing by 0.1% methane are quite clear).

Although not mentioned at all here, the injection mixtures are produced in an identical manner in the injection mixture vessel, but whereas a new test mixture needs to be made every day, one vessel of injection mixture can last for weeks (obviously the exact length of time depends on the injection duration used and the injection pressure). The injection mixture strength was kept constant for all tests, at $\lambda = 4.57$ (9.9% CH_4 - this includes correction for gas purity).

6.4 PERFORMING A TEST

To start the tests for a day the computer, oscilloscope and piezo channel are turned on and left to warm up for ten minutes. The power to the timing control box is also turned on, along with power to the ignition coils and gas injector. The atmospheric pressure is recorded (during the testing this was checked at regular intervals but typically did not vary during the day). The vacuum pump is started and the bomb evacuated.

When the bomb reaches the maximum vacuum (approximately 0.03 bar absolute) it is filled with the test mixture to between 0.5 and 1 bar absolute to flush it of the previous explosion's products. The bomb is then re-evacuated and filled with the test mixture to 0.5 bar (gauge). This pressure is used because it eliminates the possibility that the charge might be contaminated with outside air and because it is a help to the pressure transducer in the bomb, as the transducer is operating in the lower portion of its range (see Section 4.2.3). A higher initial pressure means a higher explosion pressure and a greater pressure rise effectively increases the sensitivity of the transducer. The mixture is then left to sit in the bomb for at least 10 minutes. It was discovered during preliminary explosion testing that any shorter duration than this leads to inconsistencies in the explosions.

Immediately before the test the ignition timing and injection duration are set on the timing control box. The injection pressure is also set. To perform the tests the "Ground" switch on the piezo channel is depressed. This earths the pressure

transducer output to remove any stray voltage in the cable connecting the transducer to the piezo channel. The switch is then released and the "Fire" button on the timing control box is depressed immediately. It is now necessary to wait while the oscilloscope samples the output of the transducer and the ionisation probes. This may be a considerable length of time (up to five seconds). If the mixture has not ignited the above procedure can be repeated as many times as is thought necessary to confirm a non-ignition (see Appendix E).

If the mixture does produce a successful ignition, the pressure and ionisation traces on the oscilloscope are held by pressing the "Hold" button. This ensures the traces will not be lost due to stray triggering of the oscilloscope. The vacuum pump is restarted and the bomb is evacuated to just above atmospheric pressure (0.1 bar). The Kitagawa gas detector tube and pump are now used to take the CO_2 sample. Strictly, these tubes are calibrated for use at a constant atmospheric pressure but the size of the smallest bomb used (250 mm long) is such that the small amount of gas drawn off makes virtually no difference to the pressure. Having the pressure above atmospheric makes it simpler to tell when the pump has drawn though a large enough sample. The bomb is then evacuated in preparation for the next test.

6.5 RECORDING TEST RESULTS

A manual system is the primary means for gathering data from the explosions. Each test is given a unique number, and a special form is used to record all the

relevant data. Before the test, the test mixture λ, the initial and atmospheric pressures, the ambient and initial bomb temperatures and the ignition timing and injection duration are recorded. The oscilloscope settings are also logged. The explosion is then carried out, and afterward the pressure rise, the time of each ionisation probe signal, the number of ignition attempts, the CO_2 produced and the time to maximum pressure (TMP) are recorded.

To supplement this information, the data recorded on the oscilloscope (the pressure trace and the ionisation probe trace) is downloaded to a personal computer using the Metrabyte Dash-8 data acquisition system (see Section 4.6.3). This is done primarily as a backup and it has proven useful in that the pressure and ionisation traces of many tests could be compared to one another, which made small differences significantly easier to determine.

CHAPTER 7

RESULTS AND DISCUSSION

7.1 INTRODUCTION

This Section will cover the results obtained by the test programme. Over 250 individual tests were carried out, with test mixture strengths ranging from $\lambda = 6$ to $\lambda = 9$ (7.7% CH_4 in O_2 to 5.3% CH_4 in O_2). All equivalence ratios and mixture strengths given in this Chapter have been corrected for the impurity of the gases using Equation (6.7) in Section 6.3. Not all the individual test data has been presented, it only being given in those cases where it is necessary to illustrate a particular point.

The injection pressure used for all tests was 5 bar gauge, and the injection mixture was 9.9% CH_4-O_2 ($\lambda = 4.57$). All tests were conducted at room temperature, and since this varied slightly the maximum pressures obtained were corrected to a standard initial temperature of 25°C, and an initial pressure of 1.5 bar absolute (see, for example, Green[101] for method of correction).

7.2 IGNITION BY SPARK ALONE

7.2.1 Leanest Ignitable Mixture

The first series of tests to be undertaken attempted to find the lean limit of flammability of methane-oxygen mixtures the combustion rig when only the electric spark was used for ignition. This was done so that the effectiveness of using the methane-oxygen puff as the ignition enhancer could be determined. The smallest (250 mm long) bomb was used initially for these tests. The tests were repeated in the longer (500 mm and 1000 mm) bombs, there being no change in the leanest mixture ignitable by the electric spark alone. It was found that the leanest mixture ignitable with the low energy ignition system (12 V) was that of λ = 6.26 (7.4% CH_4), while the high energy ignition (24 V) could be used down to λ = 7.31 (6.4% CH_4). The mixture of strength λ = 7.31 will be defined as the ELLOF.* The testing procedure proved to be easily repeatable, and the resolution was good, for example a mixture of 7.4% CH_4 would always ignite, whereas one of 7.3% CH_4 would never ignite.

7.2.2 Minimum Ignition Energy

The energy available in the spark was measured as described in Section 5.4.2, these values being 3.95 mJ and 6.87 mJ for the 12 V and 24 V sparks respectively. The

---

* Equipment Lean Limit Of Flammability

energy in a spark can be considered to be the minimum ignition energy of the leanest mixture ignitable with that spark. Therefore we can say that the minimum ignition energy of a methane-oxygen mixture of λ = 6.26 is 3.95 mJ (and hence is 6.87 mJ for a mixture of λ = 7.31). Much empirical data has been gathered by various researchers (see Section 3.5) regarding the minimum ignition energy of different combustible mixtures, and literature sources agree (within an order of magnitude) with the above stated values.[64,65,66] Considering the relative crudity of the spark energy measuring device, order of magnitude agreement is acceptable.

7.3 EFFECT OF INJECTED PUFF ON IGNITION

7.3.1 Puff Ignition Versus Spark Alone

For a mixture that could be ignited by the spark alone the main benefit provided by the injection of a small puff of methane-oxygen was the increased speed of ignition. This can be seen in Figure 7.1.

A mixture (λ = 6.084) in the 250 mm bomb was ignited by a spark occurring 25 ms after the "fire" button was depressed (hereafter pushing the "fire" button will be referred to as the test start). A second test used exactly the same mixture but injected a puff of 9.9% methane-oxygen, the injection ending at 15 ms ATS (After Test Start). This gave an injection duration of 11 ms, remembering that there is a delay of 4 ms between the test start and the relay activating (see Section 4.5.2).

The spark then occurred at 25 ms ATS (this sequence of events is shown figuratively in Figure 7.2).

As can be seen in Figure 7.1 the major differences between the two tests is the rate at which combustion commences when the puff is used as the ignition source. The puff provides a much more rapid initial rate of burning and it can be seen that the second test has a TMPI (Time to Maximum Pressure from Ignition) of 125 ms compared to 145 ms for the spark alone. This represents an increase in the average flame speed of approximately 13.5% (the average flame speed is an approximation and is defined by assuming the flame moves at a constant speed from the beginning to the end of the bomb, and that the occurrence of the spark represents the flame at the beginning of the bomb, and the point of maximum pressure the end of the bomb). By observation we can show that this time saving is made up in the initiation of the flame, because beyond 60 ms ATS the pressure traces of the two tests lie almost parallel to each other. This is similar to the observations of Pitt *et al*,[107,108,109] who compared a puff jet ignition system to a plasma jet ignition and a high energy capacitor discharge ignition. The puff jet used by Pitt was in principle the same as that used here but the injector was placed in the engine or bomb in such a way that it could create a puff around the spark electrodes, rather than injecting through the spark plug itself. The system proved especially beneficial for lean mixtures. The puff jet was shown to produce similar ignition characteristics to a high energy plasma jet ignition, but with significantly less electrode erosion and energy consumption. Speed of ignition was shown to be much superior to a conventional capacitor discharge system in engine testing.

It is important to compare the amount of energy available in the injected puff to that available in the spark alone. We can calculate the total number of moles injected using the procedure in Section 5.3.3. Thus if we multiply the number of moles of methane injected (calculated from the equivalence ratio of the injection mixture, allowing for impurities) by its calorific value (50 MJ/kg = 800 KJ/mol[92]) we can obtain the energy injected. For the tests described above this energy is 3.68 J, compared to 6.87 mJ for the high energy (24 V) spark alone. This confirms that the puff jet is a very effective means of obtaining a high energy ignition system with relatively little complication, as claimed by Pitt. It is also easy to vary the energy in the puff simply by increasing the duration of the puff.

7.3.2 Shape of the Pressure Trace

An unusual effect is displayed in the pressure traces of Figure 7.1 this being the "Double Hump". The rate of pressure rise increases after ignition as one would expect (the flame is not moving at a constant speed - the expansion of the burnt gas causes the pressure in the bomb to rise, and this causes the burning velocity to rise, which in turn increases the rate of pressure rise. See Section 3.6.1). It then reaches a plateau where the rate of pressure rise decreases before eventually increasing again up to the point of maximum pressure. It will be noticed that this "Hump" occurs both with and without injection. It is the author's opinion that the "Hump" represents the point at which the flame changes from three to two dimensional propagation.

After ignition, the flame burns as a hemisphere, that is in three dimensions. The rate of pressure rise is a function of the quantity of reactants consumed, and the quantity of reactants consumed is a function of the flame front area. When the flame hemisphere reaches its maximum size (ie. the diameter of the bomb) it can progress as a hemisphere no further, and assumes an increasingly planar (ie. two dimensional) shape as it proceeds along the bomb.* A planar shape has considerably less surface area than a hemisphere of the same diameter, and hence the rate of reactant consumption would decrease. Since the rate of pressure rise is a function of this, it too would decrease. A contributing factor may be that the hemispherical flame has a low surface area/volume ratio compared to the cylinder like volume behind a planar flame front. This would reduce the heat losses for the hemispherical flame, which would increase the reaction rate due to the higher temperature (reaction rate is dependant on temperature according to the Arrhenius Factor $e^{-E/RT}$).

7.3.3 Effect of Changing Injection Duration

To observe the effect of increasing puff duration, injection timings ranging up to 60 ms ATS were studied. The effect of increasing injection duration can be seen in Figure 7.3. The mixture is the same as that used in the test described above, ie. λ = 6.084. The slower igniting mixture used a puff ending 15 ms ATS and the faster

---

* Not strictly true. In a horizontal bomb the flame does become approximately planar for only a short distance, then assuming an "hook" like shape due to buoyancy effects. See Section 3.7.3.

50 ms ATS. In both tests the spark occurred 5 ms AEI (After the End of Injection), that is at 20 ms ATS and 55 ms ATS respectively.

The 50 ms ATS puff provides a much greater energy input than the smaller one, 21.22 J compared to 3.68 J. As can be seen the larger puff provides a much more efficient ignition, offering a similar improvement over the 15 ms ATS puff as that puff did over none at all. This is shown by comparing the values of TMPI, 110 ms for the 50 ms ATS puff compared to 135 ms for the 15 ms ATS puff. This again represents an increase of approximately 18% in the average flame speed, compared to an 13.5% increase for the 15 ms ATS puff over none at all.

It might be thought that such a large puff would significantly alter the overall strength of the mixture in the bomb. The fact that this is not so is demonstrated in Appendix E.

For the testing programme, the main advantage of long injection durations was the fact that it assured reliable ignition. Even if the test mixture would not ignite, the puff would, and it could be seen that only the puff had burnt from the magnitude of the pressure trace. Short (approximately 10 ms ATS) puffs proved quite hard to ignite, probably due to ease with which a small puff can move away from the spark electrodes. In this case it was difficult to tell whether a test mixture did not burn because it would not ignite at all, or whether just the puff would not ignite.

7.3.4 Effect of Changing Ignition Timing

Tests were also carried out in an attempt to determine when the spark should occur relative to the end of the injection pulse for the best results. It was immediately discovered that triggering the spark before the injection had ended was counterproductive. Even for mixtures that would ignite with the spark alone, firing the spark before the end of injection produced much less reliable ignition. It is thought that this was due to the very high velocity and turbulence of the injection mixture gas stream as it flowed past the spark plug electrodes. This creates velocity fields with gradients of such magnitude that ignition or flame propagation beyond the ignition kernel is impossible due to the area variation phenomena (flame stretch - see Section 3.2.4).[45,110] Turbulence itself causes an increase in the ignition energy due to increased heat dissipation.[111] Turbulent straining may also be significant depending on the turbulence scale.[112]

Triggering the spark exactly at the end of injection was an improvement. The best method proved to be triggering the spark at least 5 ms AEI. A delay of around 10 ms was the best compromise in terms of reliability of ignition, although for long injection durations (40 ms ATS) delays of up to 40 ms AEI were used without problems. The delay was probably necessary to let the turbulence level produced by the puff injection decrease a little. This would improve the ease of ignition for the reasons stated in the preceding paragraph. Long delays (greater than 20 ms AEI) could not be used for short injection durations (less than 20 ms ATS). It appeared the puff either moved away from the electrodes or diffused sufficiently

into the test mixture in the bomb that it produced no noticeable effect (the test mixture behaved as though no injection had taken place). The length of delay did not have any noticeable effect on the speed of ignition or the rate of pressure rise.

7.4 THE LEAN LIMIT OF FLAMMABILITY

The definition of the lean limit of flammability for a given set of initial conditions is the leanest mixture which will ignite and burn completely. Tests were carried out using progressively leaner test mixtures in an attempt to find this limit. Testing was carried out in the 250 mm long bomb, the 500 mm and finally the 1000 mm long bomb.

There were three main measures of the completeness of the combustion, namely the pressure rise, the carbon dioxide level produced by the explosion, and the average flame speed. As anticipated, using the injected puff allowed much leaner mixtures to be ignited than the electric spark alone. Mixture strengths ranged from λ = 7.6 (6.2% CH_4) to as lean as λ = 8.9 (5.3% CH_4).

7.4.1 Peak Pressure

The pressure rise produced for each test was recorded. Each was then divided by the adiabatic pressure rise predicted for a mixture of that concentration (Section

5.2). This fraction will be hereafter called the FAPPR (Fraction of Adiabatic Peak Pressure Rise) of the explosion. It was hoped that this would produce a linear relationship (each explosion should have approximately the same heat losses) which would decrease sharply when the lean limit was encountered. The results for the 250 mm bomb can be seen in Figure 7.4 and those for the 500 mm bomb can be seen in Figure 7.5. The graph for the 1000 mm bomb is not given here as it produced some unusual effects that will be discussed in Section 7.6.2.

As can be seen from both Figure 7.4 and Figure 7.5, the FAPPR starts with a value of approximately 0.47 when λ is around 7.5. The FAPPR drops slightly as λ becomes leaner. This is not unexpected as the reaction rate and hence the flame speed drop as a natural consequence of the mixture becoming leaner. This increases the time available for heat losses to occur from the burnt gases, and hence the FAPPR will fall.

When λ = 8.35, the FAPPR v λ curve takes a sudden drop. This is interpreted as the ELLOF. The combustion of the puff is no longer producing sufficient energy to produce self sustaining combustion in the test mixture. It can be seen from Figure 7.4 and Figure 7.5 that the behaviour of the 250 mm bomb and the 500 mm bomb is essentially the same, with the lean limit occurring at an almost identical value of λ.

Although some combustion is taking place below the lean limit, this is primarily due to burning of the puff and some of the internal mixture which has been enrichened

by entrainment with the puff. When the mixture is at or very close to the lean limit, the amount of internal mixture that is enrichened is quite significant, as only a very slight increase in the concentration of the methane is required to make the mixture combustible. The exact amount of entrainment seems to vary significantly with each explosion, especially at the lean limit. This is evidenced by the large spread in the FAPPR for mixtures at the limit. This is probably due to the fact that the entrainment process is governed by the turbulence induced by the injection of the puff, and will vary from test to test.

The size of the injection puff is also significant, as a bigger puff can enrich more of the test mixture and hence lead to a greater FAPPR. This can be seen in Figure 7.6. The smaller pressure rise was for an injection ending 15 ms ATS, while the greater was for an injection ending 40 ms ATS. In both cases the ignition occurred 5 ms AEI, and the test mixture strength was λ = 8.499.

Increasing the ignition delay for limit mixtures also tended to increase the FAPPR, due to the greater time available for entrainment. The effect was not nearly as marked as for increasing the injection duration as can be seen in Figure 7.7. The smaller pressure rise had an ignition 5 ms AEI, and the greater 10 ms AEI. Injection for both cases ended 15 ms ATS, and the test mixture strength was λ = 8.499. Increasing the injection delay further did not generally produce any greater improvement in the FAPPR. Very long delays should be detrimental, but this could not be observed due to the limitations of the timing control box.

7.4.2 Average Flame Speed

The rate of reaction in a combustible mixture is a function of, amongst other things, the relative concentrations of the fuel and oxidiser (ie. the mixture strength). As the concentration of the fuel becomes less (ie. the mixture becomes leaner, λ increasing), the reaction rate decreases. In a constant volume bomb this leads to a reduction in the average flame speed (hereafter abbreviated as AFS).

If a graph of the AFS v λ was plotted, it would be expected that the AFS would gradually decrease as λ increased. When λ reached the lean limit it would be expected the AFS would begin to increase once again, to a limit of infinity. This is because the AFS is inversely proportional to the TMPI, and if the mixture in the bomb fails to burn completely, the TMPI would decrease and hence the AFS would increase.

Graphs of the AFS v λ were plotted for the 250 mm and 500 mm bomb (that of the 1000 mm bomb is not given here for the same reasons as in the previous Section). These are shown in Figure 7.8 and Figure 7.9. As can be seen they follow the predicted trend closely. If we define the minimum point of the curve as the lean limit then it can be seen that the limit is approximately at $\lambda = 8.35$. This closely matches the result found in the previous Section. However the minimum on both graphs is not particularly sharp, but more intensive testing could probably resolve this to a greater degree.

There is some spread in the values of AFS for a given mixture strength, especially for the 250 mm bomb. For the most part this is probably due to the improved ignition initiation (see Section 7.3.3) obtained when larger injection puffs were used although some variability in the AFS at around the lean limit due to random variations in the initiation of the combustion process is not unknown.[45,113]

7.4.3 Carbon Dioxide Production

The final measure of the completeness of an explosion was the quantity of the CO_2 produced. The quantity of CO_2 produced in an adiabatic explosion could be predicted using the method described in Section 5.2. The actual CO_2 produced was then divided by the adiabatic value to produce the FACP (Fraction of Adiabatic Carbon dioxide Production). This was plotted against λ to produce the graphs shown in Figure 7.10 and Figure 7.11 (250 mm and 500 mm bomb respectively).

The first point of interest is the large spread of results, even for mixtures of the same strength. A significant part of this is due to the relatively poor accuracy of the gas detector tubes used. For a typical mixture that burnt completely, about 7% of the products (by volume) would be CO_2. The gas detector tubes could only read to ± 0.5% CO_2, that is the total error possible in the quantity of CO_2 measured was typically ± 7% (0.5/7). By itself this error is not large enough to explain the spread of results, and a contributing factor is probably how quickly the sample was taken. As the temperature in the bomb dropped, the water produced in the explosion

condensed out, and this would increase the concentration of the CO_2 relative to the other remaining gaseous products. If the sample was taken quickly, less water would have condensed, and this would have lowered the relative concentration of the CO_2. Therefore because all samples were not taken exactly the same time after the explosions a significant inaccuracy may have occurred here. Although the gas detector tubes had the virtue of simplicity, these results show that for accurate gas sampling in the future some other method (eg gas chromatograph, mass spectrometer) would be desirable. However it must be emphasized that some degree of scatter in the combustion products, even in a controlled combustion environment, is expected, this being especially so near the lean limit of flammability.[101]

The condensation of the water in the products explains why some explosions produce a FACP value of greater than unity. The concentration of CO_2 predicted by the adiabatic flame temperature program described in Section 5.2 assumes the water is still in vapour form, whereas in practice the majority of water would have condensed by the time the sample was taken. If desired the program could be modified to accommodate this.

Both Figure 7.10 and Figure 7.11 the same trend as observed in previous Sections, that is there is a significant fall in the FACP at the lean limit. This point is still approximately at $\lambda = 8.35$, but the trend is much less marked than for the graphs of FAPPR v λ and AFS v λ. It is probable that the trend would be clearer if the problems regarding the CO_2 measurement were solved.

7.4.4 Comparison with the Accepted Lean Limit

It will be remembered from Sections 1.3 and 6.2 that one of the intended objectives of this investigation was to see whether a flame front could propagate from a flammable mixture into one below the normally accepted or ideal lean limit of flammability,* and continue burning. From the discussion in the preceding Sections it is clear that the ELLOF for methane-oxygen mixtures at the stated initial conditions (1.5 bar absolute, 25°C) and in the present rig configuration (horizontal bomb, 250 mm and 500 mm long) is at λ = 8.35 (5.65% methane).

The generally accepted ILLOF of methane in oxygen is λ = 8.93[45,70] (5.3% methane). However this limit has been obtained for upward flame propagation in a tube, and it is well known that the mode of propagation is critical in determining the flammability limits (see Section 3.4.2). Two other studies by Bone,[90] and Hsieh and Townend[89] used horizontal bombs of 50 mm diameter and 45 mm diameter respectively. Both these studies found a flammability limit of λ = 8.42 (5.60% methane). The ELLOF obtained by this investigation is therefore in close agreement with these.

It is therefore clear that combustion has not been sustained below the normally accepted ILLOF. This confirms the findings of Karim *et al*,[95] who used a 2.5 m long, 95 mm diameter vertical tube to study stratified methane-air mixtures. The bottom half of the tube could be filled with a rich mixture and the top with a lean

---

* Hereafter abbreviated as ILLOF (Ideal Lean Limit Of Flammability)

mixture. A plate valve separating the two halves could then be opened and the tube left for a certain time to produce a known concentration gradient as the two mixtures diffused into one another. The flame propagated upward, and it was found that "...a rapidly propagating flame through the lower half of the tube soon came to an abrupt end, once it reached the severe concentration interphase between the two mixtures." They then concluded that "...mixtures below the flammability limit do not get consumed by a rapidly propagating flame."

Another study by Liebman *et al* [114] used a quite similar method and did find an extension of the lean limit for downward propagating flames in methane-air mixtures from 6.1% methane to 5.7%. Much gentler concentration gradients were used than those of Karim *et al*, and the authors state that the flame only propagated to the limit point, that is it did not continue propagating in the limit mixture. This is basically a matter of defining where the flame is extinguished. A flame that is propagating and reaches a severe concentration interphase cannot die instantaneously, but will carry on a short distance until there is insufficient heat to cause any further reaction. Thus even though the limit mixture burnt a little, it is not the same as saying sustained combustion in that limit mixture is possible.

Having said this however, it is clear that the use of the puff jet ignition has significantly extended the ELLOF, from λ = 7.31 (6.4% methane) to λ = 8.35 (5.65% methane). This demonstrates that the stratified charge created by the injected puff is a useful method of improving flame propagation characteristics (especially flame initiation) in a non-ideal situation (for example, an engine).

7.5 COMBUSTION GENERATED TURBULENCE

An interesting observation can be made by comparing the graphs of AFS v λ (Figure 7.8 and Figure 7.9). The AFS for a given mixture is higher in the 500 mm bomb than the 250 mm bomb. This difference is quite marked, especially at the lean limit (0.35 m/s for the 500 mm bomb, 0.2 m/s for the 250 mm bomb). This was a most unexpected result. It was expected that the value of the AFS would remain constant for a given mixture for different bomb lengths.

Initially this difference was attributed to the reduced surface area/volume ratio of the 500 mm bomb compared to the 250 mm one. This would lead to reduced heat losses and hence a faster reaction rate (and therefore a higher AFS). However the reduced surface area/volume ratio would only reduce heat losses by 9.4%, whereas the AFS has increased by as much as 75%.

It therefore seemed that some mechanism was increasing the reaction rate (and hence AFS) as the flame progressed along the bomb, this mechanism being in addition to the rise in reaction rate due to the compression of the unburnt gas.

It is hypothesised that the mechanism responsible for this reaction rate increase is the self-generation of turbulence by the flame as it progresses along the bomb. The causes of and circumstances leading to FGT have been discussed in Section 3.7 and in reviewing this it will be seen that the mixtures used for the testing programme described in this thesis are susceptible to the some of the phenomena reported.

For example, the mixtures have a great deal of stoichiometric imbalance (ie. they are very lean) and the deficient component (methane) has a high diffusivity compared to the excess component (oxygen). This should lead to flame wrinkling by diffusional stratification. Some test explosions produced audible vibrations, and this is consistent with the phenomena described by Lewis and Von Elbe[45] for slow burning mixtures. However just because a test mixture could produce FGT does not mean it does, but evidence was obtained in the test programme to suggest that the creation of FGT is definitely occurring, and it is further suggested that it is responsible for some unusual effects observed.

7.6 EVIDENCE AND CONSEQUENCES OF FGT

7.6.1 Flame Ionisation Probes

As stated in Section 7.5, the variation in AFS with bomb length gave the initial clue that some mechanism was acting to accelerate the flame. The confirmation of that mechanism came from the ionisation probe trace. These probes (described in Section 4.2.2) recorded the time it took for the flame to reach a certain position in the bomb. For the majority of the testing programme the probes were mounted along the top of the bomb. All tests in which complete combustion occurred showed that the flame appeared to be reaching the end of the bomb a significant amount of time before the point of maximum pressure. This is shown in Figure 7.13 (test mixture equivalence ratio λ = 7.20 (6.5% methane), 250 mm

bomb, arrangement of ionisation probes as shown in Figure 7.12). At first it was thought that this was due to post flame front reactions,[96] but the length of delay was too great for this explanation to be feasible. In addition tests with the thermocouple probes and fibre optic probes (described in Section 4.2.2) showed the point of maximum light emission from the explosion coincided with the point of maximum pressure. It was thought that this showed the flame was continuing to propagate in some manner after it had passed the final ionisation probe.

In response the above it was felt that the most likely explanation was that the flame was propagating along the top of the bomb at a greater rate than the bottom, due to the buoyancy effects described in Section 3.7.3. To verify this some tests were conducted with the bomb upsidedown, ie. the ionisation probes on the bottom. An identical mixture (λ = 7.20) to the test described in the previous paragraph was fired with identical initial conditions and the ionisation trace recorded. This is also shown on Figure 7.13 for ease of comparison.

As can be seen there is clear evidence that buoyancy significantly affects the flame propagation. The virtually identical pressure traces show that the flame propagation is the same for each test. The flame reaches the first and second probes slightly later on the bottom than the top. This is consistent with the flame shape obtained by Smith,[83] and Coward and Hartwell.[81,82] However, after this the flame propagation along the bottom of the bomb must virtually cease, as evidenced by the long delay between the second and third probe peaks on the bottom. This implies that induction of the unburnt mixtures below the flame front is taking place,

and hence a considerable bulk swirl motion is being imparted to the mixture. The flattened shape of the final probe peak on the bottom of the bomb implies the flame front was travelling in a direction parallel to the probe centreline when it came into contact with it (established from preliminary tests with the ionisation probes), that is it was no longer travelling parallel to the bomb centreline. The probable path of the flame front from these observations is thus sketched in Figure 7.14.

It is thought that the cone shaped flame described in Section 3.6.2 as typical of closed vessel explosions (and shown in Figure 3.6) will not develop, as the trapped unburnt mixture can escape under the flame front (that is along the bottom of the bomb), due to the flame front's assymetery. This is supported by the virtual ceasing of flame propagation along the bottom of the bomb after half distance. This effect probably assists the buoyancy significantly in the creation of swirl in the mixture.

7.6.2 Flame Quenching by Turbulence

The final series of tests to be carried out used the 1000 mm long bomb. It might be expected that this bomb would behave in much the same manner as the smaller two bombs used (ie. 250 mm and 500 mm), but this proved not to be the case.

Figure 7.15 shows the graph of FAPPR v λ for the 1000 mm bomb. As can be seen this differs significantly from those of the two smaller bombs (Figure 7.4 and

Figure 7.5 for the 250 mm and 500 mm bombs respectively). For a mixture burning to completion the FAPPR is approximately 0.4, the same as for the smaller bombs. However the graph, instead of falling slightly as λ increases, and then dropping sharply as the ELLOF is encountered, begins to drop at a steady rate when λ is approximately 7.7. This behaviour implies that there is no definite lean limit in the 1000 mm bomb, and that mixtures of $\lambda > 7.7$, although successfully ignited, somehow extinguish themselves after a certain distance of propagation. Ionisation probe traces tended to confirm this but the records were not reproducible due to data sampling limitations. This is quite different to the smaller two bombs where a definite lean limit of $\lambda = 8.35$ existed, and if a mixture was successfully ignited it burnt completely.

The propagation distance is function of λ, that is as λ increases the propagation distance decreases. This trend is confirmed by the graphs shown in Figure 7.16 and Figure 7.17, these showing AFS v λ and FACP v λ for the 1000 mm bomb respectively. The AFS v λ graph shows a minimum at approximately $\lambda = 7.7$, giving the same limit for complete combustion as does Figure 7.15. The graph of FACP v λ also shows a gradual decline, rather than a sharply defined limit as would be expected from the earlier results.

Since the flame appears to be extinguishing itself after a certain propagation distance, the question must be asked regarding what mechanism is responsible for the quenching. As explained in Section 3.2.3, if the combustion were truly adiabatic, then once a flame front was established in a quiescent mixture, and

propagating under steady conditions, it could not be extinguished. However, as explained in Section 7.6.1, for all the tests described in this research it seems certain that the flame is generating its own turbulence as it propagates, and this turbulence offers a possible solution.

Turbulent propagation of flames is generally associated with increased reaction rates and hence higher values of AFS. Increasing turbulence leads to a higher reaction rate, until a point is reached at which increasing turbulence inhibits flame propagation.[101,115,116] This phenomenon is known as gas phase quenching. Many models have been presented to explain this process, but it is still not well understood. The exact flame quenching mechanism put forward by each model is dependent on the mode of flame propagation studied. The mechanism is generally one in which the surface area increase of the flame (attributed to such things as small and large scale eddies, flame stretch and cellular flamelets) causes the heat loss to the unburnt gas to exceed the heat production by chemical reaction, hence causing quenching.

Therefore it seems possible that flames in the 1000 mm bomb are being quenched by their own self generated turbulence. Since the FGT is self increasing, it is possible that it attains a level high enough to induce gas phase quenching of the flame. Alternatively the FGT can increase the flame velocity to such an extent that a detonation wave develops, but this could not occur for the mixtures used in the testing programme because of their very lean condition (lean limit of detonability of methane-oxygen is approximately $\lambda = 7.5$[117,118]). The quenching of the

combustion by FGT also offers a solution to the observation that leaner mixtures are quenched more quickly than richer ones. As the mixture becomes leaner, its flame speed drops slightly due to its slightly decreased reaction rate. This decrease is only small, as evidenced by Figure 7.16. Thus the turbulence generated would also decrease slightly for a given distance of flame propagation. However, near the lean limit the amount of heat loss from the reaction required for quenching decreases rapidly as the limit is approached.[45,93] Therefore the level of turbulence generated by different mixtures for a given distance of propagation remains approximately constant relative to the amount of heat loss required for quenching. As leaner mixtures require less heat loss for quenching, they propagate a shorter distance.

No model has been discovered which describes the quenching of flames in tubes or bombs by their own FGT, but it is possible that with further work one could be developed. It is also interesting to speculate on the effects of using a still longer bomb. It would seem likely that flames below the lean limit of detonability (λ = 7.5) would eventually be quenched by increasing FGT, and those richer than λ = 7.5 would continue to propagate as detonation waves.

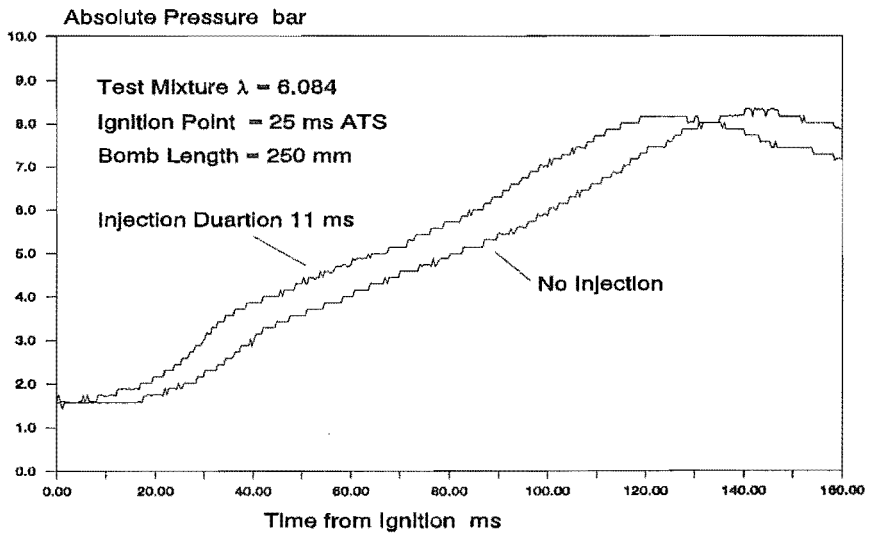

Figure 7.1 Effect of Puff Size on Ignition Speed

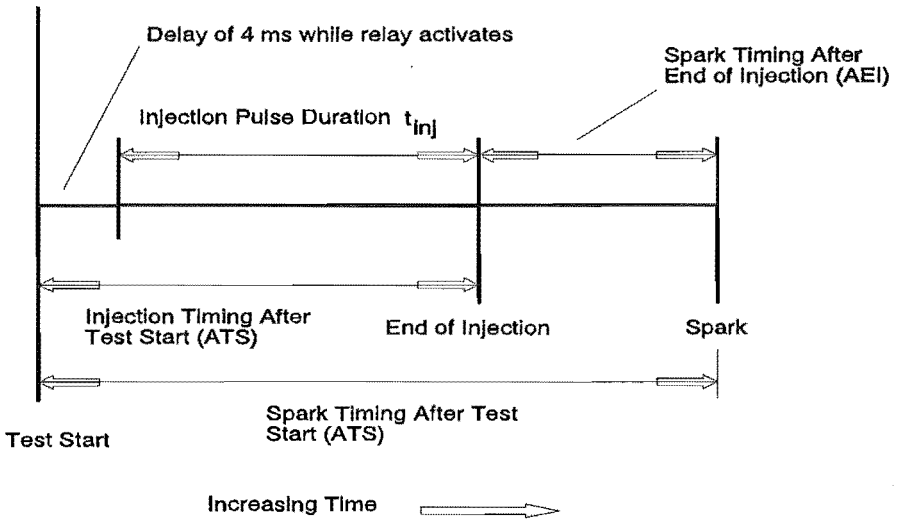

Figure 7.2 Injection and Ignition Timing

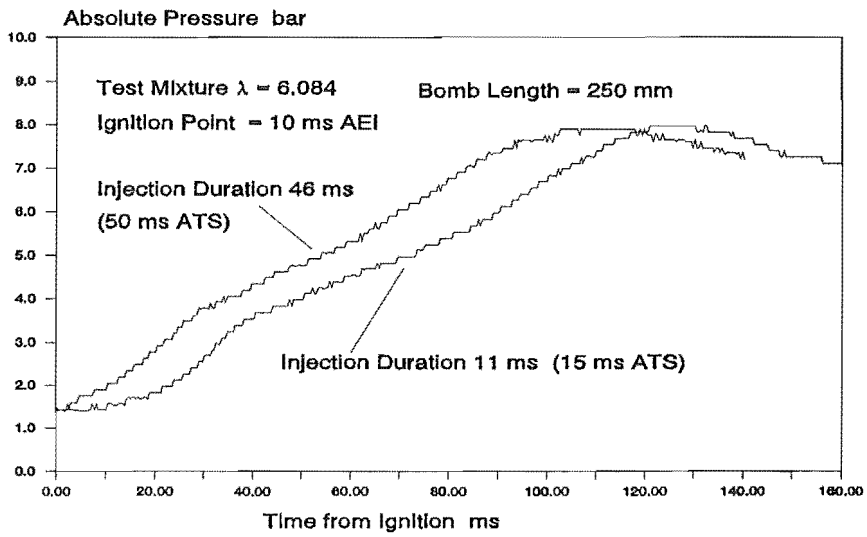

Figure 7.3 Effect of Puff Size on Ignition Speed

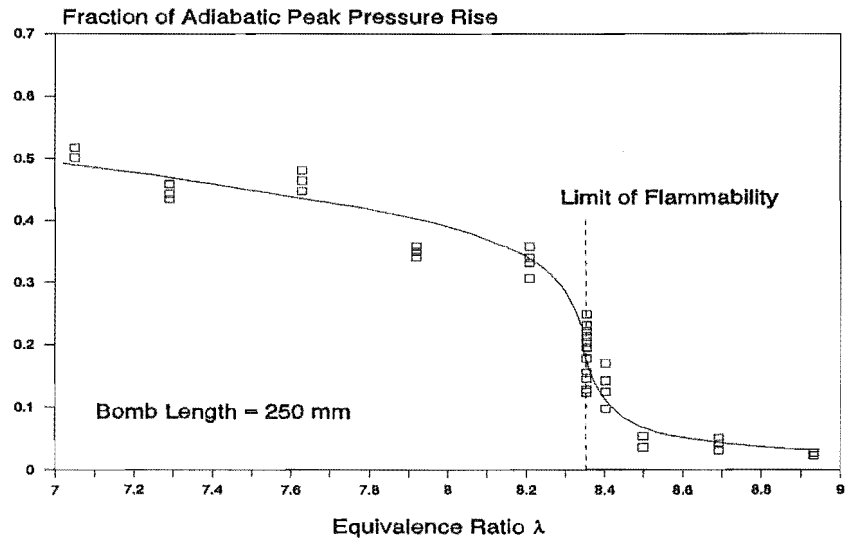

Figure 7.4 FAPPR versus λ for 250 mm Bomb Length

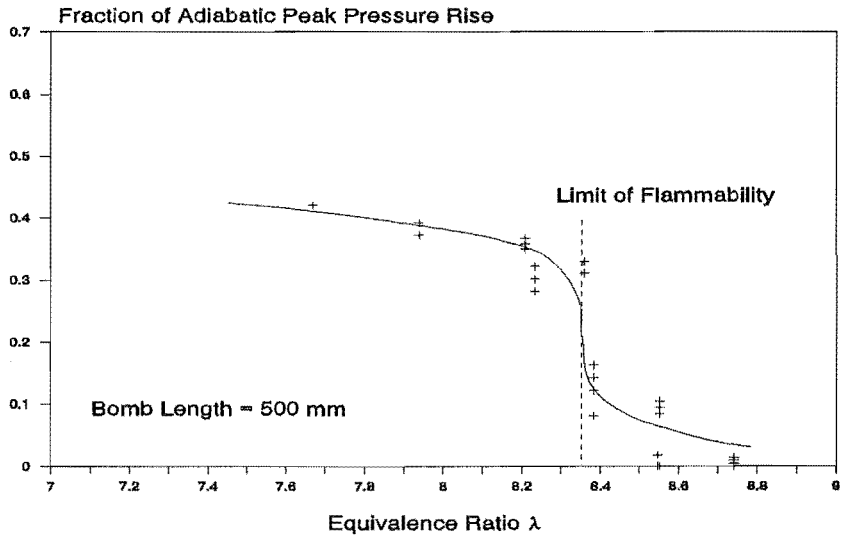

Figure 7.5 FAPPR versus λ for 500 mm Bomb Length

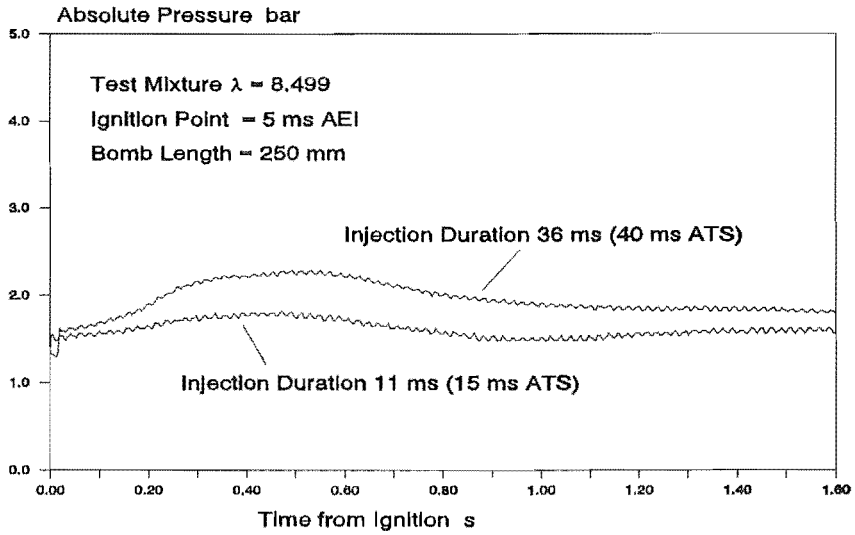

Figure 7.6 Effect of Larger Puff on Mixtures Below the Lean Flammability Limit

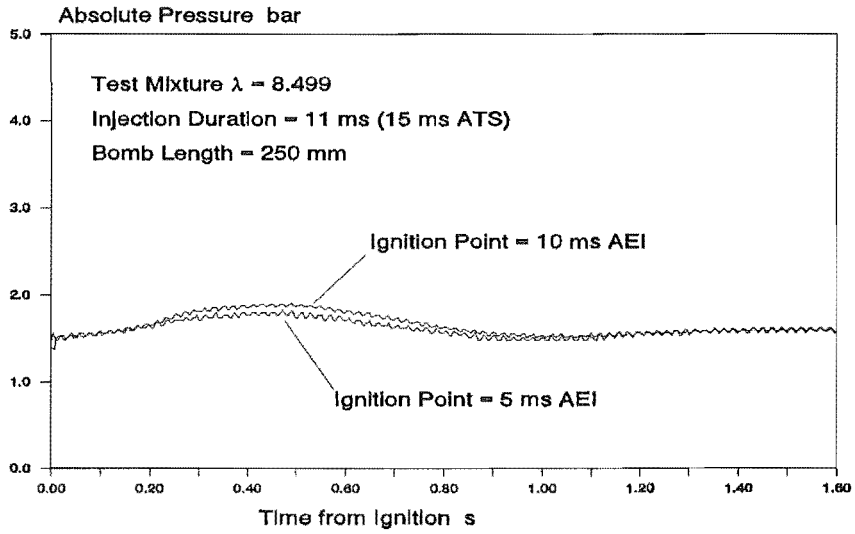

Figure 7.7 Effect of Greater Ignition Delay for Mixtures Below the Lean Flammability Limit

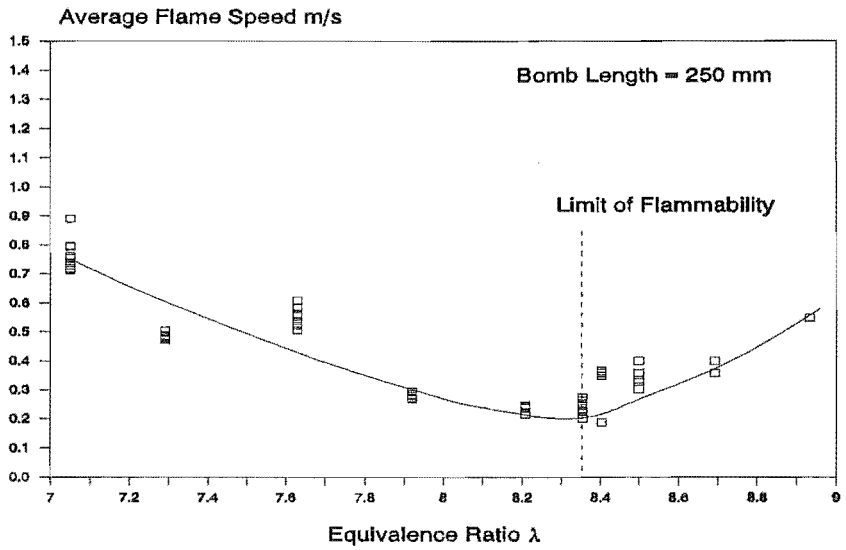

Figure 7.8 AFS versus λ for 250 mm Bomb Length

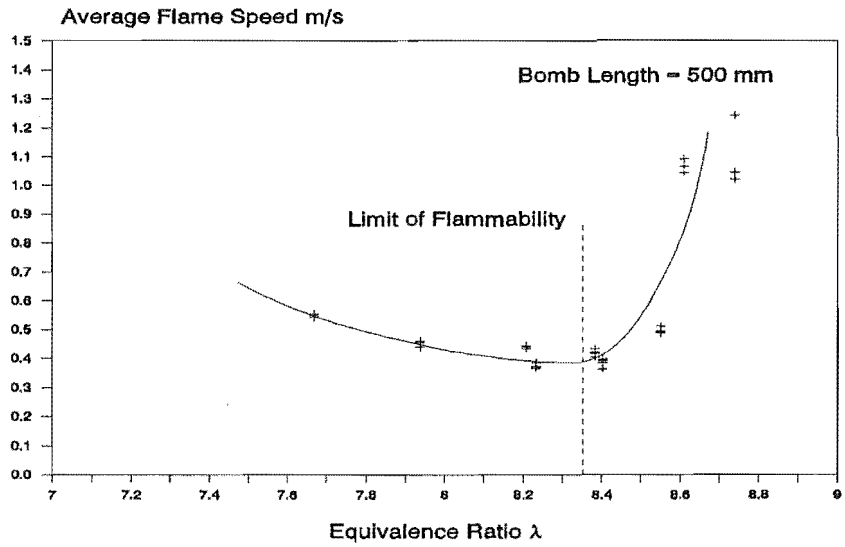

Figure 7.9 AFS versus λ for 500 mm Bomb Length

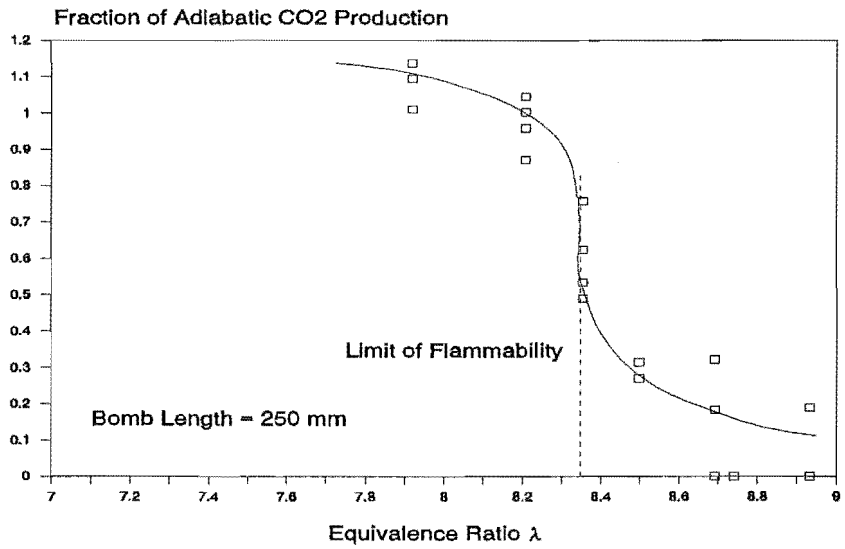

Figure 7.10 FACP versus λ for 250 mm Bomb Length

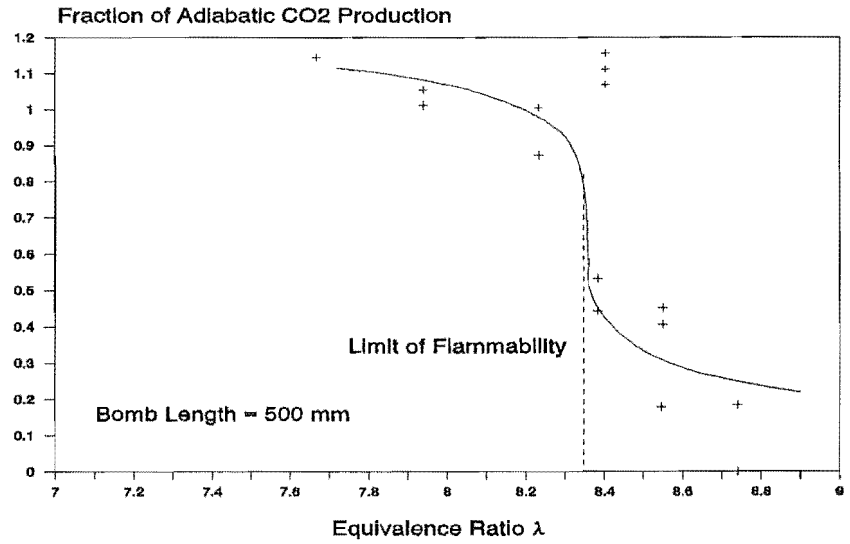

Figure 7.11 FACP versus λ for 500 mm Bomb Length

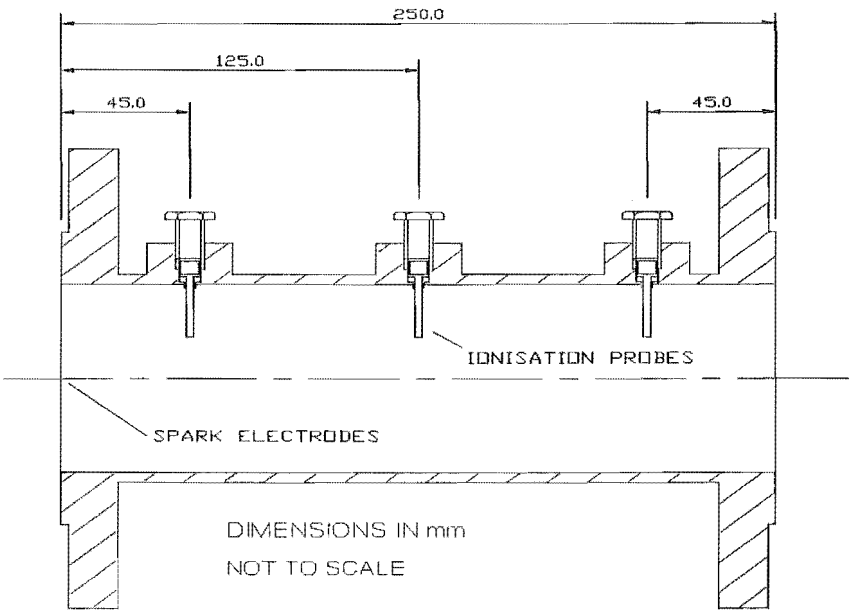

Figure 7.12 Setup of Three Ionisation Probes on 250 mm Long Bomb

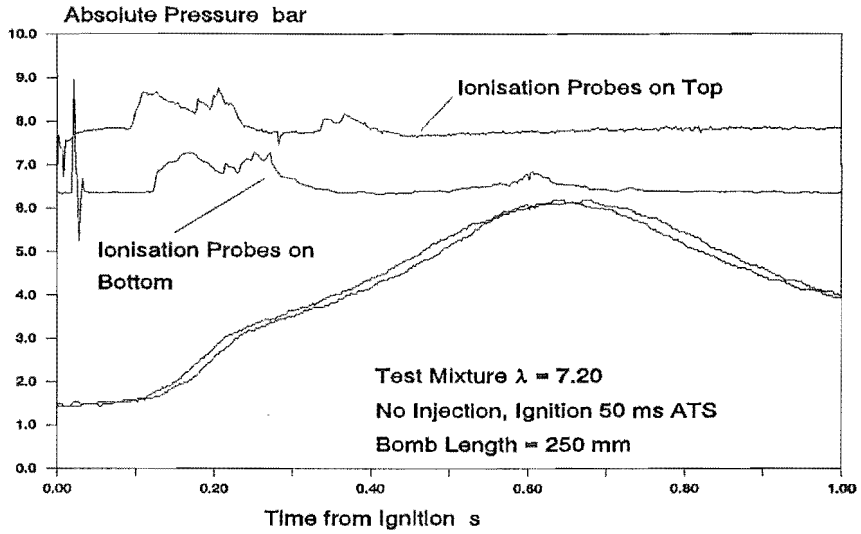

Figure 7.13 Ionisation Probe Traces Along Top and Bottom of Bomb

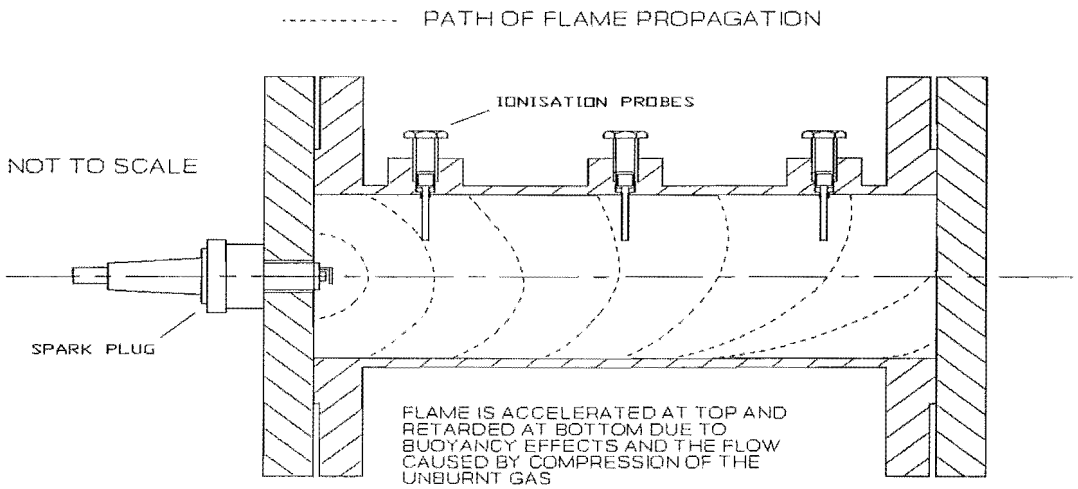

Figure 7.14 Probable Path of Flame in Bomb

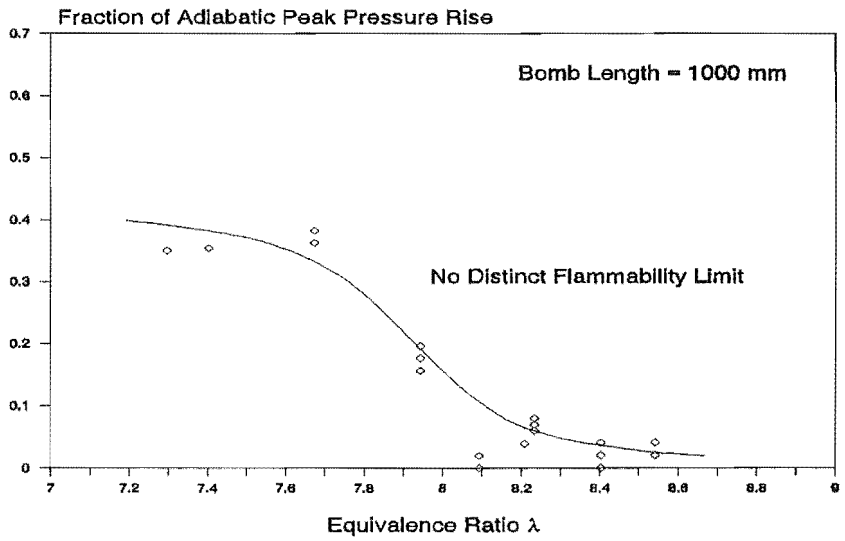

Figure 7.15 FAPPR versus λ for 1000 mm Bomb Length

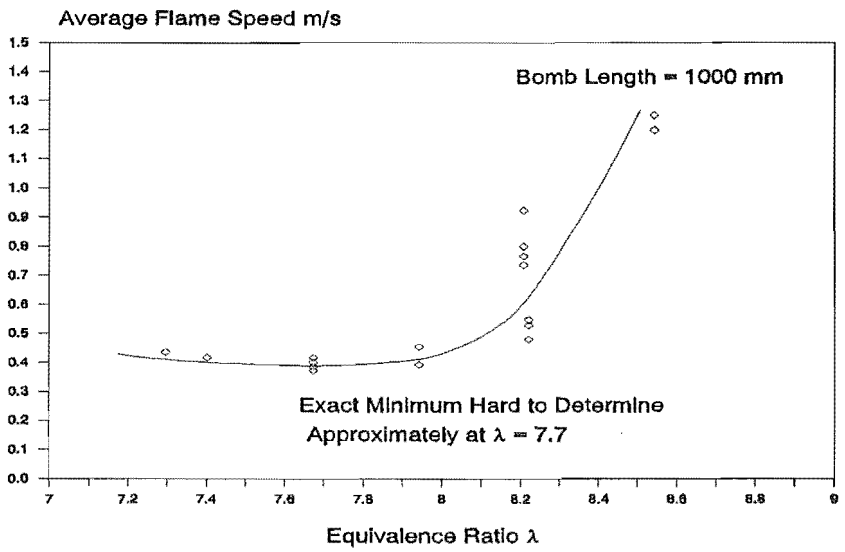

Figure 7.16 AFS versus λ for 1000 mm Bomb Length

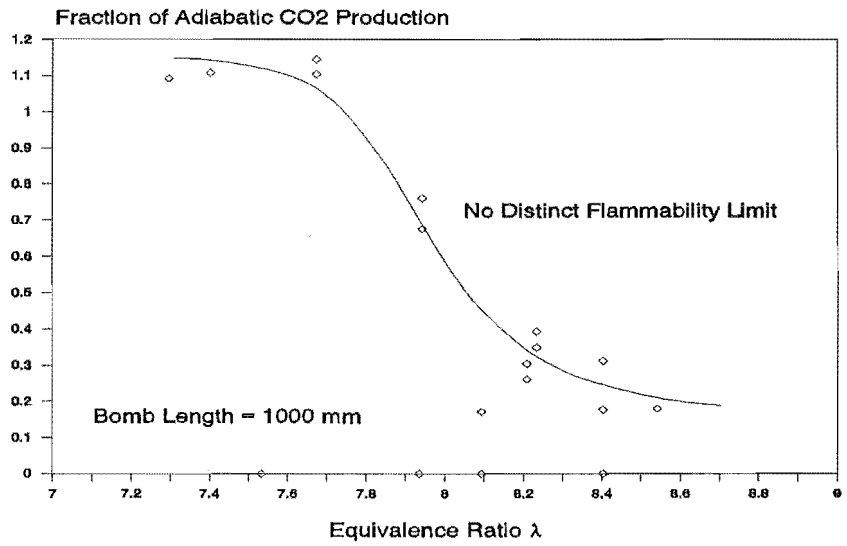

Figure 7.17 FACP versus λ for 1000 mm Bomb Length

CHAPTER 8

CONCLUSIONS AND RECOMMENDATIONS

8.1 CONCLUSIONS

The work described in this thesis has enabled the following conclusions to be drawn for the combustion of lean methane-oxygen mixtures in a cylindrical constant volume bomb.

(a) The puff jet ignition system, injecting a premixed 9.9% methane-oxygen mixture, is an efficient and reliable method of ignition for very lean methane-oxygen mixtures.

(b) Even with premixed injection, it has been shown that a delay of approximately 10 ms between the end of the injection and the firing of the spark is desirable for reliable ignition. This is attributed to the decay of the turbulence produced in the puff.

(c) Injection durations of greater than 20 ms improved the reliability of ignition but did not alter the leanest mixture for which complete combustion is possible.

The study of the propagation of the flame in the combustion rig shows the following.

(a) The use of charge stratification as a method of ignition does not extend the ideal lean limit of flammability of methane-oxygen mixtures. This shows that mixtures below the flammability limit are not consumed by a propagating flame. However the puff injection is a suitable means for extending the equipment lean limit of flammability in non-ideal situations.

(b) The equipment lean limit of flammability obtained using the puff jet ignition (for methane-oxygen mixtures in the 250 mm and 500 mm long bombs) is $\lambda = 8.35$ (5.65% CH_4). For the mode of flame propagation (horizontal, cylindrical constant volume bomb) this value is in agreement with that given by other researchers.

(c) For the longest bomb used (1000 mm) the results with lean mixtures ($\lambda > 7.7$) show that the flame dies out in the bomb after successful ignition has been achieved, and that therefore a clear lean flammability limit does not exist in this case.

(d) Experimental evidence shows that the flame is accelerating as it propagates, and it is proposed that the mechanism for this acceleration is the self generation of turbulence by the flame. Tests

also show that buoyancy of the hot gas behind the flame is probably responsible for a significant degree of this turbulence. It is proposed that turbulence induced gas phase quenching is the most likely cause of the partial burning of a successfully ignited charge in the 1000 mm bomb.

The above stated points show that all the major objectives intended of this work (as given in Sections 1.3 and 6.2) have been achieved. In addition some unusual combustion effects have been observed and a possible explanation for the cause of these has been proposed. It is realised that the majority of the conclusions reached may not have any immediate application to a practical engine using charge stratification, but it hoped that they will help further the fundamental understanding of the combustion process.

8.2 RECOMMENDATIONS FOR FUTURE WORK

8.2.1 Combustion Apparatus

Now that a successful combustion rig has been built studies of a similar nature can be made on a whole range of fuel-oxidiser combinations. With a little modification, the test conditions (mode of flame propagation, initial pressure or temperature, etc) can be varied. The following areas of the rig are considered to need improvement.

(a) Ionisation Probes. For studies that concentrate on stoichiometric fuel-oxidiser mixtures the present system should suffice. Improvement needs to be made for near limit mixtures, to eliminate noise and sensitivity problems. Whether the ionisation probes could be retained is unclear, but the phototransducer with fibre-optic cable probes described briefly in Section 4.2.2 could be the answer if developed further.

(b) Gas Sampling. A mass spectrometer or gas chromatograph would be highly desirable to replace the inaccurate gas detector tubes used at present. This would allow for the study of pollutant production mechanisms, which should be of interest in the future.

(c) Vacuum System. A rotary vacuum pump would be an improvement on the present venturi pump, both in terms of more efficient evacuation of the bomb and mixing cylinders, and also the speed of evacuation for very large vessels, for which the venturi was intolerably slow.

(d) Timing Control Box. The replacement of the present device (which uses electro-mechanical relays) with a fully digital system would enable closer control of injection and ignition timings, especially in the 0-10 ms range.

8.2.2 Combustion Research

It is felt that future research should include the following areas:

(a) Theoretical investigation of burning velocities from rate constants and reaction mechanisms. This could possibly be the first step toward a complete model of the flame. The effects of including flame generated turbulence could be studied.

(b) Experimental determination of the flame generated turbulence ahead of the flame front, using, for example, hot-wire anemometry or laser anemometry.

(c) Experimental investigation of whether the puff jet ignition system can reduce cycle to cycle variation in an engine running on very lean mixtures.

REFERENCES

(1) BLACKMORE, D AND THOMAS, A "Fuel Economy of the Gasoline Engine" First Edition Macmillan Press Ltd London (1977) 268p.

(2) PERKINS, H "Air Pollution" First Edition McGraw Hill Book Company New York (1974) 407p.

(3) QUADER, A "Lean Combustion and the Misfire Limit in Spark Ignition Engines" SAE Paper 741055 (1974)

(4) HANSEL, J "Lean Automotive Engine Operation" SAE Paper 710164 (1971)

(5) PATTERSON, D "Cylinder Pressure Variations - a Fundamental Problem" SAE Paper 660129 (1966)

(6) PETERS, B "Mass Burning Rates in a Spark Ignition Engine Operating in the Partial Burn Regime" Paper C92/79 Proceedings of IMechE Conference on Fuel Economy and Emissions in Lean Burn Engines p.63 (1979)

(7) DANIEL, W "Why Engine Variables Affect Exhaust Hydrocarbon Emissions" SAE Paper 700108 (1970)

(8) KAISER, E, ROTHSCHILD, W AND LAVOIE, G "The Effect of Fuel and Operating Variables on Hydrocarbon Species Distribution in the Exhaust from a Multi-Cylinder Engine" Combustion Science and Technology Vol 32 p.245 (1983)

(9) NEWHALL, H AND EL MESSERI, I "A Combustion Chamber Designed for Minimum Exhaust Emissions" SAE Paper 700491 (1970)

(10) NEWHALL, H AND STARKMAN, E "Direct Spectroscopic Determination of Nitric Oxide in Reciprocating Engine Cylinders" SAE Paper 670122 (1967)

(11) HEYWOOD, J "Pollutant Formation and Control in Spark Ignition Engines" Progress in Energy and Combustion Science Vol 1 p.135 (1976)

(12) BLUMBERG, P AND KUMMER, J "Prediction of NO Formation in Spark Ignition Engines - an Analysis of Methods of Control" Combustion Science and Technology Vol 4 p.73 (1971)

(13) KOMIYAMA, K AND HEYWOOD, J "Predicting NO Emissions and Effects of EGR in Spark Ignited Engines" SAE Paper 730475 (1973)

(14) NEWHALL, H "Kinetics of Engine Generated Nitrogen Oxides and Carbon Monoxide" Twelfth Symposium on Combustion (International) p.603 (1969)

(15) PISCHINGER, F AND KLEINSCHMIDT, W "Study of NO, NO_2 and CO Formation in Spark Ignited Engines Using Extended Reaction Kinetics" Combustion Institute European Symposium p.457 (1973)

(16) GREEN, R AND ZAVIER, C "Charge Stratification in a Spark Ignition Engine" IMechE Proceedings Vol 206 p.59 (1992)

(17) DATE, T, YAGI, S, ISHIZUYA, A AND FUJI, L "Research and Development of the Honda CVCC Engine" SAE Paper 740605 (1974)

(18) BISHOP, I AND SIMKO, A "A New Concept of Stratified Charge Combustion - Ford Combustion Process" SAE Paper 680041 (1968)

(19) MITCHELL, E, COBB, J AND FROST, R "Design and Evaluation of a Stratified Charge Multifuel Military Engine" SAE Paper 680042 (1968)

(20) WOOD, C "Performance of a Stratified Charge Engine" SAE Paper 790434 (1979)

(21) ZAVIER, C "Charge Stratification for an Internal Combustion Engine" Master of Engineering (Mechanical) Thesis University of Canterbury

(1991) 165p.

(22) MELVIN, A "Natural Gas - Basic Science and Technology" First Edition IOP Publishing Ltd Bristol (1988) 221p.

(23) BRITISH PETROLEUM CO. LTD. "Gas Making and Natural Gas" First Edition Ben Johnson and Company Ltd York (1972) 305p.

(24) FOX, A "The Future Climate for the Exploration of Gas" Proceedings of an Institute of Petroleum Conference on the Outlook for Natural Gas p.21 (1972)

(25) PEEBLES, M AND GELLARD, M "Natural Gas in the Future Energy Picture" Proceedings of an Institute of Petroleum Conference on the Outlook for Natural Gas p.237 (1972)

(26) SHARMA, S AND MOHAN, C "Fuels and Combustion" First Edition Tata McGraw Hill Publishing Company Ltd. New Delhi (1984) 500p.

(27) FIRTH, A "Gas Sales to the Domestic Market" Proceedings of an Institute of Petroleum Conference on the Future of Natural Gas p.165 (1972)

(28) BELL, C, BOULTER, S, DUNLOP, D AND KEILLER, P "Methane: Fuel of the Future - an Assessment" First Edition Prism Press Dorchester (1973) 85p.

(29) FRISTROM, R AND WESTENBERG, A "Flame Structure" First Edition McGraw Hill Book Company Ltd. New York (1965) 424p.

(30) FENIMORE, C AND JONES, G "Rate of Reaction of Methane with H Atoms and OH Radicals in Flames" Journal of Physical Chemistry Vol 65 p.2200 (1961)

(31) WONG, E AND POTTER, A "Reaction Rates of Hydrogen, Ammonia and Methane with Mixtures of Atomic and Molecular Oxygen" Journal of Chemical Physics Vol 39 p.2211 (1963)

(32) FENIMORE, C AND JONES, G "Formation of Carbon Monoxide in Methane Flames by Reaction of Oxygen Atoms with Methyl Radicals" Journal of Physical Chemistry Vol 65 p.1532 (1961)

(33) WIRES, R, WATERMEIER, L AND STREHLOW, R "The Dry Carbon Monoxide-Oxygen Flame" Journal of Physical Chemistry Vol 63 p.989 (1959)

(34) TSATSARONIS, G "Prediction of Propagating Laminar Flames in Methane, Oxygen and Nitrogen Mixtures" Combustion and Flame Vol 33 p.217 (1978)

(35) WARNATZ, J "The Structure of Laminar Alkane-, Alkene- and Acetylene Flames" Eighteenth Symposium on Combustion (International) p.369

(1981)

(36) WESTBROOK, C AND DRYER, F "A Comprehensive Mechanism for Methanol Oxidation" Combustion Science and Technology Vol 20 p.125 (1979)

(37) BURKE, S AND SCHUMANN, T "Diffusion Flames" Industrial Engineering Chemistry Vol 20 p.998 (1928)

(38) FRISTROM, R, GRUNFELDER, C AND FAVIN, S "Methane-Oxygen Flame Structure" Journal of Physical Chemistry Vol 64 p.1386 (1960)

(39) WESTENBERG, A AND FAVIN, S "The Theory of a Spherical Premixed Laminar Flame" Combustion and Flame Vol 3 p.161 (1960)

(40) FRISTROM, R "Structure of Laminar Flame Fronts" Sixth Symposium on Combustion (International) p.96 (1956)

(41) FRISTROM, R, AVERY, W AND GRUNFELDER, C "Reactions of Simple Hydrocarbons in Flame Fronts" Seventh Symposium on Combustion (International) p.304 (1959)

(42) HIRSCHFELDER, J AND CURTISS, C "Theory of Propagation in Flames" Third Symposium on Combustion, Flame and Explosion Phenomena (International) p.121 (1949)

(43) VON KARMAN, T "Present Status of the Theory of Laminar Flame Propagation" Sixth Symposium on Combustion (International) p.1 (1956)

(44) SPALDING, D "The Theory of Inflammability Limits and Flame Quenching" Proceedings of the Royal Society (London) Vol A240 p.83 (1957)

(45) LEWIS, B AND VON ELBE, G "Combustion, Flames and Explosions of Gases" Second Edition Academic Press New York (1961) 725p.

(46) MELVIN, A AND MOSS, J "Evidence for the Failure of the Flame Stretch Concept for Premixed Flames" Combustion Science and Technology Vol 7 p.189 (1973)

(47) STREHLOW, R AND SAVAGE, L "The Concept of Flame Stretch" Combustion and Flame Vol 31 p.209 (1978)

(48) MATALON, M "On Flame Stretch" Combustion Science and Technology Vol 31 p.169 (1983)

(49) CHUNG, S AND LAW, C "An Invariant Derivation of Flame Stretch" Combustion and Flame Vol 55 p.123 (1984)

(50) LINNETT, J AND SIMPSON, J "Limits of Inflammability" Sixth Symposium on Combustion (International) p.20 (1956)

(51) GERSTEIN, M AND STINE, W "Analytical criteria for Flammability Limits" Fourteenth Symposium on Combustion (International) p.1109 (1973)

(52) EGERTON, A AND THABERT, S "Flame Propagation: Measurement of Burning Velocities of Slow Flames and Determination of Limits of Combustion" Proceedings of the Royal Society (London) Vol A211 p.445 (1952)

(53) EGERTON, A AND BADAMI, G "The Determination of Burning Velocities of Slow Flames" Proceedings of the Royal Society (London) Vol A228 p.297 (1955)

(54) DIXON-LEWIS, G AND ISLES, G "Limits of Inflammability" Seventh Symposium on Combustion (International) p.475 (1959)

(55) ANDREWS, G AND BRADLEY, D "Limits of Flammability and Natural Convection for Methane Air Mixtures" Fourteenth Symposium on Combustion (International) p.1119 (1973)

(56) ROSEN, G "Ignition of Combustible Gases" Journal of Chemical Physics Vol 30 p.298 (1959)

(57) DE SOETE, G "The Influence of Isotropic Turbulence on the Critical Ignition Energy" Thirteenth Symposium on Combustion (International)

p.735 (1971)

(58) BALLAL, D AND LEFEBVRE, A "The Influence of Flow Parameters on Minimum Ignition Energy and Quenching Distance" Fifteenth Symposium on Combustion (International) p.1473 (1975)

(59) MALY, R "Ignition Model for Spark Discharges and the Early Phase of Flame Front Growth" Eighteenth Symposium on Combustion (International) p.1747 (1981)

(60) AKINDELE, O, BRADLEY, D, MAK, P AND McMAHON, M "Spark Ignition of Turbulent Gases" Combustion and Flame Vol 47 p.129 (1982)

(61) MERZANOV, A AND AVERSON, A "The Present State of Thermal Ignition Theory - An Invited Review" Combustion and Flame Vol 16 p.89 (1971)

(62) DESHAIES, D AND JOULIN, G "On the Initiation of a Spherical Flame Kernel" Combustion Science and Technology Vol 37 p.99 (1984)

(63) TROMANS, P AND FURZELAND, R "An Analysis of Lewis Number and Flow Effects on the Ignition of Premixed Gases" Twentyfirst Symposium on Combustion (International) p.1891 (1986)

(64) GUEST, P, BLANC, M, LEWIS, B AND VON ELBE, G "Ignition of Explosive Gas Mixtures by Electric Sparks" Journal of Chemical Physics Vol 15 p.798 (1947)

(65) GUEST, P, BLANC, M, LEWIS, B AND VON ELBE, G "Ignition of Gas Mixtures by Electric Sparks" Third Symposium on Combustion, Flame and Explosion Phenomena (International) p.363 (1949)

(66) CALCOTE, H, GREGORY, C, BARNETT, C AND GILMER, R "Spark Ignition - Effect of Molecular Structure" Industrial Engineering Chemistry Vol 44 p.2656 (1952)

(67) ROSE, H AND PRIEDE, T "Ignition Phenomena in Hydrogen-Air Mixtures" Seventh Symposium on Combustion (International) p.436 (1959)

(68) LLEWELLYN-JONES, F "Arcing Phenomena at Electrical Contacts" Journal of the Institute of Electrical Engineers Vol 96 p.60 (1949)

(69) BALLAL, D AND LEFEBVRE, A "The Influence of Spark Discharge Characteristics on Minimum Ignition Energy in Flowing Gases" Combustion and Flame Vol 24 p.99 (1975)

(70) BOND, J "Sources of Ignition" Butterworth Heinemann London (1991) 156p.

(71) MORGAN, J "Note on the Vibrational Movements Which Occur During the Inflammation of Combustible Gases" Philosophical Magazine Vol 3 p.1161 (1927)

(72) MAXWELL, G AND WHEELER, R "Some Characteristics of Motor Fuels" Industrial Engineering Chemistry Vol 20 p.1041 (1928)

(73) ELLIS, O AND WHEELER, R "The Movement of Flames in Closed Vessels: After Burning" Journal of the Chemical Society Vol 130 p.310 (1927)

(74) DAVID, W "Turbulence in Internal Combustion Engines" The Engineer Vol 164 p.733 (1937)

(75) DAVID, W AND LEAH, A "Fuel Economy in Petrol Engines" IMechE Proceedings Vol 143 p.289 (1940)

(76) DAVID, W, LEAH, A AND PUGH, B "Latent Energy and Dissociation in Flame Gases" Philosophical Magazine Vol 31 p.156 (1941)

(77) KARLOVITZ, B, DENNISTON, D AND WELLS, F "Investigation of Turbulent Flames" Journal of Chemical Physics Vol 19 p.541 (1951)

(78) SCURLOCK, A AND GROVER, J "Propagation of Turbulent Flames" Fourth Symposium on Combustion (International) p.645 (1953)

(79) LEWIS, B, VON ELBE, G AND MANTON, J "Nonisotropic Propagation of Combustion Waves in Explosive Gas Mixtures" Journal of Chemical Physics Vol 20 p.153 (1952)

(80) MARKSTEIN, G "Cell Structure of Propane Flames Burning in Tubes" Journal of Chemical Physics Vol 17 p.428 (1949)

(81) COWARD, H AND HARTWELL, F "Studies in the Mechanism of Flame Movement: Part 1" Journal of the Chemical Society Vol 135 p.1996 (1932)

(82) COWARD, H AND HARTWELL, F "Studies in the Mechanism of Flame Movement: Part 2" Journal of the Chemical Society Vol 135 p.2676 (1932)

(83) SMITH, O, WESTBROOK, C AND SAWYER, R "Lean Limit Combustion in an Expanding Chamber" Seventeenth Symposium on Combustion (International) p.1305 (1978)

(84) BURRELL, G AND OBERFJELL, G "Limits of Inflammability in Mixtures of Methane and Air" Bureau of Mines Technical Paper 119 (1915)

(85) JONES, G, HARRIS, E AND MILLER, W "Explosive Properties of Acetone-Air Mixtures" Bureau of Mines Technical Paper 544 (1933)

(86) COWARD, H AND HARTWELL, F "The Limits of Inflammability of Firedamp in Atmospheres which contain Blackdamp" Safety in Mines Research Board Paper 19 (1926)

(87) EGERTON, A AND POWELLING, J "The Limits of Flame Propagation at Atmospheric Pressure" Proceedings of the Royal Society (London) Vol A193 p.172 (1948)

(88) WHITE, A "Limits for the Propagation of Flames in Inflammable Gas-Air Mixtures" Journal of the Chemical Society Vol 125 p.2387 (1924)

(89) HSIEH, M AND TOWNEND, D "The Inflammation of Mixtures of Air with Diethyl Ether and with Various Hydrocarbons at Reduced Pressures" Journal of the Chemical Society p.332 (1939)

(90) BONE, W, NEWITT, D AND SMITH, C "Gaseous Combustion at High Pressure" Proceedings of the Royal Society (London) Vol A117 p.553 (1928)

(91) ROGLINGSON, W, MACPHERSON, J, MONTGOMERY, P AND WILLIAMS, B "Effect of Temperature on the Upper Flammable Limit of Methane, Ammonia and Air Mixtures" Journal of Chemical and Engineering Data Vol 5 p.349 (1960)

(92) ADLER, U (ED) "Bosch Automotive Handbook" Second Edition Robert Bosch GmbH Stuttgart (1986) 706p.

(93) GAYDON, A AND WOLFHARD, H "Flames - Their Structure, Radiation and Temperature" Third Edition Chapman and Hall London (1970) 402p.

(94) CAMPBELL, A "Development and Use of a Test Rig for Monitoring the Combustion of Fuels in a Spark Ignition Engine with Particular Reference to the Use of Methanol in Transport Vehicles" Master of Engineering (Mechanical) Thesis University of Canterbury (1983) 245p.

(95) KARIM, G, TSANG, P, SARPAL, G AND BADR, O "A fundamental Study into Flame Propagation Through Stratified Mixtures" Paper C255/76 Proceedings of an IMechE Conference on Stratified Charge Engines p.121 (1976)

(96) SPENCER, R "Adaptive Control of the Ignition Timing of Spark Ignition Engines Utilising the Combustion Flame Light Emissions" Master of Engineering (Mechanical) Thesis University of Canterbury (1985)

(97) TROLOVE, H "Calibration of Piezoelectric Pressure Transducers" Final Year Project Report Department of Mechanical Engineering University of Canterbury (1991) 50p.

(98) GLASSON, N "Hydrogen Fuelling of an Internal Combustion Engine" Ph.D Thesis University of Canterbury (1992) 280p.

(99) ROGERS, G AND MAYHEW, Y "Thermodynamic and Transport Properties of Fluids" Third Edition Basil Blackwell (1980) 25p.

(100) FEHLING, H AND LESER, T "Combustion with Oxygen and Oxygen Enriched Air" Journal of the Institute of Fuel Vol 21 p.221 (1948)

(101) GREEN, R "The Influence of Turbulence on the Quenching Effects in the Combustion Process in Constant Volume Explosion Flames" Ph.D Thesis University of Leeds (1975) 270p.

(102) DOW CHEMICAL CO. "JANAF Thermochemical Data Tables" (1971)

(103) KREYSIG, E "Advanced Engineering Mathematics" John Wiley and Sons New York (1983) 1050p.

(104) MASSEY, B "Mechanics of Fluids" Fifth Edition Van Nostrand Reinhold (UK) Ltd Wokingham (1983) 625p.

(105) BARTKOWIAK, R "Electric Circuit Analysis" Harper and Row New York (1985) 688p.

(106) WHITE, W "The Modern Calorimeter" The Chemical Catalogue Company Inc. New York (1928) 194p.

(107) PITT, P AND CLEMENTS, R "The Effects of Plasma Jet Ignition on a Methane Fuelled Internal Combustion Engine" Combustion Science and Technology Vol 30 p.327 (1983)

(108) PITT, P, RIDLEY, J AND CLEMENTS, R "An Ignition System for Ultra Lean Mixtures" Combustion Science and Technology Vol 38 p.217 (1984)

(109) FISHER, P, PITT, P, RIDLEY, J AND CLEMENTS, R "Puff Jet Ignition of Methane in an Internal Combustion Engine" Combustion Science and Technology Vol 46 p.137 (1986)

(110) BOLT, J, AND HARRINGTON, D "The Effects of Mixture Motion Upon the Lean Limit and Combustion of Spark Ignited Mixtures" SAE Paper 670467

(111) DE SOETE, G "Propagation Behaviour of Spark Ignited Flames in Early Stages" Proceedings of IMechE International Conference on Combustion in Engineering Vol 1 p.93 (1983)

(112) DANESHYAR, H, MENDES-LOPES, J AND LUDFORD, G "Effect of Strain Fields on Burning Rates" Nineteenth Symposium on Combustion (International) p.413 (1982)

(113) KALGHATGI, G "Spark Ignition, Early Flame Development and Cyclic Variation in I.C. Engines" SAE Paper 870163 (1988)

(114) LIEBMAN, I, CORRY, J AND PERLEE, H "Dynamics of Flame Propagation Through Layered Methane-Air Mixtures" Combustion Science and Technology Vol 2 p.365 (1971)

(115) BRADLEY, D AND SHEPPARD, C "Limitations to Turbulence Enhanced Burning Rates in Lean Burn Engines" Proceedings of an IMechE Conference on Combustion in Engines: Technology and Applications p.17 (1988)

(116) CHOMIAK, J AND JAROSINSKI, J "Flame Quenching by Turbulence" Combustion and Flame Vol 48 p.241 (1982)

(117) MARSHALL, A "Explosives" J and A Churchill London (1915) 623p.

(118) ZELDOVITCH, I AND KOMPANEETS, A "Theory of Detonation" Academic Press London (1960) 285p.

(119) GUPTA, C AND PRAKASH, R "Engineering Thermodynamics" Fourth Edition Nem Chand and Bros, Roorkee (1981) 953p.

(120) KEENAN, J "Principles of General Thermodynamics" John Wiley and Sons New York (1965) 788p.

(121) HSIEH, J "Principles of Thermodynamics" Scripta Book Company Washington DC (1975) 510p.

(122) ESBACH, O "Handbook of Engineering Fundamentals" First Edition John Wiley and Sons New York (1936)

(123) HOLDER, D AND NORTH, R "Schlieren Methods" Notes on Applied Science No. 31 National Physical Laboratory London (1963) 106p.

APPENDIX A

ADIABATIC FLAME TEMPERATURES: PROGRAM AND DATA

A.1 FLOW CHART FOR AIDTEMP.OXY

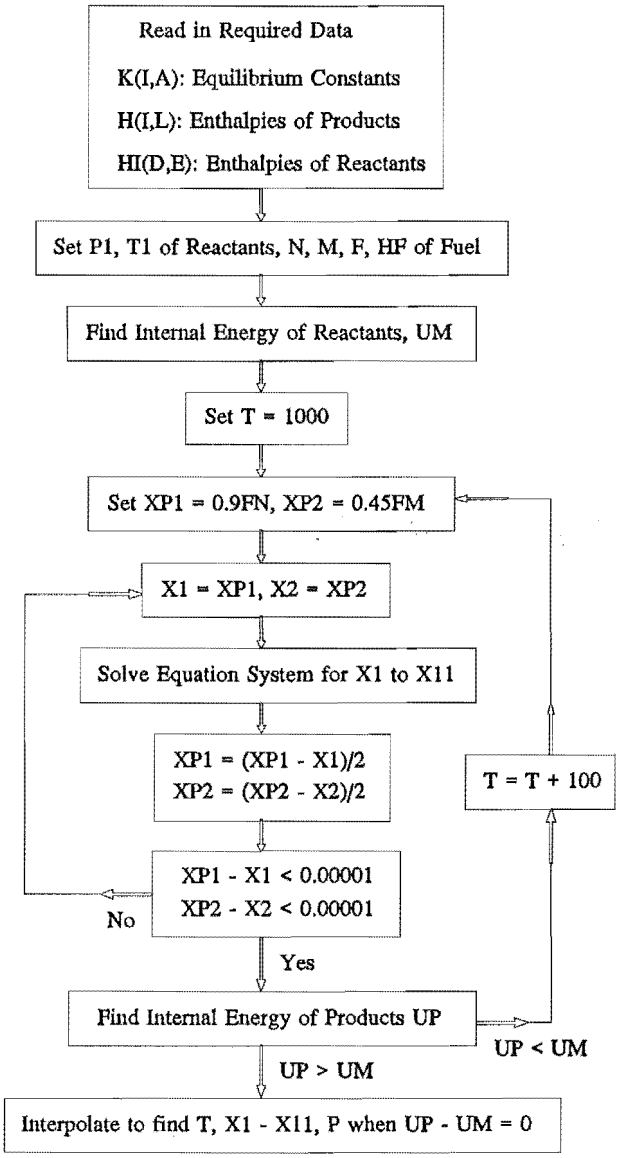

Figure A.1 Flowchart for AIDTEMP.OXY

A.2 AIDTEMP.OXY

```
10 COLOR 11:CLS
15 CLEAR
20 WIDTH "lpt1:",170
25 REM dimension arrays for data constants input
30 DIM H(31,11)
40 DIM K(31,8)
50 DIM UP(31)
60 DIM X(31,11)
70 DIM T(31)
80 DIM B(31)
90 DIM UTEST(31)
100 DIM HI(3)
115 DIM XF(11)
116 REM read in equilibrium constants and enthalpies
120 OPEN "I",#1,"hidat.oxy"
140 FOR E=1 TO 3
150 INPUT #1,HI(E)
160 NEXT E
200 OPEN "I",#2,"hdat.oxy"
210 FOR I=1 TO 31
220 FOR L=1 TO 11
230 INPUT #2,H(I,L)
```

```
240 NEXT L
250 NEXT I
260 OPEN "I",#3,"kdat.oxy"
270 FOR I=1 TO 31
280 FOR A=1 TO 8
290 INPUT #3,K(I,A)
295 K(I,A)=10^K(I,A)
300 NEXT A
310 NEXT I

315 CLS
320 CLOSE:PRINT:PRINT:PRINT"   Welcome to AIDTEMP.OXY"
330 PRINT"   This program can calculate the final adiabatic flame   temperature"
340 PRINT"    for any hydrocarbon fuel of composition CnHm burning lean
       in"
341 PRINT"   oxygen under constant volume conditions."
345 PRINT"      SET YOUR PRINTER TO 20 CHAR/INCH BEFORE
CONTINUING"
350 PRINT:INPUT "   What is the initial temperature (K)";T1
360 INPUT "   What is the initial pressure (atm)";P1
380 INPUT "   No. of Carbon atoms in fuel";N
390 INPUT "   No. of Hydrogen atoms in fuel";M
400 INPUT "   Percent by volume of fuel in mixture";F
410 IF F>=100/(N+M/4+1)-.1 THEN PRINT "   That mixture is too rich.
```

```
      Choose another.":GOTO 400
420 INPUT "  Enthalpy of fuel at initial temp (KJ/mol)";HF
430 F=F/100
440 PRINT:PRINT"  Now calculating internal energy of mixture UM..."
445 REM calculate UM using quadratic interpolation
450 RI=(T1-200)/100
470 HII=HI(1)+RI*(HI(2)-HI(1))+.5*RI*(RI-1)*(HI(3)-2*HI(2)+HI(1))
490 UM = F*HF + (1-F)*HII - .0083144*T1
495 GOSUB 2000
500 PRINT "  UM = "UM" KJ/mol"
505 PRINT "  The final results will be written to "HDR$"FINAL."FIL$
510 PRINT:INPUT "  Are these figures correct";A$
520 IF A$="y" THEN 530 ELSE CLS:GOTO 320
530 PRINT "  MAKE SURE YOUR PRINTER IS ON LINE AND YOU HAVE
A GOOD SUPPLY OF PAPER"
540 INPUT "  Press ENTER to start",A$
550 PRINT "  Now Performing Calculation...."

555 REM start printing initial data
560 LPRINT "Carbon Atoms :> "N
570 LPRINT "Hydrogen Atoms :> "M
580 LPRINT "Percentage of fuel in oxygen :> "F*100
590 LPRINT "Initial Pressue :> "P1"atm"
600 LPRINT "Initial Temperature :> "T1"K"
```

```
610 LPRINT "Internal Energy of Mixture :> ";
620 LPRINT USING "##.###";UM;
630 LPRINT " KJ/mol"
640 LPRINT
650 LPRINT " T(K)" TAB(11) "CO2" TAB(19) "H2O" TAB(27) "OH" TAB(35)
      "C" TAB(43) "H" TAB(51) "O" TAB(59) "CH4";
660 LPRINT TAB(67) "O3" TAB(75) "CO" TAB(83) "O2" TAB(91) "H2" TAB(99)
      "UP(KJ/mol)" TAB(110) "E(mols)"
670 LPRINT STRING$(116,45)

675 REM set constants for iteration
680 I=1
740 XP1 = .9*F*N
750 XP2 = .45*F*M
770 T(I) = 1000 + 100*(I-1)
780 B(I) = (P1*T(I))/T1

785 REM begin iteration
790 X(I,1)=XP1:X(I,2)=XP2
800X(I,10)=1-F-.5*(F*N+X(I,1)+X(I,2)+X(I,3)-X(I,4)+X(I,6)-X(I,7)+3*X(I,8))
810 X(I,9) = SQR((X(I,1)^2*K(I,1))/(X(I,10)*B(I)))
820 X(I,11) = (X(I,9)*X(I,2))/(X(I,1)*K(I,2))
830 X(I,4) = SQR((X(I,9)^2*K(I,3))/(X(I,10)*B(I)))
840 X(I,3) = SQR((X(I,2)^2*K(I,4))/(X(I,11)*B(I)))
```

```
850 X(I,5) = SQR((X(I,11)*K(I,5))/B(I))

860 X(I,2) =.5*(F*M-2*X(I,11)-X(I,3)-X(I,5)-4*X(I,7))

870 X(I,6) = SQR((X(I,10)*K(I,6))/B(I))

900 X(I,7) = (X(I,9)*X(I,11)^3*B(I)^2)/(X(I,2)*K(I,7))

930 X(I,8) = SQR(X(I,10)^3*K(I,8)*B(I))

940 X(I,1) = F*N-X(I,9)-X(I,4)-X(I,7)

960 XP1 = .5*(X(I,1)+XP1)

970 XP2 = .5*(X(I,2)+XP2)

980 TEST1=ABS(XP1-X(I,1))

990 TEST2=ABS(XP2-X(I,2))

995 REM test for accuracy of calculated mole fractions

1000 IF TEST1<.000001 AND TEST2<.000001 THEN 1010 ELSE 790


1005 REM if accuracy OK then calculate internal energy of products

1010 E = .5*F*(N+M) + (1-F) -

      .5*(X(I,1)+X(I,2)-X(I,4)-X(I,5)-X(I,6)-3*X(I,7)+X(I,8))

1020 UP(I)=0

1030 FOR L=1 TO 11

1040 UP(I) = UP(I) + X(I,L)*H(I,L)

1050 NEXT L

1060 UP(I) = UP(I) - E*.0083144*T(I)

1070 LPRINT T(I)" ";

1080 FOR L=1 TO 11

1090 LPRINT USING "###.####";X(I,L);
```

```
1100 NEXT L
1110 LPRINT USING "######.####";UP(I);
1120 LPRINT USING "#####.####";E
1130 UTEST(I) = UP(I)-UM
1135 REM if UP<UM then increase temperature and begin iteration again
1140 IF SGN(UTEST(I))=1 THEN 1150 ELSE I=I+1:GOTO 740

1145 REM quadratic interpolations to find final temp, mole fractions & pressure
1150 C6 =
     ((2*(UTEST(I)-UTEST(I-1)))/(UTEST(I)-2*UTEST(I-1)+UTEST(I-2)))-
     1
1160 C7 = (2*UTEST(I-2))/(UTEST(I)-2*UTEST(I-1)+UTEST(I-2))
1170 R1 = .5*(-1*C6+SQR(C6^2-4*C7))
1180 R2 = .5*(-1*C6-SQR(C6^2-4*C7))
1190 TONE = 100*R1 + T(I-2)
1200 TTWO = 100*R2 + T(I-2)
1210 IF TONE<T(I) AND TONE>T(I-1) THEN TFINAL=TONE
1220 IF TTWO<T(I) AND TTWO>T(I-1) THEN TFINAL=TTWO
1230 R3 = (TFINAL-T(I-2))/100
1240 EF=0
1250 FOR L=1 TO 11
1260 XF(L) = X(I-2,L) + R3*(X(I-1,L)-X(I-2,L)) +
     .5*R3*(R3-1)*(X(I,L)-2*X(I-1,L)+X(I-2,L))
1270 EF = EF + XF(L)
```

```
1280 NEXT L
1290 R4 = (TFINAL-T(I-2))/100
1300 BF = B(I-2) + R4*(B(I-1)-B(I-2)) + .5*R4*(R4-1)*(B(I)-2*B(I-1)+B(I-2))
1310 PFINAL = EF*BF

1315 REM print final results
1320 LPRINT STRING$(116,45)
1330 LPRINT USING "#####";TFINAL;
1340 LPRINT "  ";
1350 FOR L=1 TO 11
1360 LPRINT USING "###.####";XF(L);
1370 NEXT L
1380 LPRINT USING "######.####";UM;
1390 LPRINT USING "#####.####";EF
1400 LPRINT
1410 LPRINT "Final Temperature :> "TFINAL"K"
1420 LPRINT "Final Pressure :> "PFINAL"atm"

1425 REM write results to file
1430 OPEN "A",#1, HDR$+"final."+FIL$
1440 WRITE #1,T1,P1,N,M,F,UM
1450 WRITE #1,TFINAL,PFINAL,EF
1460 FOR L=1 TO 11
1470 WRITE #1,XF(L)
```

```
1480 NEXT L
1490 CLOSE #1
1500 CLS:GOTO 320


2000 FIL$=""
2020 N$=STR$(N):M$=STR$(M)
2030 HDR$=MID$(N$,2,1)+MID$(M$,2,1)
2050 F$=STR$(100*F)
2060 Z=1
2070 IF Z>LEN(F$) THEN 2120
2080 A$=MID$(F$,Z,1)
2090 IF A$=" " OR A$="0" OR A$="." THEN Z=Z+1:GOTO 2070
2100 FIL$=FIL$+A$
2110 Z=Z+1:GOTO 2070
2120 IF LEN(FIL$)=3 THEN RETURN ELSE FIL$=FIL$+"0":GOTO 2120
```

A.3 DATA USED IN THE CALCULATION OF FLAME TEMPERATURES

Table A.1 Enthalpies of Combustion Products at T(i) (kJ/mol)

T (K)	CO_2	H_2O	OH	C	H	O	CH_4	O_3	CO	O_2	H_2
1000	-360.11	-215.83	59.92	11.82	232.59	264.03	-36.70	177.91	-88.85	22.70	20.68
1100	-354.62	-211.64	63.01	14.01	234.67	266.12	-29.33	183.44	-85.51	26.21	23.72
1200	-349.03	-207.32	66.15	16.25	236.75	268.21	-21.61	189.04	-82.11	29.76	26.80
1300	-343.35	-202.89	69.33	18.55	238.82	270.30	-13.57	194.68	-78.67	33.34	29.92
1400	-337.61	-198.33	72.56	20.87	240.90	272.39	-5.27	200.36	-75.20	36.96	33.08
1500	-331.80	-193.68	75.83	23.23	242.98	274.47	3.28	206.07	-71.69	40.60	36.29
1600	-325.93	-188.92	79.14	25.62	245.06	276.55	12.04	211.80	-68.16	44.27	39.54
1700	-320.02	-184.07	82.49	28.02	247.14	278.64	20.99	217.56	-64.60	47.96	42.83
1800	-314.07	-179.13	85.88	30.44	249.22	280.72	30.09	223.35	-61.01	51.67	46.17
1900	-308.08	-174.12	89.30	32.88	251.30	282.80	39.34	229.15	-57.42	55.41	49.54
2000	-302.06	-169.04	92.75	35.32	253.37	284.89	48.72	234.96	-53.80	59.18	52.95
2100	-296.01	-163.89	96.23	37.78	255.45	286.97	55.24	240.54	-50.17	62.96	56.40
2200	-289.94	-158.68	99.74	40.25	257.53	289.05	67.84	246.39	-46.52	66.77	59.88
2300	-283.84	-153.41	103.27	42.73	259.61	291.14	77.55	252.26	-42.86	70.60	63.39
2400	-277.72	-148.09	106.83	45.22	261.69	293.22	85.24	258.13	-39.19	74.45	66.93
2500	-271.58	-142.72	110.41	47.72	263.77	295.30	97.18	260.02	-35.51	78.33	70.50
2600	-265.43	-137.31	114.00	50.22	265.85	297.39	107.09	269.92	-31.83	82.22	74.10
2700	-259.26	-131.85	117.62	52.73	267.92	299.48	117.07	275.82	-28.13	86.14	77.72
2800	-253.07	-126.36	121.26	55.25	270.00	301.56	127.10	281.73	-24.43	90.08	81.37
2900	-246.87	-120.84	124.91	57.77	272.08	303.65	137.18	287.66	-20.71	94.04	85.04
3000	-240.65	-115.28	128.57	60.30	274.16	305.75	147.31	293.59	-17.00	98.01	88.74
3100	-234.59	-109.96	132.82	62.88	276.41	308.07	157.47	299.53	-13.27	102.17	92.52
3200	-228.34	-104.34	136.51	65.42	278.49	310.17	167.68	305.48	-9.54	106.20	96.05
3300	-222.08	-98.70	140.22	67.98	280.57	312.27	177.91	311.44	-5.80	110.24	100.03
3400	-215.82	-93.03	143.95	70.54	282.65	314.38	188.18	317.40	-2.05	114.31	103.81
3500	-209.54	-87.35	147.68	73.10	284.73	316.49	198.48	323.37	1.70	118.39	107.61
3600	-203.25	-81.63	151.42	75.67	286.81	318.60	208.81	329.35	5.45	122.48	111.44
3700	-196.96	-75.90	155.18	78.25	288.89	320.72	219.16	335.34	9.21	126.59	115.28
3800	-190.65	-70.15	158.95	80.83	293.24	322.84	229.54	341.33	12.97	130.72	119.14
3900	-184.33	-64.38	162.72	83.43	293.06	324.96	239.93	347.33	16.74	134.85	123.03
4000	-178.01	-58.59	166.51	86.02	297.39	327.09	250.35	353.34	20.51	139.01	126.93

Table A.2 Equilibrium Constants used in Combustion Calculations

(LK = $\log_{10}$K, definition of K given in equations following table)

T (K)	LK1	LK2	LK3	LK4	LK5	LK6	LK7	LK8
1000	-20.428	-0.148	-20.918	-22.576	-17.288	-19.606	1.417	-22.168
1100	-17.748	0.014	-19.852	-19.858	-15.174	-17.206	2.490	-20.800
1200	-15.516	0.146	-18.958	-17.590	-13.410	-15.202	3.388	-19.658
1300	-13.630	0.254	-18.198	-15.666	-11.912	-13.504	4.150	-18.690
1400	-12.016	0.344	-17.542	-14.016	-10.626	-12.048	4.803	-17.860
1500	-10.618	0.421	-16.970	-12.586	-9.508	-10.784	5.370	-17.138
1600	-9.400	0.485	-16.468	-11.334	-8.528	-9.678	5.865	-16.506
1700	-8.326	0.541	-16.022	-10.228	-7.662	-8.700	6.301	-15.946
1800	-7.374	0.588	-15.622	-9.244	-6.892	-7.830	6.688	-15.448
1900	-6.460	0.632	-15.262	-8.366	-6.200	-7.050	7.034	-15.004
2000	-5.756	0.668	-14.938	-7.572	-5.576	-6.350	7.344	-14.602
2100	-5.066	0.700	-14.642	-6.856	-5.012	-5.714	7.617	-14.252
2200	-4.440	0.728	-14.370	-6.202	-4.498	-5.136	7.870	-13.900
2300	-3.868	0.754	-14.122	-5.608	-4.028	-4.608	8.101	-13.610
2400	-3.346	0.776	-13.892	-5.062	-3.596	-4.124	8.312	-13.320
2500	-2.866	0.797	-13.680	-4.560	-3.198	-3.678	8.505	-13.080
2600	-2.426	0.814	-13.482	-4.096	-2.830	-3.266	8.682	-12.840
2700	-2.018	0.830	-13.298	-3.668	-2.490	-2.884	8.846	-12.630
2800	-1.636	0.846	-13.126	-3.268	-2.174	-2.530	8.998	-12.420
2900	-1.286	0.859	-12.966	-2.898	-1.878	-2.200	9.140	-12.240
3000	-0.958	0.871	-12.814	-2.552	-1.602	-1.892	9.270	-12.060
3100	-0.664	0.869	-12.672	-2.232	-1.348	-1.610	9.392	-11.864
3200	-0.378	0.878	-12.538	-1.926	-1.106	-1.340	9.506	-11.710
3300	-0.108	0.888	-12.412	-1.642	-0.878	-1.086	9.613	-11.566
3400	0.142	0.895	-12.290	-1.374	-0.664	-0.846	9.712	-11.430
3500	0.380	0.902	-12.176	-1.118	-0.462	-0.620	9.806	-11.302
3600	0.604	0.909	-12.068	-0.880	-0.270	-0.408	9.894	-11.180
3700	0.816	0.915	-11.784	-0.654	-0.088	-0.206	9.978	-11.066
3800	1.016	0.921	-11.866	-0.440	0.084	-0.014	10.056	-10.958
3900	1.206	0.926	-11.772	-0.236	0.246	0.168	10.131	-10.856
4000	1.384	0.930	-11.682	-0.044	0.402	0.340	10.201	-10.760

The following eight equations define the equilibrium constants given in Table A2, where P_i is the partial pressure of i.

$$K1 = \frac{P_{CO}^2 \, P_{O_2}}{P_{CO_2}^2} \tag{A.1}$$

$$K2 = \frac{P_{CO} \, P_{H_2O}}{P_{CO_2} \, P_{H_2}} \tag{A.2}$$

$$K3 = \frac{P_C^2 \, P_{O_2}}{P_{CO}^2} \tag{A.3}$$

$$K4 = \frac{P_{OH}^2 \, P_{H_2}}{P_{H_2O}} \tag{A.4}$$

$$K5 = \frac{P_H^2}{P_{H_2}} \tag{A.5}$$

$$K6 = \frac{P_O^2}{P_{O_2}} \tag{A.6}$$

$$K7 = \frac{P_{CO} \, P_{H_2}^3}{P_{CH_4} \, P_{H_2O}} \tag{A.7}$$

$$K8 = \frac{P_{O_3}^2}{P_{O_2}^3} \qquad \text{(A.8)}$$

The initial enthalpy of the mixture before combustion is calculated using the enthalpy of the fuel (entered by the user) and the enthalpy of oxygen (lines 440 to 490 in AIDTEMP.OXY). The oxygen enthalpy was given for 3 temperatures (200, 300 and 400 K), so the program can calculate the initial enthalpy for a modest range of initial temperatures. The oxygen enthalpies used are -2.868, 0.054 and 3.301 kJ/mol for 200, 300 and 400 K respectively.

APPENDIX B

CALCULATION OF MOLAR FLOWRATES

No real gas behaves exactly according to the perfect gas equation of state, that is their behaviour does not exactly conform to

$$Pv = RT \tag{B.1}$$

To overcome this problem there have been put forward many (at least 125, according to Gupta and Prakash[119]) modifications to the perfect gas equation although most are of little use either because of poor accuracy or difficult solution. This Appendix details how the molar flowrates of oxygen* measured using the method described in Section 5.3 can be calculated using two of the better known alternative equations of state.

B.1 THE VAN DER WAALS EQUATION

This equation was one of the first (1873) to attempt to represent the behaviour of real gases. It can be written as

---

* Methane flowrates can be calculated as well, the method being identical. However, the empirical constants used in some of the equations will need to be changed to suit methane rather than oxygen.

$$\left(P + \frac{a}{v^2}\right)(v - b) = RT \qquad \text{(B.2)}$$

In comparison with Equation (B.1) it can be seen there have been two modifications;

(1) A new term (a/v^2) has been added to the pressure term P.

(2) A new term b has been subtracted from the volume term v.

These deviations arise because real gases have intermolecular forces. These forces prevent the molecules nearest the container wall from exerting their full pressure on the wall. This is known as the internal pressure of the gas and it was suggested by Van der Waals that it was proportional to the square of the density and equal to a/v^2. Thus the constant a accounts for the reduction in pressure due to long range attractive forces. For an ideal gas the molecules occupy no space so the total volume and the free volume are the same. In a real gas the free volume will be equal to the total volume less the volume of the molecules. This reduction in volume leads to more molecule collisions and hence a rise in pressure. Thus the constant b takes into account this rise in pressure, and also the small rise due to short range repulsive forces between the molecules.

The problem we are interested in is finding the number of moles in the injection mixture vessel before injection commences and after it has finished. The constants

a and b vary for different gases. For oxygen, we have from Gupta and Prakash[119] a = 0.13925 Nm^4/mol^2 and b = 31.4e-06 m^3/mol (for methane constants see, for example, Keenan[120] or Hsieh[121]). Since we know the pressure and temperature in the injection mixture vessel before and after injection we can rearrange Equation (B.2) in terms of the specific volume v, giving

$$v^3 - \left(b + \frac{RT}{P}\right)v^2 + \left(\frac{a}{P}\right)v - \frac{ab}{P} = 0 \qquad \text{(B.3)}$$

This cubic equation can be solved relatively easily, using a method such as that given by Esbach[122]. Thus it is a simple matter to get the moles present ($n = V/v$) at the initial and final states if we know the volume of the injection mixture vessel, and if we know the time taken for the injection we can calculate the molar flowrate.

B.2 THE BEATTIE-BRIDGEMAN EQUATION

This is a much more complex and accurate five constant equation. It can be written as

$$P = \frac{RT(1-\epsilon)}{v^2}(v+B) - \frac{A}{v^2} \qquad \text{(B.4)}$$

where

$$A = A_0\left(1-\frac{a}{v}\right); \quad B = B_0\left(1-\frac{b}{v}\right); \quad \epsilon = \frac{c}{vT^3} \qquad \text{(B.5)}$$

For oxygen the constants are given below (for methane see Keenan[120] or Hsieh[121]).

A_0	0.15063 Nm^4/mol^2
a	0.0256e-03 m^3/mol
B_0	0.0462e-03 m^3/mol
b	0.0042e-03 m^3/mol
c	48.0 m^3K^3/mol

Equation (B.4) is not easy to solve, so a brief BASIC computer program BBMASFL.BAS was written so an iterative method could be used. This program is included at the end of this Section. The method is crude but speed was not of concern. A specific volume is assumed and all five constants calculated. The pressure is then calculated and if this pressure is greater than the actual pressure the specific volume is increased in small steps until the pressure is less than the actual pressure. Interpolation is then used to find the actual specific volume. The moles present before and after injection, and hence the flowrate can be calculated in the same way as for the Van der Waals Equation.

BBMASFL.BAS BASIC Program to Calculate Molar Flowrates of Oxygen using the Beattie-Bridgeman Equation

```
10 CLS:KEY OFF
15 PRINT "THIS PROGRAM CALCULATES O2 FLOWRATES USING THE
      BEATTIE-BRIDGEMAN EQN"
16 PRINT:PRINT
20 INPUT "What is the initial pressure (bar)";PINT:PINT=PINT*100000!
30 INPUT "What is the initial temperature (deg C)";TIN
40 INPUT "What is the final pressure (bar)";PFINAL:PFINAL=PFINAL*100000!
50 INPUT "What is the final temperature (deg C)";TFINAL
60 INPUT "What is the time taken for the pressure drop (s)";TIM
70 PRINT:PRINT

80 REM find mols at initial conditions
90 V=.0001 REM Assume specific volume
95 REM Calculate constants
100 A = .15063*(1-(.0000256/V))
110 B = .0000462*(1-(-.0000042/V))
120 E = 48/(V*(273.15+TIN)^3)
125 REM Calculate Pressure
130 P = 8.3144*(273.15+TIN)*(1-E)*(V+B)/(V^2) - A/(V^2)
140 IF P<PINT THEN 200
150 PPREV = P
```

```
160 V = V + .00001
170 GOTO 100
195 REM interpolate to find actual initial specific volume
200 VINT = ((PINT-PPREV)/(P-PPREV))*.00001 + (V-.00001)
210 NINT = .0018368/VINT REM find initial mols
220 PRINT USING "Initial No of moles = #.###";NINT

280 REM find mols at final conditions
290 V=.0001 REM assume specific volume
295 REM calculate constants
300 A = .15063*(1-(.0000256/V))
310 B = .0000462*(1-(.0000042/V))
320 E = 48/(V*(273.15+TFINAL)^3)
325 REM calculate pressure
330 P = 8.3144*(273.15+TFINAL)*(1-E)*(V+B)/(V^2) - A/(V^2)
340 IF P<PFINAL THEN 400
350 PPREV = P
360 V = V + .00001
370 GOTO 300
395 REM interpolate to find final specific volume
400 VFINAL = ((PFINAL-PPREV)/(P-PPREV))*.00001 + (V-.00001)
410 NFINAL = .0018368/VFINAL REM find final mols
420 PRINT USING "Final No of moles = #.###";NFINAL
```

```
495 REM calculate flowrate from difference in mols
500 NDIFF = NINT - NFINAL
520 NFLOW = NDIFF/TIM
530 PRINT:PRINT:PRINT
540 PRINT USING "Vol Flowrate = #.#### millimols/s";NFLOW*1000
```

APPENDIX C

CALCULATION OF SPLINE APPROXIMATION

A spline interpolation from Kreysig[103] was used to approximate the apparent molar flowrate variation as the injection pulse duration changed.

The apparent molar flowrate had been measured for four different lengths of injection pulse duration, and for infinite duration (ie. the injector constantly open). The spline was intended to give a piecewise equation that could be used to calculate the apparent molar flowrate for any given injection duration. The tests were done for both methane and oxygen, but the method shown for calculating the spline will only be that for oxygen. This is not important as the procedure for methane is identical. The known data is shown in Table C.1.

Table C.1 Summary of Measured Flowrate Data for Oxygen

Node	0	1	2	3	4
Duration t_{inj} ms	10	20	40	60	?
x (t_{inj} - 20)	-10	0	20	40	?
Flowrate (y)	4.094	4.780	5.507	5.854	6.097
$dy/dx = y'$	?	?	?	?	0

where the flowrate y is in mmols/s and t_{inj} is the injection pulse duration. Each interval (ie. between each node) will be approximated by a different polynomial

$$x = -10 \rightarrow 0, \quad y_0(x) = a_3x^3 + a_2x^2 + a_1x + a_0 \tag{C.1}$$

$$x = 0 \rightarrow 20, \quad y_1(x) = b_3x^3 + b_2x^2 + b_1x + b_0 \tag{C.2}$$

$$x = 20 \rightarrow 40, \quad y_2(x) = c_3x^3 + c_2x^2 + c_1x + c_0 \tag{C.3}$$

$$x = 40 \rightarrow x_4, \quad y_3(x) = d_3x^3 + d_2x^2 + d_1x + d_0 \tag{C.4}$$

The problem is to now determine the constants for these equations. Since there are sixteen unknowns we must find sixteen equations. For a classical spline solution the method would be to now apply the boundary conditions as follows;

1. Eight boundary condition equations (hereafter BCEs) can be found from letting each polynomial equal the known value of y at each node (eg. $y_0(x=-10) = -1000a_3 + 100a_2 - 10a_1 + a_0 = 4.094$).
2. Three BCEs can be found from the equality of the gradients at each interior node (eg. $dy_0(0)/dx = dy_1(0)/dx$).
3. Three BCEs can be found from the equality of the double gradients at the interior nodes (eg. $d^2y_0(0)/dx^2 = d^2y_1(0)/dx^2$).
4. The remaining two BCEs can be found from equating to the known slopes at the end (eg. $dy(x_4)/dx = 0$).

This requires us to assume a value for x_4, because we do not know at what injection duration the flowrate becomes the same as the continuous one, and also a value for the slope at x_0. This was done but the spline it produced was too oscillatory because there was no condition that constrained the gradients at the interior nodes to the positive.

The next step was to assume a gradient at all of the interior nodes. This estimation was done by assuming straight lines connected each node, and calculating the gradients of these lines. It was then assumed that the gradient at the node was the average of the gradient leading to it and the gradient leaving it. These new boundary conditions are summarised in Table C.2.

Table C.2 Oxygen Flowrate Data with Estimated Nodal Gradients

Node	0	1	2	3	4
Duration t_{inj} ms	10	20	40	60	?
x (t_{inj} - 20)	-10	0	20	40	?
Flowrate (y)	4.094	4.780	5.507	5.854	6.097
$dy/dx = y'$	?	0.0523	0.027	?	0

As can be seen however, this still required a guess for x_4 and the slope at x_0. This was overcome by assuming that the rate of change of the gradient decreased by a factor g between each set of nodes as one goes from x_0 to x_4, as shown in Table C.3.

Table C.3 Required Oxygen Nodal Gradients and Double Gradients

Node	0	1	2	3	4
Duration t_{inj} ms	10	20	40	60	t_4
x (t_{inj} - 20)	-10	0	20	40	x_4
Flowrate (y)	4.094	4.780	5.507	5.854	6.097
$dy/dx = y'$	y_o'	0.0525	0.0269	y_3'	0
$d^2y/dx^2 = y''$	y_{01}''	-0.001	y_{23}''	y_{34}''	

This enables us to set up five compatibility equations that relate all the unknowns on the right hand side of Table C.3.

$$y_3' = 0.5\left[\left(\frac{y_4-y_3}{x_4-x_3}\right) + \left(\frac{y_3-y_2}{x_3-x_2}\right)\right] \tag{C.5}$$

$$y_{23}'' = \frac{y_3'-y_2'}{x_3-x_2} \tag{C.6}$$

$$y_{34}'' = \frac{y_4'-y_3'}{x_4-x_3} \tag{C.7}$$

$$y_{34}'' = g\, y_{23}'' \tag{C.8}$$

$$y_{34}'' = g^2\, y_{12}'' \tag{C.9}$$

Equations (C.8) and (C.9) can be combined to give

$$1 = \frac{y_{34}''\, y_{12}''}{\left(y_{23}''\right)^2} \tag{C.10}$$

Thus if we assume a value of x_4 then we can calculate our unknowns from Equations (C.5) to (C.7), and check how accurate our assumption was by seeing if Equation (C.10) is true. A simple interpolation was set up using LOTUS 123 and this gave the results shown in Table C.4.

Table C.4 Estimated Oxygen Nodal Gradients and Double Gradients

Node	0	1	2	3	4
Duration t_{inj} ms	10	20	40	60	91.2
x (t_{inj} - 20)	-10	0	20	40	71.2
Flowrate (y)	4.094	4.780	5.507	5.854	6.097
$dy/dx = y'$	y_o'	0.0525	0.0269	0.0126	0
$d^2y/dx^2 = y''$	y_{01}''	-0.0013	-7.1e-04	-4e-04	

It also gave $g = 0.56$ and hence we can solve for the final two unknowns y_{01}'' and y_o'.

$$y_{01}'' = \frac{1}{g} y_{12}'' \tag{C.11}$$

$$y_0' = y_1' - y_{01}'' (x_1 - x_0) \tag{C.12}$$

Thus all the gradients needed have been calculated and are shown in Table C.5.

We can now write the 16 BCEs, as we have 8 from the letting the polynomials equal the known values of y at the nodes and another 8 from letting the differential of the polynomials equal the slope at each node.

Table C.5 Nodal Values used in BCEs for Oxygen

Node	0	1	2	3	4
Duration t_{inj} ms	10	20	40	60	91.2
x (t_{inj} - 20)	-10	0	20	40	71.2
Flowrate (y)	4.094	4.780	5.507	5.854	6.097
$dy/dx = y'$	0.0754	0.0525	0.0269	0.0126	0

At x = -10 we have

$$300a_3 - 20a_2 + a_1 = y_0' = 0.0754 \quad \text{(C.13)}$$

$$-1000a_3 + 100a_2 - 10a_1 + a_0 = y_0 = 4.094 \quad \text{(C.14)}$$

At x = 0

$$a_1 = y1' = 0.0525 \quad \text{(C.15)}$$

$$a_0 = y_1 = 4.780 \quad \text{(C.16)}$$

$$b_1 = y_1' = 0.0525 \quad \text{(C.17)}$$

$$b_0 = y_1 = 4.780 \quad \text{(C.18)}$$

At x = 20

$$1200b_3 + 40b_2 + b_1 = y_2' = 0.0269 \quad \text{(C.19)}$$

$$8000b_3 + 400b_2 + 20b_1 + b_0 = y_2 = 5.507 \quad \text{(C.20)}$$

$$1200c_3 + 40c_2 + c_1 = y_2' = 0.0269 \quad \text{(C.21)}$$

$$8000c_3 + 400c_2 + 20c_1 + c_0 = y_2 = 5.507 \quad \text{(C.22)}$$

At $x = 40$

$$4800c_3 + 80c_2 + c_1 = y_3' = 0.0126 \quad \text{(C.23)}$$

$$64000c_3 + 1600c_2 + 40c_1 + c_0 = y_3 = 5.854 \quad \text{(C.24)}$$

$$4800d_3 + 80d_2 + d_1 = y_3' = 0.0126 \quad \text{(C.25)}$$

$$64000d_3 + 1600d_2 + 40d_1 + d_0 = y_3 = 5.854 \quad \text{(C.26)}$$

At $x = 71.2$

$$9075d_3 + 110d_2 + d_1 = y_4' = 0 \quad \text{(C.27)}$$

$$166375d_3 + 3025d_2 + 55d_1 + d_0 = y_4 = 6.097 \quad \text{(C.28)}$$

These were rewritten in matrix form and solved using PC-MATLAB 3.13, although solving by hand would not be too difficult. This yielded the constants given in Table C.6.

The constants have been given to eight decimal places, because it is essential for the splines to work best that as many decimal places as possible are used.

Table C.6 Spline Constants for Oxygen

a_3	-9.3e-05	c_3	1.2e-05
a_2	-2.54e-03	c_2	-1.4375e-03
a_1	5.25e-02	c_1	7.0e-02
a_0	4.78	c_0	4.586
b_3	1.675e-05	d_3	-3.05814747e-06
b_2	-1.1425e-03	d_2	3.08175922e-04
b_1	5.25e-02	d_1	2.62503414e-03
b_0	4.78	d_0	5.45163860

The method for calculating the spline for methane flowrates is identical. The only change is the values of y and y'. These values are summarised in Table C.7 and the constants for the spline are given in Table C.8.

Table C.7 Nodal Values used in BCEs for Methane

Node	0	1	2	3	4
Duration t_{inj} ms	10	20	40	60	91.2
x (t_{inj} - 20)	-10	0	20	40	71.2
Flowrate (y)	4.881	6.744	7.878	8.292	8.685
$dy/dx = y'$	0.2584	0.1134	0.0305	0.0153	0

Table C.8 Spline Constants for Methane

a_3	-8e-06	c_3	1.1e-05
a_2	-7.37e-03	c_2	-1.37e-03
a_1	1.134e-01	c_1	7.21e-02
a_0	6.744	c_0	6.896
b_3	7.625e-05	d_3	-2.71875e-06
b_2	-4.36e-03	d_2	2.98125e-04
b_1	1.134e-01	d_1	4.5e-03
b_0	6.744	d_0	7.809

APPENDIX D

SCHLIEREN METHODS - EQUIPMENT AND PROCEDURE

D.1 INTRODUCTION

Schlieren methods originated in Germany where they were used to detect inhomogeneous regions in optical glass, which are often in the form of streaks (schliere).[123] The principle of the method is that many types of engineering phenomena involve changes in the relative density through the field of study (eg. motion of air past aeroplane wings, the mixing of liquids or gases). The density change produces a corresponding change in the refractive index of the medium under study. This can be visualised or photographed by using optical methods that depend on the effects of refractive index changes on the transmission of light.

The general layout of the Schlieren system used is shown in Figure D.1. Some of the light rays passing through the test section are refracted because of the slightly different density at various points. These produce a slightly displaced image on the screen and this shows as regions of varying lightness and darkness.

D.2 TEST EQUIPMENT

The test section was a specially built vessel with two 50 mm by 40 mm perspex windows. This vessel was 250 mm long and identical in dimensions to the combustion bomb vessels (see Section 4.2). A special endcap was built that allowed the spark plug to be recessed so the end of the electrode could be seen through the windows. This is shown in Plate D.1. The injection system was identical to that used for the combustion and flowrate testing, although only methane was injected to form the gas puff as its lower density would help distinguish the puff from the gas in the vessel. This gas was air, which was used because of simplicity and also because its density is approximately that of lean methane-oxygen mixture. The internal pressure of the bomb before injection was 0.5 bar gauge and the injection pressure was 5 bar gauge, these being the same pressures as used for the combustion tests.

The light used was an Optical Works Ltd Argon Jet Light Source. This device can operate in two modes, either a steady low level source, used for setting up the mirrors, knife edge and test section, or a short (0.2 microseconds) high intensity light pulse, for taking still photographs. The light pulse is created by jumping a spark of 3 J between two tungsten electrodes. Argon (at 0.3 bar) is introduced in the location of the electrodes and is used to help stabilise and intensify the spark. The light travels from the source to the first 150 mm mirror, which focuses it into a parallel beam for travel through the test section. The beam then reaches a second 150 mm mirror, which focuses the light on to a knife edge, which in turn

focuses the image at a Nikon F3 camera. The film used for the photography was 400 ASA, push processed to 1600 ASA. The entire system except the camera can be seen in Plate D.2 and Plate D.3.

The light pulse is triggered by a digital timer specially built for Zavier[21] in the Department of Electrical and Electronic Engineering. This provides a variable delay between the start of injection and the triggering of the light source from 0 to 100 ms in steps of 0.01 ms.

D.3 SETUP AND TESTING

The rig was set up using approximately the dimensions given in Figure D.1. The steady light source was then turned on and the beam directed through the test section. The knife edge was moved toward the second mirror until the mirror focused the light onto the variable slit. The lens was removed from the camera and the camera positioned until an image of the appropriate size was focused directly onto the shutter. The knife edge gap was adjusted to give the best focus.

To obtain the best results it was then necessary to move the second mirror down slightly, to reduce the light level on the camera shutter. The image would stay in focus but the background would become very grey, and any dirt on the test section windows stood out in high relief. This step was necessary because although it proved possible to see the puff with the mirror in the normal position, it

photographed very poorly. The injector was then tested several times to ensure that the puff could be seen and that the injector was working satisfactorily.

The testing was carried out in the reverberation room in the Department of Mechanical Engineering, which had the twin advantages of being absolutely dark and vibration free. To start the test the light source was switched on and the EHT switch also set to on (this provides power to the transformer which provides the voltage for the light generating spark). The argon gas valve was opened and the whole light source was allowed to warm up. The methane supply valve was opened and the injection pressure set to 5 bar. The test vessel was flushed using compressed air from the Departmental ring main and the internal pressure set to 0.5 bar. The required delay was set on the digital timer. When everything was ready all the room lights were switched off and the camera shutter opened. A microswitch was then triggered, closing a 3 V circuit to start the injector, and sending a 12 V pulse to the digital timer. The timer registered this and triggered the argon light source after the preset delay. The camera shutter was then closed, the film wound on and everything was reset for the next test.

This system proved to work very well, giving excellent pictures of the puff, five of which are shown in Plate D.4. The only major difficulty was that using greater time delays than about 15 ms was pointless as the puff became so big that it filled the entire window.

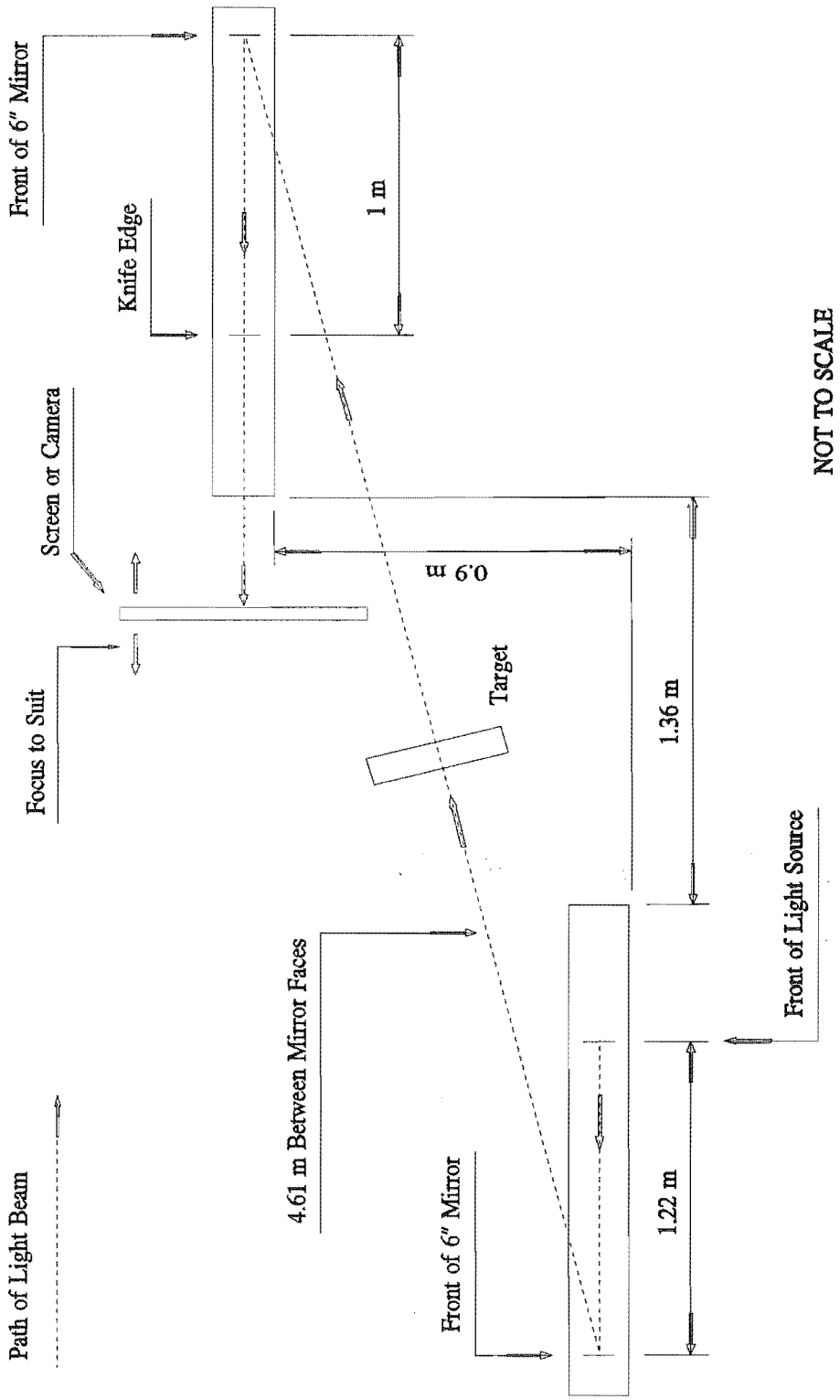

Figure D.1 Approximate Setup of Schlieren Apparatus

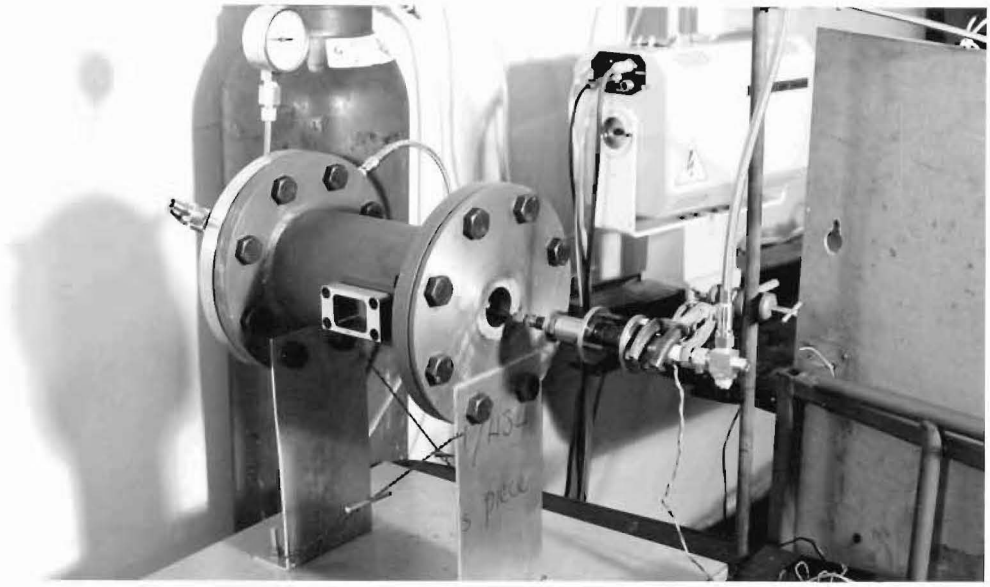

Plate D.1 Vessel Used for Schlieren Photography

Plate D.2 Schlieren Apparatus

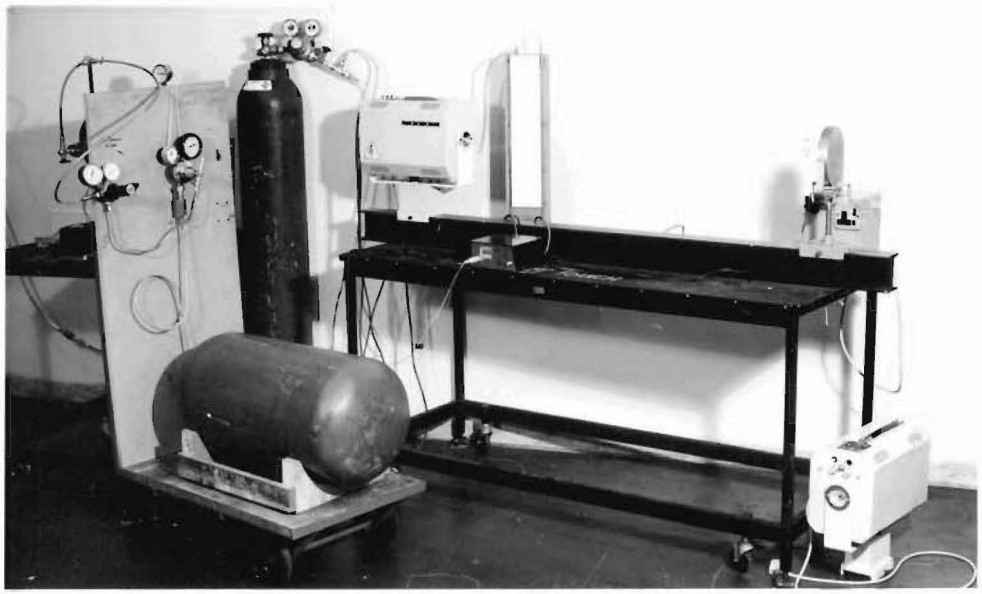

Plate D.3 Schlieren Apparatus

t_{inj} = 8ms

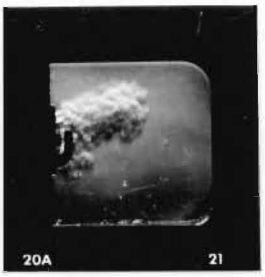

t_{inj} = 9ms

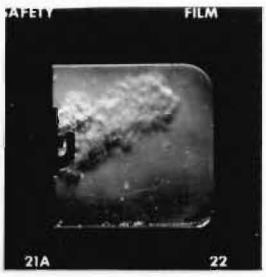

t_{inj} = 10ms

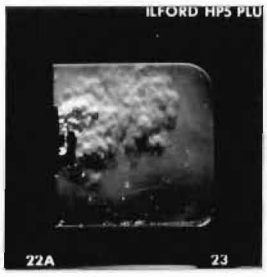

t_{inj} = 11ms

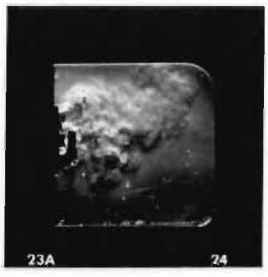

t_{inj} = 12ms

Plate D.4 Schlieren Photographs of Injected Gas Puff (Injection Pressure = 5 bar gauge)

APPENDIX E

DEFINITION OF NON-IGNITION

It was necessary during testing to define how many attempts would be made to ignite a test mixture. This definition has a direct bearing on how the limit of flammability is defined.

For ignition using only the electric spark to ignite a homogenous mixture this matter was straight forward, and for all tests using only the spark ten attempts were made to ignite the mixture. For mixtures where the injected puff of methane-oxygen was the intended ignition source the problem became more serious because if a puff was injected and did not burn it would alter the overall λ of the mixture in the bomb (the puff would generally be richer in methane than the mixture in the bomb).

The obvious solution would be to replace the mixture in the bomb after only one injection attempt, but this was rejected on the grounds of wasting both the test mixture and time. Therefore a calculation was performed to show how the overall λ in the bomb would change if the injected puff(s) were just left to distribute themselves evenly around the bomb. Consider the following. In the bomb we have a mixture of w moles of methane-oxygen at P_i and T_i. Into this we inject n moles of a different methane-oxygen mixture. We can say that

$$w = w_{O_2} + w_{CH_4} \tag{E.1}$$

$$n = n_{O_2} + n_{CH_4} \tag{E.2}$$

Now we can define λ_1 and λ_2 as the equivalence ratios of the mixture in the bomb before and after injection respectively.

$$\lambda_1 = \left(\frac{w_{O_2}}{w_{CH_4}}\right)\frac{1}{C} \tag{E.3}$$

$$\lambda_2 = \left(\frac{w_{O_2} + n_{O_2}}{w_{CH_4} + n_{CH_4}}\right)\frac{1}{C} \tag{E.4}$$

where C is the stoichiometric value of the O/F ratio (equals 2 for methane-oxygen). If instead of injecting just one puff of n moles we inject N puffs, each of n moles, Equation (E.4) becomes

$$\lambda_2 = \left(\frac{w_{O_2} + Nn_{O_2}}{w_{CH_4} + Nn_{CH_4}}\right)\frac{1}{C} \tag{E.5}$$

We can now substitute Equation (E.3) into Equation (E.5) eliminating C

$$\lambda_2 = \lambda_1\left(\frac{w_{O_2} + Nn_{O_2}}{w_{CH_4} + Nn_{CH_4}}\right)\frac{w_{CH_4}}{w_{O_2}} \tag{E.6}$$

With further manipulation this gives

$$\lambda_2 = \lambda_1 \left(\frac{1 + N \dfrac{n_{O_2}}{w_{O_2}}}{1 + N \dfrac{n_{CH_4}}{w_{CH_4}}} \right) \tag{E.7}$$

Thus we now have a relationship expressing how the equivalence ratio of the mixture in the bomb will change for N injections.

We can assume that the injected puff is composed of 10% methane in oxygen. This was approximately true for all the tests conducted. The maximum injection duration used in the testing was 60 ms, and from this information we can calculate n_{O2} and n_{CH4} from Equations (5.30) and (5.31) in Section 5.3.3. For any given λ_1 we can calculate w_{O2} and w_{CH4} from the perfect gas equation since we know P_i and V (the volume of the bomb), and can assume T_i.

Table E.1 shows how λ_1 is affected by the number of injection puffs introduced into the bomb, where the injection duration is 60 ms and the volume is that of the smallest bomb size (1.96 litres).

As can be seen the effect on the overall λ is minimal for the richer mixtures. However as the mixture in the bomb becomes leaner the effect becomes progressively worse. It was decided to limit the number of ignition attempts to four, this keeping the maximum possible decrease in λ to just over 1% in the worst possible case. This translates approximately to an increase in the concentration of

methane in the mixture of 0.056%. This limit was considered acceptable for the test programme undertaken.

Table E.1 Changes in Mixture Strength with Number of Injected Puffs

No. Puffs	1	2	3	4	5	6	7	8	9	10
λ_1 = 5	4.998	4.997	4.995	4.994	4.992	4.990	4.989	4.987	4.986	4.984
% dec.	0.033	0.065	0.097	0.129	0.161	0.193	0.224	0.256	0.287	0.317
λ_1 = 6	5.994	5.988	5.983	5.977	5.971	5.966	5.960	5.955	5.949	5.944
% dec.	0.097	0.192	0.287	0.382	0.475	0.568	0.660	0.752	0.843	0.933
λ_1 = 7	6.989	6.978	6.967	6.956	6.945	6.935	6.942	6.914	6.903	6.893
% dec.	0.159	0.317	0.473	0.628	0.781	0.933	1.084	1.233	1.382	1.529
λ_1 = 8	7.892	7.965	7.948	7.930	7.914	7.897	7.880	7.864	7.847	7.831
% dec.	0.221	0.439	0.655	0.869	1.081	1.291	1.499	1.704	1.908	2.110
λ_1 = 9	8.975	8.950	8.925	8.900	8.876	8.852	8.828	8.805	8.782	8.759
% dec.	0.282	0.560	0.835	1.108	1.377	1.643	1.907	2.167	2.425	2.680

APPENDIX F

ESTIMATION OF ERRORS IN THE MIXING PROCESS

A problem was how to accurately measure the pressure in the test and injection mixture vessels, since accuracy is of the greatest importance as the concentration of the mixture depends upon it.

Hardie Technologies Ltd (the suppliers) were unable to provide much in the way of information for the SenSym SSX 300 G pressure transducer used for the pressure measurement. Therefore a programme was undertaken to measure the response of the transducer. The QuickBASIC program which reads the pressure signal through the Metrabyte Dash-8 A/D board was modified to read in millivolts, and the pressure was applied to the transducer using the Barnet Instruments Industrial Deadweight Tester (note that this was not the same procedure that was used to calibrate the AVL piezoelectric pressure transducer, which required the deadweight tester to be operated in a dynamic mode). The response of the SSX 300 G was recorded for a range of pressures from 0 to 20 bar in steps of 0.2 bar. This procedure automatically took into account errors in reading the signal from the A/D board. The response was very repeatable, varying by less than 0.01 mv (ie. ± 0.05 mv, approximately ± 0.00125 bar). The repeatability was better at lower pressures (0-5 bar) than high pressures (15 to 20 bar). The signal at a given pressure generally fluctuated between two extreme values due to the intermittent

sampling via the multiplexer, but the spread of this fluctuation could be reduced by increasing the number of samples the program took. This had a penalty in that it took longer to complete a sampling cycle. It was important that this time be no more than about a second, as it became too easy to overfill the mixing vessels if the sample time was any longer. Therefore 2000 samples were taken per reading, this translating into a signal spread of approximately ± 0.004 mv (± 0.0015 bar). The spread of the signal was the same at all pressures. The actual pressure was always taken to be the mean of this spread. Lastly, a very small error of 6.6e-05 bar was associated with the measurement of atmospheric pressure, but this will be neglected in the following.

To give an example of how these inaccuracies will affect the concentration let us consider a 6% methane in oxygen mixture with a total pressure of 18 bar absolute (hence methane partial pressure is 1.08 bar). This was typical of the mixtures used in the test programme.

The error in the pressure of methane is calculated by adding the absolute errors before the fill commences and after the fill has finished (ie. the pressure before the fill has an error of some amount associated with it and the pressure after the fill also has an associated error). Each of these errors (ie. before and after the fill) is comprised of the error of variation (± 0.0015 bar) and the error of repeatability (± 0.00125 bar). This gives the error at each "end" of the methane measurement as ± 0.00275 bar. Thus the concentration of methane has a total error of ± 0.0055 bar. The same argument can be applied to the total pressure in the vessel after the

oxygen has been added. The absolute error at each "end" of the total pressure is also ± 0.00275 bar, so the total error in the total pressure is ± 0.0055 bar.

Thus the minimum partial pressure of methane will be 1.0745 and the maximum 1.0855 bar absolute (1.08 ± 0.0055). The minimum total pressure is 17.9945 and the maximum 18.0055 bar absolute. Thus the minimum concentration of methane in the mixture is therefore 1.0745/18.0055 = 5.97% and the maximum is 1.0855/17.9945 = 6.03%.